All-fibre wavelength versatile short pulsed laser sources

Carlos Eduardo Schmidt Castellani

Femtosecond Optics Group
Photonics, Department of Physics
Imperial College London
United Kingdom

October 2013

Thesis submitted for the degree of Doctor of Philosophy of Imperial College London and for the Diploma of the Imperial College

Declaration of Originality

All the work reported in this thesis is the result of my own work realized during my PhD unless stated otherwise in which case the appropriate references are made.

Copyright Declaration

Abstract

Pulsed lasers operating in the picosecond or femtosecond regimes find a wide range of applications in optical sciences, such as spectroscopy, laser surgery, material processing and optical communications. Among the existing sources of short-pulses, mode-locked fibre lasers play an important role mainly due to their robust and compact nature, and also due to their ability to generate outputs over a wide range of repetition-rates, pulse durations, pulse shapes, peak powers and optical wavelengths.

Considering the case of wavelength versatility, Raman amplification can be used to fill the spectral gaps that are not covered by the emission band of traditional rare-earth doped elements such as ytterbium and erbium, allowing the generation of light at unconventional wavelengths. Additionally, another contribution has come from the recent development of new nanomaterials such as graphene and carbon nanotubes that can be used as saturable absorbers over a broadband wavelength range.

The experimental work reported in this thesis is mainly focused in combining the wavelength versatility allowed by Raman gain and carbon nanotubes and graphene to generate short-pulsed fibre lasers at different wavelengths. High power ytterbium and erbium lasers and also a high power Raman laser operating at 1450 nm are used as pump sources to seed the Raman gain and carbon nanotubes and graphene are the saturable absorbers used as mode-lockers. All the fibres utilized in the oscillators are highly non-linear single mode silica fibres doped with GeO_2.

The lasers operate in the dissipative soliton regime, generating chirped pulses with durations on the order of hundred of picosecond that are suitable for external compression. We demonstrate for example an erbium-pumped Raman oscillator generating 500 ps pulses that are linearly compressed to 2 ps. The results presented in this document are a contribution towards making fibre based lasers more universal devices in terms of wavelength operation.

Acknowledgments

First of all I would like to thank my supervisor Roy Taylor for all the support, help and knowledge received during my PhD. Equally important I cannot forget to mention my co-supervisor Sergei Popov, who helped me immensely with many laser issues, and also Paul Brown, Simon and Martin from the workshop not only for their material support given but also for being good friends through these years. I am also immensely thankful to all my colleges with whom I coincide in the lab during these years, even if it was only for a short time. John the wisest guy I've ever met and a great source of inspiration, Ed for giving me many good advices and being a great friend, Marko for being a funny guy, Olivier for helping me improve my French, Ben for being a very good office-mate, Robbie for being simply Robbie, Tim for being a very good attacking partner on the photonics football team, Meng for being for a long time with me the only foreign students in the group, Rob for being a nice guy and lastly Dora for being a nice friend.

More importantly I need to thank the help and support I got from my family, that even being on the other side of the ocean were always at my side. My mother, my father, my grandmothers, both my brothers, my uncle Fausto and my other uncles, my beloved girlfriend Daria, all my cousins, and many others. Without them this would have been even harder. Lastly I would also like to thank CAPES for the financial support I received along this years, which allowed me to pursue this great opportunity of doing my PhD in England.

For my grandmother Jovelina who passed away during my studies in England

Contents

List of Figures

1 Introduction

All-fibre integrated laser configurations delivering high-power short-pulses across a range of wavelengths is now an established reality over many years. The extensive development of optical fibre-based technologies that occurred in the last decades have allowed an unprecedented growth in both temporal and spectral versatility of fibre lasers sources.

Highly non-linear single mode fibres with small cores and high levels of GeO_2 doping are now ubiquitous tools in laser physics research permitting many non-linear effects to be observed over reduced fibre lengths. Combining these fibres with the high optical power levels that can readily be obtained from Erbium- or Ytterbium-doped amplifiers creates an ideal platform to excite non-linear effects that can be used for efficient wavelength conversion such as stimulated Raman scattering (SRS) and parametric amplification. In more recent years, the growth of bismuth and especially of thulium fibre laser technology has extended the spectral range over which non-linear wavelength conversion in fibre can occur.

In the temporal domain, newly developed nanomaterials such as carbon nanotubes (CNT) and graphene became an interesting alternative to the traditionally used saturable absorber mirrors (SESAM). Among other interesting features, such as fast response time and low fabrication costs, both graphene and carbon nanotubes can be used as optical saturable absorbers over a broadband wavelength range, that can be larger than 1 μm for CNTs and that virtually can cover any wavelength in the broad absorption band of graphene (500 - 2000 nm), different from SESAMs that traditionally work at specific wavelengths, on ranges that usually are not broader than a few tens of nanometers.

Still on the time domain of mode-locking, lots of research effort has been lately dedicated towards lasers operating in the the so-called dissipative soliton regime. The usage of optical cavities presenting net normal dispersion has allowed the direct generation of long pulses, with duration up to tens of nanoseconds, that are

chirped in nature, therefore suitable for external compression. Such lasers present an alternative route to higher power levels than possible from the standard soliton mode-locked lasers due to its capacity to increase the pulse energy levels achievable from an oscillator.

This thesis concentrates on the implementation of non-linearity and nanomaterial based saturable absorbers into mode-locked laser cavities. Raman amplification is used together with carbon nanotubes and graphene, generating short-pulses at a number of different wavelengths, confirming the spectral versatility of this approach. All the systems designed operate in the dissipative soliton regime. The present chapter is intended to be an overview of the field, focusing mainly on the physical phenomena that are directly or indirectly involved in the experiments realised in the lab. Section 1.1 describes the basic physics of light propagation in optical fibres divided into its linear and non-linear aspects. Section 1.2 summarizes some of the techniques used to generate short pulses in fibre lasers and finally the section 1.3 is dedicated mainly to the physics of Raman lasers. The experimental results are shown in detail in the following chapters.

1.1 Linear and non-linear optics overview

The invention of low-loss optical fibres that started in the mid-sixties was beyond doubt one of the most important technology advancements in physical sciences that happened in the 20th century. Its capacity to guide light over tens of kilometres without adding significant loss was essentially responsible for the birth of a new era in the telecommunication field [1]. Indeed, this fact was lately recognized in 2009 when the Nobel prize of physics was awarded to Charles Kuen Kao for his "groundbreaking achievements concerning the transmission of light in fibers for optical communication".

The first experimental demonstration of the idea of guiding light through means of total internal reflection dates back to the mid 1800s when both D. Colladon and J. Thyndall showed light being guided by water jets [2]. However, it took nearly another century until experimental investigations of light guidance in a glass fibre waveguide was finally realised [3]. In the early sixties the telecommunication industry started to pay attention to this new evolving technology and the main effort during that time was to try to reduce the fibre losses that were initially approxi-

mately 1000 dB/km. This value was gradually reduced over the next decades. By the early seventies fiber losses were already down to 20 dB/km [4], but it was not until 1976 that the first fibres presenting less then 1 dB/km loss were experimentally demonstrated [5, 6]. In 1978 by applying the Modified Chemical Vapour Deposition (MCVD) method and by using germanium instead of titanium as the core dopant the current loss of 0.2 dB/km at 1.55 μm was finally achieved [7]. This loss value close to the theoretical limit paved the way to a revolution in optical sciences.

1.1.1 Light in optical fibres

An optical fibre is in its basic form simply a cylindrical glass core of refractive index n_1 surrounded by a cylindrical cladding made of a glass material that has a refractive index n_2 lower then n_1. This scenario is illustrated in Fig. 1.1. Typical fibres, such as step-index standard telecom fibres (STF), have both core and cladding constituted of silica glass (SiO_2). The difference in the refractive index is usually achieved by doping the core with elements such as germanium dioxide (GeO_2) and phosphorus pentoxide (P_2O_5) that increase n_1, while the cladding is doped with materials such as boron and fluorine that cause the inverse effect [8].

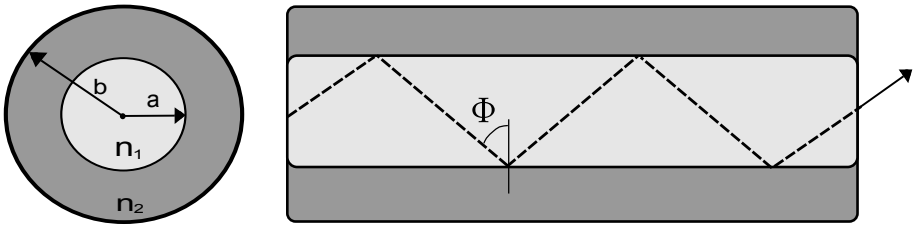

Figure 1.1: Transverse and longitudinal section of a step-index standard optical fibre of core radius a and cladding radius b showing light propagation through total internal reflection. n_1 and n_2 represent the refractive index of both materials.

As a first approach, the physical phenomenon behind light guidance in standard optical fibres can be understood by geometric optics by means of total internal reflection [1], as exemplified in Fig. 1.1. If a ray of light is incident at a interface between two transparent media at an angle Φ higher then a certain critical angle Φ_{crit} defined by Eq. 1.1, than no light is transmitted and everything is reflected. This geometric approach generally serves as a good insight on light propagation in optical fibres. However, if the core diameter and the wavelength in case have close

values a field analysis solving Maxwell's equations is necessary for a more accurate understanding [1].

$$\Phi_{crit} = arcsin(\frac{n_2}{n_1}) \tag{1.1}$$

Another important concept regarding light propagation in optical fibres is the number of modes that are allowed to propagate. If one solves Maxwell's equations applying the boundary conditions posed by the fibre [1], one will find that the possible solutions define that only certain particular transverse electromagnetic field patterns are permitted. A fibre that guides just the fundamental mode is called single-mode fibre (SMF), while if it supports also other high-order modes then the fibre is called multi-mode fibre (MMF).

The parameter that determines the number of guided modes propagating in a fibre for each given wavelength is the so-called V parameter, defined by Eq. 1.2. There, k_0=$2\pi/\lambda$, a is the core radius, λ is the wavelength of light and n_1 and n_2 are the refractive index of core and cladding, respectively. For a fibre to be single mode it is necessary to fabricate it with a V value lower then 2.405. However, it is important to notice that the number of modes in a fibre is wavelength dependent, and for a given fibre, the wavelength at which high-order modes cease to propagate is called the cut-off wavelength.

$$V = k_0 a \sqrt{{n_1}^2 - {n_2}^2} \tag{1.2}$$

The core size is the main structural difference between multi-mode and single-mode fibres. Usual core size values are on the range of 1-5 μm for SMFs and 25-100 μm for MMFs. In long distance telecommunication systems, single-mode fibres are preferably used because on a multi-mode fibre each different mode travels with a different group velocity causing dispersion and therefore signal distortion at high-repetition rates. Their reduced core sizes also make SMFs ideal hosts for the generation of nonlinear effects even when using moderate optical powers. MMFs are mainly used for short-distance optical fibre communications where the effects of dispersion are not very significant.

1.1.2 Attenuation

As mention previously, one of the main traits of optical fibres that made them so widely used is their capacity of guiding light with very low loss. In STFs, the attenuation at its lowest point around the wavelength of 1550 nm, can be below 0.2 dB/km, which means that light would have to travel 50 km until it reaches 10 % of its initial value. The physical mechanisms behind losses in optical fibres are chiefly ultraviolet (UV) absorption and Rayleigh scattering at short wavelengths and molecular vibration at longer wavelengths [9].

In the wavelength region from 0.5 to 2 μm the loss in silicate fibres is limited mainly due to Rayleigh scattering and to a lower degree also by material absorptions. The Rayleigh scattering arises from local microscopic fluctuations in density, which causes local random fluctuations in the refractive index, and it can be estimated in dB/km by the eq. 1.3, where C_r is a constant in the range of 0.7-0.9 dB.μm^4/km.

$$\alpha_r = \frac{C_r}{\lambda^4} \tag{1.3}$$

Typical α_r values at 1.55 μm are on the range of 0.12-0.15 dB/km [8]. Low Rayleigh scattering losses can be obtained by taking special care about temperature and speed of pull during the drawing process of the fibre. In ref. [10] this was demonstrated by experimentally fabricating a fibre with total losses of just 0.16 dB/km at 1.55 μm. Alternatively, other glasses, such as K_2O-MgO-SiO_2 and Na_2O-B_2O_3-SiO_2, have been proposed as candidates for ultra-low loss optical fibres demonstrating losses due to Rayleigh scattering as low as 0.05 dB/km at 1.55 μm [11].

The loss due to material absorption in the range from 0.5 to 2 μm is mainly due to impurities in the fibre. The most significant contribution comes from OH ions, which has harmonics of its vibration resonance peak at approximately 1.4 μm. In state-of-the-art fibres, however the peak at 1.4 μm is usually reduced to less than 0.5 dB/km, and it virtually disappears in the so-called dry fibres [12], that are already commercially available. The intrinsic absorption loss of the silica glass is not very significant in the 0.5 to 2 μm range. It is indeed less than 0.1 dB/km in the wavelength range from 0.8 to 1.6 μm [1]. This value gets higher only for wavelengths lower than 0.4 μm where electronic resonances cause high ultra-violet

absorption [13], and for wavelengths beyond 2 μm where vibrational resonances become significant. To extend the operation of optical fibres beyond the silica transparency window limit in the region of 2 μm, alternative materials have to be used, such as fluoride [14], germanium dioxide [15], or chalcogenide glasses [16].

Another loss mechanism in optical fibres are the so-called waveguide losses, that arise from perturbations on the waveguide structure that appear during the fabrication process. Particularly significant can be the presence of imperfections on the core-cladding interface, which can cause light to leak into the cladding. Usually, during the fabrication process of an optical fibre a lot of care is taken in order to ensure that the core radius does not vary significantly along the fibre length, which allows such losses to be kept typically below 0.03 dB/km.

1.1.3 Dispersion

In optical fibres, dispersion is always related to the dependence of the phase velocity of light to other parameters. In multi-mode fibres it arises mainly from the fact that light guided at different modes present different velocities (intermodal dispersion), which is completely suppressed in single mode-fibres, in which dispersion appears chiefly due to the fact that light at different wavelengths travel at different speeds. Its immediate effect is to cause broadening of short-pulses, which can be very detrimental in telecommunication systems. In nonlinear and ultrafast optics, dispersion has to be taken into account because it plays a very important role in a number of different phenomena, such as soliton propagation [17], mode-locking [18] and parametric processes [19].

The dispersion in single-mode fibres, known as group velocity dispersion (GVD) arises from both material and waveguide contributions. Material dispersion comes from the fact that in a glass, the refractive index is wavelength dependent, and the waveguide dispersion is due to the fact that part of the light might be guided in the cladding, which has a different refractive index. The waveguide contribution to dispersion is also wavelength dependent because the mode field diameter of a propagating beam, therefore the amount of light which propagates in the cladding, is strongly dependent on wavelength.

Mathematically speaking, dispersion can be accounted from expanding the mode propagation constant β into a Taylor series around frequency ω_0, as shown in Eq.

1.4 [8].

$$\beta(\omega) = n(\omega)\frac{\omega}{c} = \beta_0 + \beta_1(\omega - \omega_0) + \frac{1}{2}\beta_2(\omega - \omega_0)^2 + ... \tag{1.4}$$

where

$$\beta_m = (\frac{d^m\beta}{d\omega^m})_{\omega=\omega_0} \tag{1.5}$$

The term β_1 is the group velocity, which is related to the propagation speed of the envelope of an optical pulse, whereas β_2 accounts for the first order derivative of β_1. In other words, β_2, known as the GVD parameter, is a measure of how much β_1 varies with frequency, being responsible for pulse broadening.

Finally, the dispersion parameter D can be defined as

$$D = \frac{d\beta_1}{d\lambda} = -\frac{2\pi c}{\lambda^2}\beta_2 = -\frac{\lambda}{c}\frac{d^2n}{d\lambda^2} \tag{1.6}$$

For fused silica, both β_2 and D have zeros around 1.27 μm. In an optical fibre, this point in which D is zero is know as the zero-dispersion wavelength and it is usually denoted by λ_0 or λ_D. In practical optical fibres the zero-dispersion wavelength is slightly shifted towards longer wavelengths due both to contributions that come from waveguide dispersion and from changes on the material dispersion induced by dopants in the core. The dispersion parameter as a function of wavelength for a single-mode silica fibre can be seen in Fig. 1.2, where λ_0 is around 1.31 μm. For wavelengths close to λ_0, or for ultra-short pulses (few femtosoconds) high-order dispersive effects become significant and have to be taken into account [24]. This is usually done by including in equation 1.4 and 1.5, the coefficient β_3, known as third order dispersion (TOD) parameter.

The zero-dispersion wavelength is a very important parameter because it defines whether the the light is going to propagate in the normal or the anomalous dispersion regime. For wavelengths higher than λ_0, or for positive values of D, higher frequencies travel faster than lower frequencies, which is known as anomalous dispersion. In this regime, dispersion and self-phase modulation (SPM) can act together to generate optical solitons [17]. And this phenomenon can be used in mode-locked lasers to shape the output pulses [21]. In the opposite case, for wavelengths lower than λ_0, or negative D, the lower frequencies travel faster than

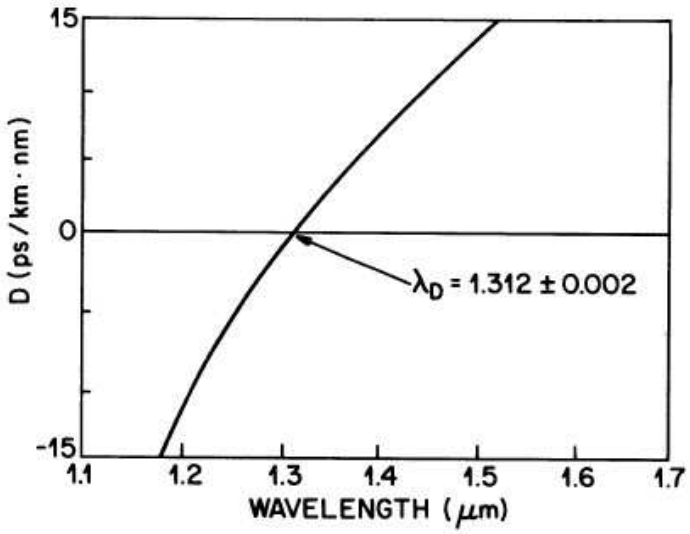

Figure 1.2: Measured dispersion parameter as a function of wavelength in a single-mode silica fibre. Taken from Ref. [20]

the higher frequencies, in what is called normal dispersion. In mode-locked lasers, the combination of normal dispersion and SPM can lead to the formation of high energy linearly chirped optical pulses [22, 23].

Dispersion shifted fibres (DSF) with up-shifted zero dispersion wavelength can be build by tailoring the waveguide dispersion. This is done by adjusting fibre design parameters such as the core radius a and the core-cladding index difference (Δ) defined by

$$\Delta = \frac{n_1 - n_2}{n_1}. \tag{1.7}$$

DSFs were developed to have the zero dispersion wavelength around 1.55 μm where the fibre attenuation is minimum, providing a low attenuation and low dispersion host for pulse propagation in telecommunication systems. However, with the later development of wavelength division multiplexing (WDM) telecommunication systems, DSFs became problematic due to the fact that four-wave-mixing (FWM) was being enhanced due to phase-matching by the operation near the zero dispersion wavelength and causing channels to interfere with each other distorting

the propagating signals. To avoid this problem, nonzero dispersion-shifted fibre (NZDSF) were produced presenting low but nonzero dispersion at 1.55 μm. Fibres with normal dispersion at 1.55 μm, known as dispersion compensating fibres (DCF), were developed to be used to compensate the dispersion induced by the propagation of optical pulses in standard fibres. The development of DCFs together with the development of optical amplifiers were responsible for allowing the propagation of pulses in telecommunication links for distances of hundreds of kilometres without the need for electronic regeneration [1].

Fibre with flat dispersion over a broad wavelength range can be made by using a multiple cladding layers [8]. Such fibres find direct application in WDM systems in which they can be used to avoid GVD mismatch between the different channels. Dispersion decreasing fibres can be designed by gradually changing the fibre core along the fibre length affecting its waveguide dispersion [25]. Dispersion decreasing fibres are generally used for adiabatic soliton compression [26, 27], where under certain conditions the pulse duration of a soliton decreases to balance for the decreasing dispersion. The dispersion profile of a DSF, a STF and a dispersion flattened fibre can be seen in Fig. 1.3.

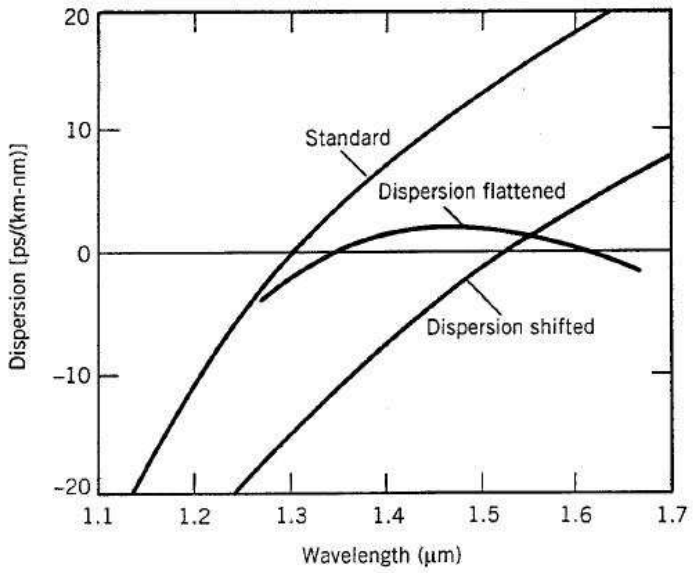

Figure 1.3: Typical dispersion profile for different kinds of fibres. Taken from Ref. [1]

1.1.4 Self- and cross-phase modulation

Any dielectric media under high intensity electro-magnetic fields starts presenting non-linear response to light. In such cases, the polarization **P** induced by electric dipoles is not linear with the electric field **E**, and can be written as [8, 28]

$$\mathbf{P} = \varepsilon_0(\chi^{(1)}.\mathbf{E} + \chi^{(2)} : \mathbf{EE} + \chi^{(3)}\vdots\mathbf{EEE} + ...). \tag{1.8}$$

where ε_0 is the vacuum permittivity and $\chi^{(j)}$ is the jth order susceptibility. The term $\chi^{(1)}$ is related to the refractive index and to attenuation, whereas the term $\chi^{(2)}$ is responsible for second harmonic generation and sum frequency generation. However, in silica glasses, or in any material that presents inversion symmetry at molecular levels, the term $\chi^{(2)}$ vanishes and the the non-linear effects related to it can not be observed under normal conditions. Therefore, in optical fibres, the lowest order non-linear effects arise from the third order susceptibility term $\chi^{(3)}$, which is responsible for phenomena such as third-harmonic generation, four-wave mixing, and non-linear refraction (also known as the Kerr effect).

Silica glasses are not known for being a strong non-linear material, and indeed its third order susceptibility is at least 100 times smaller than what is found in many crystals and liquids used for non-linear conversion [28, 29]. However, the long interaction lengths allowed by low-loss silica fibre combined with the small core diameters found in single mode fibres, usually lower then 10 μm, makes silica glass optical fibres an ideal host to observe non-linear effects even in the presence of only modest average powers [30].

Two of the most important non-linear effects present in optical fibres, self-phase modulation (SPM), [31] and cross-phase modulation (XPM) [32], arise from the fact that the refractive index in optical fibres is intensity dependent, and it can be written as

$$\tilde{n}(w, |E|^2) = n(w) + n_2|E|^2 \tag{1.9}$$

where n(w) stands for the linear part of the refractive index and n_2 is the non-linear index coefficient. $|E|^2$ is the optical intensity propagating inside the fibre.

Both SPM and XPM are related to intensity dependent phase shifts on the optical field that are self-induced in the case of SPM and caused by the presence of another

field propagating at a different wavelength, direction or polarization, in the case of XPM. The phase change of an optical field $\mathbf{E}_1$ during its propagation on the presence of another field $\mathbf{E}_2$ can be estimated by

$$\phi = nk_0L + n_2k_0L|E_1|^2 + 2n_2k_0L|E_2|^2 \tag{1.10}$$

where k_0=$2\pi/\lambda$ and L is the fibre length. The linear part contribution to the phase change is accounted by the first term on the right side of the equation. The following two terms account for SPM and XPM, respectively.

To better understand the effects cause by SPM and XPM on the propagation of short pulses in optical fibres, its important to look at the concept of chirp, which is a measure of the time dependence of the instantaneous frequency. An unchirped pulse, where the frequency distribution is uniform along the whole pulse in the time domain, undergoing SPM and XPM can acquire an up-chirp spectral broadening, lowering the frequencies on the leading edge of the pulse and raising the frequencies on the its trailing edge. This up-chirp together with normal dispersion leads to even faster temporal pulse broadening. A very important phenomenon happens when self-phase modulation acts in the presence of anomalous dispersion. The up-chirped caused by SPM under certain conditions can be perfectly balanced by the down-chirping caused by the positive dispersion, shaping the pulse as a soliton [17] that can propagate over long distances without any significant spectral and temporal broadening [33].

SPM also has an important role in the pulse shaping of mode-locked lasers. As said before, in the presence of intra-cavity anomalous dispersion the soliton mechanism can be responsible for the pulse shaping regardless of the saturable absorber response time, allowing the generation of short-pulses in the so-called soliton mode-locked lasers [21]. In the case of optical cavities with net-normal dispersion, self-phase modulation has an equally important role in the mode-locking pulse shaping, acting in a balance together with dispersion, gain and loss in the so-called dissipative soliton regime [34]. Such cavities can usually generate high energy linearly chirped optical pulses [22, 23].

As can be observed in Eq. 1.10, cross-phase modulation has twice the contribution to the phase shift of an electrical field than that of SPM, when considering two waves of same intensity propagating at different wavelengths. XPM is partic-

ularly important in Raman and parametric optical pulse amplification where the presence of the pump can phase modulate the signal causing spectral broadening [32]. In telecomunication WDM systems, XPM can lead to detrimental effects such as channel cross-talk.

1.1.5 Four-wave mixing

Another important nonlinear effect related to $\chi^{(3)}$ present in light propagation in optical fibres is four-wave mixing. FWM is a parametric phenomenon where the optical fibre plays an passive role mediating the interaction of several different optical wavelengths. In its basic form, FWM is the generation of two new frequencies ω_3 and ω_4 (Stokes and anti-Stokes frequencies) from the interaction of two pump waves ω_1 and ω_2, such as in Eq. 1.11 [8].

$$\omega_3 + \omega_4 = \omega_1 + \omega_2 \tag{1.11}$$

In quantum-mechanical terms, FWM can be understood as the annihilation of one or more photons and the generation of new photons at different frequencies conserving energy and momentum. Although, FWM is an optical process involving four different frequencies, it can still occur if two of the propagating frequencies coincide. In this case, called degenerate four-wave mixing, two photons are annihilated from the pump and one is generated at each Stokes and anti-Stokes frequency.

A crucial condition that has to be satisfied in order to make the FWM process efficient is phase-matching. Since FWM is a phase sensitive process, for its effect to accumulate over long distances all wavelengths involved have to travel at speeds close to each other in order to avoid phase-mismatch. In optical fibres this is usually achieved by having the optical frequencies close to each other, or by pumping close to the zero dispersion wavelength of the fibre.

If a previous wave is already propagating at the Stokes or at the anti-Stokes frequency, then FWM can be used to amplify it, allowing the creation of fibre optical parametric amplifiers (FOPA) and oscillators (FOPO) [19]. FOPAs can present wide spectral tunability, and can be used as an alternative gain medium for optical sources at non-conventional wavelengths [35]. Another possible way to build optical parametric amplifiers (OPA) and oscillators (OPO) is based on using sum and difference frequency generation provided by a crystal that exhibits χ^2

nonlinearity. In multi-channel telecommunication systems, FWM has to be avoided because it can also lead to signal deterioration due to signal cross-talk. This can be done in a number of ways, such as propagating the channels far away from the zero dispersion wavelength of the fibre or using unequally spaced channels [36].

1.1.6 Modulation instability and temporal solitons

Modulation instability (MI) is a non-linear phenomenon present in optical fibres that can lead to the breakup of CW or quasi-CW fields into a train of ultra-short pulses [8, 37]. MI can be physically understood by a four-wave mixing, phase-matched by the interplay of the optical Kerr effect and the chromatic dispersion, that can happen when light propagates in the anomalous dispersion regime in a region where the non-linear contribution to the phase matching condition is dominant [38]. In the temporal domain, small noise fluctuations of the CW field are amplified through the parametric process described above, also in this case called MI gain, and depending on the amount of amplification it can lead to the generation of optical solitons. This amplification scheme can be used in oscillators as a mode-locker in the generation of high-repetition rate ultra-short pulses [39].

The frequency separation under which the MI signal experiences maximum gain can be found from the expression [8]

$$\Omega_{max} = \sqrt{\frac{2\gamma P_0}{|\beta_2|}} \tag{1.12}$$

with a peak value $g_{max} = 2\gamma P_0$, where γ is the non-linear parameter of the fibre and P_0 is the signal power. The frequency separation of the MI gain sidebands is important because it determines the period of the generated pulse train, which is usually of the order of hundreds of GHz [40] or even THz [41]. The importance of modulation instability in optical fibres, however is not limited just to high repetition rate pulse formation. MI also plays a crucial role in the generation of Raman-soliton supercontinuum [42].

As mentioned before, modulation instability can lead to the generation of optical solitons. For a set of pulse shapes, the chirp induced by self-phase modulation can be perfectly counter-balanced by the chirp induced in the other direction by anomalous dispersion, creating optical pulses that propagate without any spectral

or temporal change. These are called fundamental solitons [17], and their natural shape is a sech^2. Its envelope field can be defined as

$$E(z,t) = \sqrt{P_0} sech(\frac{t}{\tau_0}) exp[iz\frac{\beta_2}{2{\tau_0}^2}] \tag{1.13}$$

where t stands for time, z is the distance along the propagation axis, P_0 is the soliton power and τ_0 the soliton duration. The soliton power and duration are related by the Eq. 1.14, also know as soliton condition:

$$N^2 = \frac{\gamma P_0 {\tau_0}^2}{|\beta_2|} \tag{1.14}$$

where N is an integer number that represents the soliton order. For $N = 1$, the pulse is a fundamental soliton and assuming that the parameters γ, β_2 and P_0 in Eq. 1.14 remain unchanged it propagates without any temporal distortion. Slow variations on the dispersion, nonlinearities, or power can be used to reduce the solution duration, which is a technique known as adiabatic pulse compression [26, 27]. For values of N higher than one, the pulse is called a high order soliton, and it propagates showing periodic temporal and spectral changes with a periodicity defined by the soliton period z_0, described by [8]

$$z_0 = \frac{\pi}{2}\frac{{\tau_0}^2}{|\beta_2|} \tag{1.15}$$

This periodic feature of high-order solitons can also be used for pulse compression, simply by removing the pulse from the fibre at the point in which it has the shortest duration. This soliton effect compressor technique has been already demonstrated many times [43, 44].

1.1.7 Photonic crystal fibres

Photonic crystal fibres (PCF), sometimes also referred to as holey fibres, belong to a different class of optical fibres. They are usually made of pure fused silica glass and have a solid or a hollow core surrounded by air holes [45, 46]. An example of a standard solid core PCF can be seen in Fig. 1.4, where the holes are arranged in a triangular latice. The two parameters that define the cladding structure are the diameter of the holes d and the distance between the centre of two consecutive holes or the pitch Λ. However, other lattices structures are possible and the holes

can also be filled with different liquids or gases in order to change the properties of the fibre.

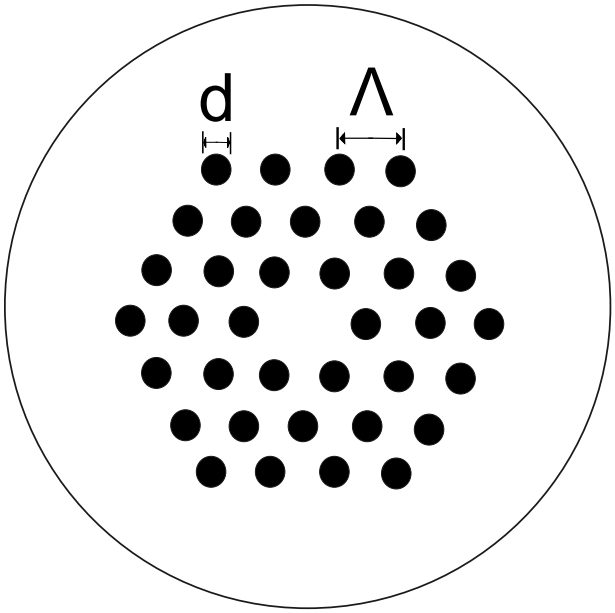

Figure 1.4: Typical structure of a solid-core PCF of hole diameter d and picth Λ.

The light guiding mechanism in PCFs is based on a photonic bandgap effect. The periodicity of the holes structure cause some frequencies to interfere destructively, not being allowed to propagate in the cladding, therefore being guided in the core. In the solid-core PCFs an analogy can me made with standard step-index fibres and the guiding mechanism can be understood as due to total internal reflection caused by a lower refractive index on the cladding region [47].

Photonic crystal fibres can present many interesting features that can not be found in conventional single-mode fibres, such as anomalous dispersion below 1.27 μm [48], single mode properties at all wavelengths [49] and high nonlinearities [50]. The most attractive feature of PCFs are the fact that fibre parameters such as, the dispersion profile, the effective area, and nonlinearities can be tailored by changing the hole geometry of the fibre [51]. The variety of different dispersion profiles found in different PCFs have found various applications in laser design, especially where dispersion plays an important role such as in supercontinuum generation [52, 53], modulation instability lasers [54] and FOPOs [55]. The main practical

drawback usually associated with PCFs is that they can present very high losses, which sometimes can be as high as hundreds of dB/km. The high levels of loss in PCFs are usually related to the absorption caused by the presence of residual OH- in the fibre and also to scattering [56]. At higher wavelengths confinement losses [57] can also be significant.

1.2 Short-pulsed laser sources

The term short-pulsed lasers, or ultra-short-pulsed lasers, usually refers to lasers that have pulse durations on the order of femtoseconds or picoseconds. However these terms do not have a strict definition and can sometimes be used to refer even to a few nanosecond laser source. Here in this thesis, short-pulsed lasers is used to refer to lasers with pulse durations lower than a nanosecond. In the literature, it can also be found the term ultrafast laser describing pulses of such time scales, and it is sometimes also used in thesis as a synonym for short-pulsed lasers.

A number of features of short-pulsed lasers sources make them attractive tools in a number of different applications [58]. The ultra-short duration of the pulses allow ultra-fast temporal resolution that can be used for example to measure the motion of molecules and electrons or chemical reaction dynamics [59]. Such applications made possible by the development of femtosecond lasers have lead Ahmed H. Zewail in 1999 to win the Nobel Prize in Chemistry "for his studies of the transition states of chemical reactions using femtosecond spectroscopy". Moreover, multi-GHz laser sources that can be obtained from mode-locked oscillators find interesting applications in high-capacity telecommunication systems [60].

More applications of short-pulsed lasers can be find due to the high peak powers, sometimes even of the order of Mega-Watts, that can readily be achieved by concentrating the energy in such short time windows. These applications range from high-harmonic generation to laser ablation and these sources are also attractive to be used to excite non-linear effects and for wavelength conversion. Other uses of short-pulsed lasers can be found in optical coherence tomography (OCT), optical frequency metrology and X-ray imaging and microscopy.

The developement of short-pulsed laser sources started just a few years after the demonstration of the first laser in 1960 [61] when in 1964 the technique of mode-locking was first proposed [62, 63], and immediately after there were a few

experimental demonstrations of mode-locked lasers [64, 65, 66]. However, some of them [65, 66] were in the so-called Q-switched mode-locking regime, where the train of short pulses are not regular and exist just inside a much longer Q-switched pulse envelope. Full mode-locking of a fibre laser was first demonstrated in 1986 [67] where pulses shorter then a nanosecond were generated in a Neodymium-doped fibre laser actively mode-locked by using intra-cavity acousto-optic loss modulation. The first demonstration of fully passive mode-locking in a fibre laser came 4 years later when in 1990 [68, 69] 2 ps pulses where produced utilising a nonlinear amplifying loop mirror (NALM).

1.2.1 Fibre lasers

There are two main categories in which solid-state lasers are usually divided, they can be either bulk or fibre-based lasers. Bulk lasers refer to solid-state lasers that use as the gain medium a bulk doped crystal or glass, whereas fibre lasers use optical glass fibres, which can be doped or not, to achieve optical gain. Since all the work described in this thesis is focused just on fibre lasers, if the reader is interested in further information about bulk lasers refer to Ref. [58] and references therein.

Fibre lasers have attracted a lot of attention especially in the last few decades due to a number of advantages they present in comparison to bulk laser systems. Amongst them we can highlight the fact that all-fibre systems can be made very compact, reliable, efficient, robust against environmental and mechanical instabilities, and often at much lower costs. Although many fibre-lasers have bulk elements inside their cavity, the current availability of optical devices in a fibre-pigtailed format, such as isolators, filters, gratings and couplers, have made all-fibre laser sources a well-established reality in both industry and academia.

Even one of the main drawbacks that fibre lasers posed in the past that was the low level of average powers that could be achieved in such configuration due to the usual reduced fibre cores, have been changing drastically during the last decade. The development of fibres with very large mode area [70, 71] have allowed fibre lasers to operate at high average powers [216], up to the order of kW for CW operation [73], making them an alternative source in high-power applications that were beforehand dominated by solid-state bulk lasers. The high levels of average power can also be found in short-pulsed systems [74], where femtosecond lasers with

hundreds of watts average power been already demonstrated [75].

Currently, fibre lasers can already cover a broad range of wavelengths, especially in the range from 1 to 2 μm, particularly due to the availability of fibre amplifiers doped with rare-earth ions such as erbium (Er^{+3}), ytterbium (Yb^{+3}), neodymium (Nd^{+3}) and thulium (Tm^{+3}). Moreover, the gaps between the emission band of such doped amplifiers can be fulfilled by alternative gain configurations such as Raman or parametric amplification, that can be also used to extend the coverage of fibre lasers to the visible region of the spectrum or even beyond 2 μm.

1.2.2 Mode-locking

Mode-locking [76] is the technique which is by far the most widely used to generate short pulses in fibre lasers. The basic concept behind its mechanism is that if the longitudinal modes that propagate in a cavity have a fixed phase relationship between them, or in other words if the phase difference between any two neighbouring modes is locked to a constant value, then a train of short pulses forms. This can be seen in Fig. 1.5 where the intensity is plotted against time for the case of 1, 3 and 5 modes locked in phase with same amplitude. It can be observed that even for the case of just 3 modes summed in phase a pulse-like output is already obtained. The more one increases the number of modes (or bandwidth), the shorter the pulses become. In the case of just one mode, also know as a single-frequency laser, the output is a CW beam and obviously no mode-locking is possible.

If there is no fixed phase relationship between the longitudinal modes in a cavity, or in other words, if the longitudinal modes have random phases in relate one to the other, then the output of the laser is CW. This can be seen in Fig. 1.6 where intensity is plotted against time for both cases where longitudinal modes are summed with and without a fixed phase relationship. The same situation is analysed for a cavity with 20 (Fig. 1.6 (a)) and 200 (Fig. 1.6 (b)) modes. As can be seen again, the higher the number of longitudinal modes the shorter the pulses become, allowing higher peak powers.

Mode-locking can be achieved in fibre lasers by passive or active techniques. In active mode-locking, either a phase or an amplitude modulation is applied to the loss in the cavity at a frequency that is a multiple of the cavity repetition rate. This is illustrated in Fig. 1.7, where the pulse formation happens in a region in time close

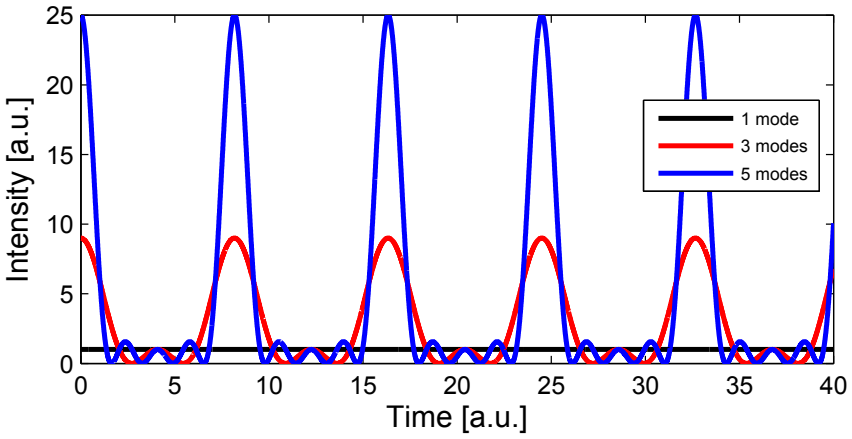

Figure 1.5: Output of a laser with one mode and with 3 and 5 modes looked in phase.

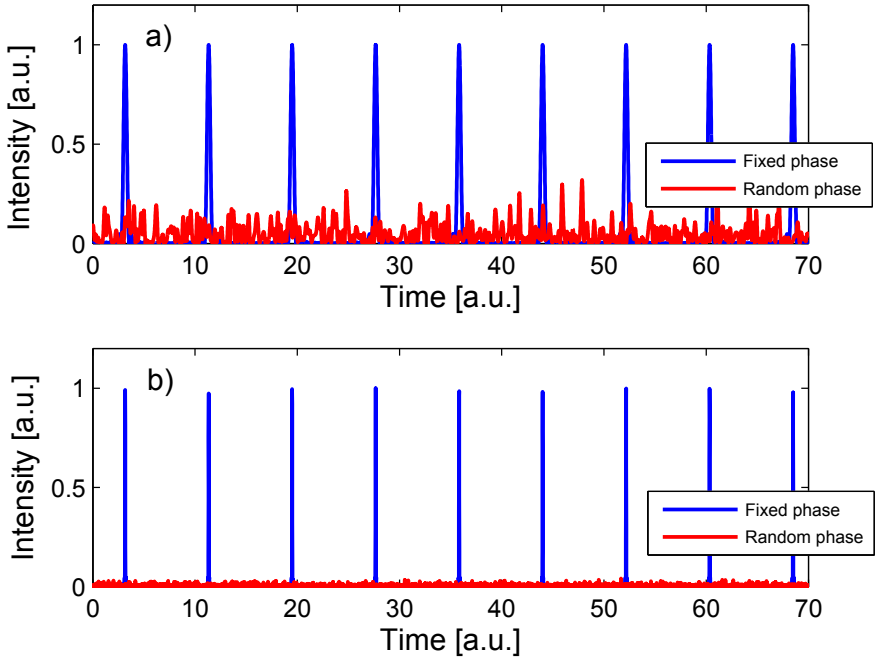

Figure 1.6: Normalized output of a laser with longitudinal modes with fixed (blue) and random (red) phase relationships. Fig. a) is the output of a laser with 20 longitudinal modes and Fig. b) a laser with 200 longitudinal modes.

to the loss minima, when the net gain becomes positive and the device lases. In practice this is usually done by using an acousto-optic or an electro-optic modulator inside the cavity. Although, active mode-locking can be a good practical solution to achieve mode-locking at high harmonics of a cavity repetition rate, usually it present many drawbacks if one compare it with other passive techniques. Specially on pulse duration, passive mode-locking easily allows the generation of femtosecond pulses (at least tens or hundreds of femtoseconds), whereas active mode-locking usually generates pulses longer than a picosecond. The necessity of an optical modulator, an electronic driver and a synchronization scheme also enhances the system's complexity.

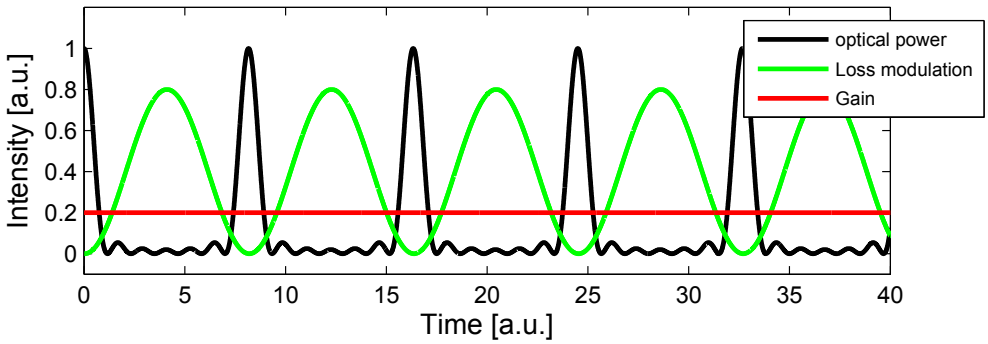

Figure 1.7: Normalized schematic of the active mode-locking mechanism through loss modulation.

The mechanism behind passive mode-locking is also a type of loss modulation. The main difference is that in this case the modulation is optically driven on a passive element (a saturable absorber), or driven by a non-linear mechanism that emulates saturable absorption, where high intensity light experience lower levels of loss than low intensity light, shaping the optical pulses over successive round-trips.

Some examples of passively mode-locking techniques that do not need a physical saturable absorber are based on non-linear phase shifts experienced by the beam at its high-intensity peaks, such as Kerr-lens mode locking [77] and non-linear polarization rotation [78], and also based on intensity-dependent frequency conversion as in the case of non-linear mirror mode locking [79]. All of them rely on the fact that the non-linearity which is induced by high-intensity light makes the peak of the pulses to experience either more gain or less loss during a round trip, making

the whole mechanism work as if a "virtual saturable absorber".

Although very short pulses can be obtained from these techniques [80], kerr-lens mode-locking and non-linear mirror mode locking are usually associated just with bulk lasers, and non-linear polarization rotation, or other techniques based on it such as mode-locking through a non-linear loop mirror (NOLM) [69], suffer from instabilities due to fluctuations in ambient temperature, and often exhibit poor self-starting performance. These drawbacks can be avoided by the usage of real saturable absorbers.

1.2.3 Saturable absorbers

A saturable absorber is basically a device which presents loss saturation under the presence of a certain amount of optical power. The main parameters used to characterise this type of device are the modulation depth, recovery time, saturation intensity and non-saturable losses. A schematic of its functioning mechanism can be seen in Fig. 1.8.

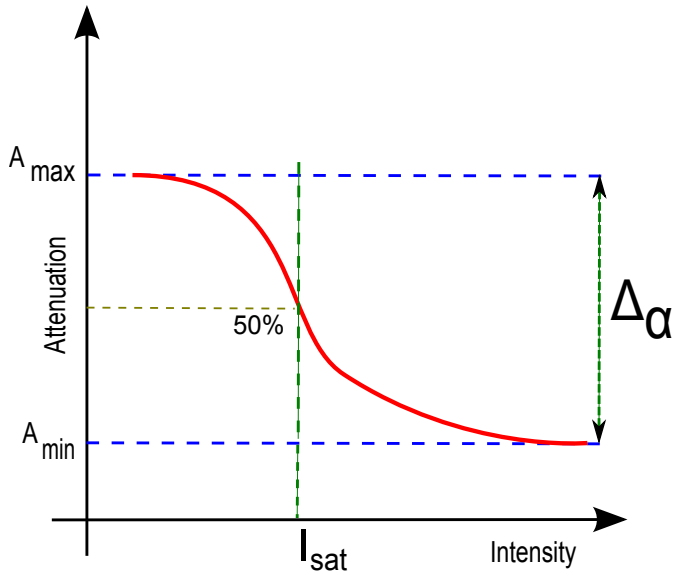

Figure 1.8: Attenuation against intensity plot of a typical saturable absorber, where I_{sat} is the saturation intensity, A_{min} and A_{max} are the minimum and maximum values of attenuation and $\Delta\alpha$ is the modulation depth.

Under low input intensities the attenuation of a saturable absorber is at its max-

imum (A_{max}), however the more the intensity increases the more the attenuation decreases, until it gets to a certain level (A_{min}) which is know as the non-saturable loss. The normalised difference between the maximum and the minimum attenuation is known as the modulation depth ($\Delta\alpha$), and for efficient mode-locking it usually has to be at least about 10%. The intensity that is necessary to decrease the attenuation of the saturable absorber by half of its modulation depth is known as the saturation intensity, which is considered to be the point at which that absorber starts to saturate. In typical saturable absorbers this value can range from a few MW/cm^2 to hundreds of MW/cm^2.

The recovery time of a absorber is the time needed for the attenuation to come back to its maximum value after being saturated. In typical saturable absorbers this recovery time can range from nanoseconds to a few femtoseconds, however the pulse shaping mechanism usually relies also on other dispersive, non-linear and filtering effects. In many cases the saturable absorber only triggers the locking mechanism and the pulse shaping itself is realised through soliton effects [21], which allows the generation of pulses with durations much shorter than the saturable absorber recovery time.

The most common and widely used saturable absorber in mode-locked lasers so far have been the semiconductor saturable absorber mirrors, or SESAMs [81]. The usage of SESAMs considerably improve self-starting and robustness against environmental perturbations, however they are usually fabricated to operate just at specific wavelength ranges that are generally not broader than tens of nanometers. In addition, the fabrication cost of SESAMs at nonstandard wavelengths can be considerably high. This might not be considered a drawback if one is building a standard Ytterbium-doped or Erbium-doped mode-locked laser, however if one is interested in more exotic gain mechanisms such as Raman gain, then the concept of a more wavelength versatile mode-locker becomes more interesting. This can be fulfilled by the usage of graphene or carbon nanotubes.

Carbon nanotubes and graphene are newly developed nanomaterials based on carbon that present interesting optical properties. Carbon nanotubes for example can present broadband saturable absorption in a single device by having a wide distribution of tubes with different diameters, that was experimentally demonstrated in [82] where a single nanotube film was used to mode-lock lasers at 1.05 μm, 1.56 μm and 1.99 μm. Graphene, also known as the universal saturable absorber due

to its zero-gap dispersion relation [83], can be used to mode-lock lasers virtually at all wavelengths. Moreover, both have low fabrication costs and can be easily incorporated in an all-fibre configuration laser. A more detailed description of the physics and the applications that are related to these materials can be found in the later chapters.

1.2.4 Dissipative solitons

Dissipative solitons are localized formations of an electromagnetic field that are maintained through an energy exchange balance between gain and loss under the presence of non-linearities, dispersion and spectral filtering [34, 84]. In fibre lasers, this type of solitons are know to be highly chirped long pulses, with pulse durations that usually range from a few picoseconds to a few tens of nanoseconds. It has been experimentally demonstrated that mode-locked lasers can support such pulsed solutions under the presence of net-normal dispersion [85], and since then a lot of attention has been dedicated to these topics [23, 86, 87].

The pulse shaping mechanism in such mode-locked systems can be understood as follows. Noise fluctuations are triggered by the saturable absorber, which over the successive round trips inserting more loss to the edges of the pulse-like structure gives rise to a proper pulse, as in any mode-locked laser. The difference here is how the pulses maintain themselves when propagating inside the cavity, since there is no interplay between the self-phase modulation and anomalous dispersion shaping the pulse as a soliton. In dissipative solitons the self-phase modulation generates new frequencies on the edge of the pulses, which act together with the normal dispersion that makes the frequencies at the front edge to travel faster than the frequencies at the trailing edge, making them temporally even more apart, broadening the pulse in duration and giving it a chirp. However, the spectral filtering present in the cavity, when it cuts the edges of the spectrum, is in reality also cutting the temporal edges of the pulse because that is the part of the pulse in which the lower and the higher frequencies remain. A similar situation happens in the saturable absorber. When the edges of the pulse receive more loss, this also means that the edges of the spectrum are "seeing" more loss, cutting the pulse spectrally.

For a number of reasons this operation regime has been studied and used as an alternative pulsed source to the traditional solitons found in anomalous dispersion

systems. One of the main factors that contribute to the recent interest in dissipative solitons is the long pulse durations that allows this regime [88, 89] allow significant scaling of the pulse energies achievable [90] overcoming the limits on pulse energy imposed by the soliton regime. Moreover, their chirped nature makes them compressible simply by propagating them through anomalous dispersion media, allowing high peak powers to be achieved. Pulses with μJ energies [91] and mega-watt peak powers [92, 93] have already been experimentally demonstrated in dissipative soliton lasers.

Another interesting trait of dissipative soliton lasers is that they allow the generation of short-pulses at wavelengths lower then 1.3 μm in more compact schemes, without the need of dispersion management techniques to achieve soliton mode-locking obtained by placing gratings or PCFs inside the cavity, reducing the system's complexity. Ytterbium-doped mode-locked lasers in particularly can take advantage of this, and indeed many experimental demonstrations of such dissipative soliton lasers have been demonstrated in such configurations [23, 88, 93]. Equally, chirped pulse amplification (CPA) schemes can be simplified by using pre-chirped pulses available direct from the output of dissipative soliton lasers, eliminating the need for a separate pulse-stretcher stage [94].

Mathematically, dissipative solitons can be described by the complex cubic-quintic GinzburgLandau equation (CGLE), which is an extension of the nonlinear Schrödinger equation to higher-order and dissipative terms [34, 84]. Although typical dissipative solitons have a square-shaped spectrum [88] and temporally are represented by linearly chirped long pulses, there is a huge variety of possible pulse shapes and spectral profiles that can become a stable pulsed solution from the CGLE [86]. Moreover, dissipative solitons are know to be more resistant and robust to perturbations and break-down as their energy is scaled than traditional solitons. These traits are particularly interesting for the mode-locking of Raman lasers, in which their typically very long lengths and high levels of noise makes it difficult to achieve a steady state without power fluctuations to suit solitonic mode-locking in anomalous dispersion fibres.

1.2.5 Other short-pulsed laser sources

Although mode-locking is by far the most used technique applied to achieve short-pulses in fibre lasers, it is definitely not the only one. Long nanosecond or microsecond pulses with high energy can be produced by Q-switched lasers [95], where the repetition rate is usually higher than the inverse of the cavity round-trip time. The mechanism behind the pulse formation in Q-switched lasers is energy accumulation during a period in which the cavity loss is kept to a high value, and sudden release of the accumulated energy through temporally reducing the overall cavity loss. Similar to mode-locking, this can be achieved actively through a loss modulator or passively by using a saturable absorber. Although high energetic pulses can be easily achieved by Q-switched lasers, their long durations usually do not allow high peak powers to be obtained.

As already mentioned in section 1.1.6, modulation instability can also be used to generate ultra-short pulses in all-fibre configurations [39]. Although the pulse formation in MI lasers can be understood as a dissipative four-wave-mixing mode-locking, their typical pulse parameters such as repetition-rate and peak powers usually differ substantially from standard mode-locked lasers by orders of magnitude. In modulation instability lasers, hundreds of GHz or even THz repetition rates are routinely obtained [40, 41]. Nevertheless, this has an immediate impact in lowering the peak powers achievable from such oscillators, that are much lower than what is usually produced in standard mode-locked lasers.

MI lasers can be obtained in very simple schemes simply by adding an anomalous dispersive nonlinear fibre with the zero dispersion not too far away from the wavelength that is oscillating in the cavity, and properly adjusting the polarization state of the propagating light. This can be readily done at 1.55 μm [40] where standard fibres are usually anomalous, however at wavelengths lower then 1.3 μm a PCF properly designed with anomalous dispersion for that spectrum region has to be used [54]. Additionally, the necessity of constant adjustment of the polarization state of light inside the cavity can cause temporal instabilities, making this approach to generate short pulses not very practical.

An interesting technique to generate wavelength versatile short-pulsed fibre lasers is to use optical parametric amplification as the gain media. As discussed in section 1.1.5, four-wave-mixing can be used to create a widely tunable fibre optical para-

metric oscillator (FOPO) [35]. This can be done either by synchronously pumping an optical cavity [55] or by direct actively mode-locking an FOPO [96]. The main issue regarding the synchronously pumping scheme is that a previous high-power short-pulsed laser source is necessary as a pump, enhancing the system's complexity. Additionally, to mode-lock a FOPO can be difficult due to the intra-cavity power levels that are necessary for the parametric conversion. So far, only active modulation schemes have been experimentally demonstrated [96], and no passive mode-locking was ever reported in such lasers.

In comparison with Raman lasers, FOPOs offer a much wider wavelength tunability in a single device. By tuning the pump wavelength around the zero dispersion wavelength of a fibre with properly designed dispersion curve, the Stokes and anti-Stokes signal can be widely tuned to satisfy the phase-matching conditions. In ref. [97] for example, a 20 nm tuning of the pump, allowed more than 200 nm tunability on the new generated waves. However, the extra care with the dispersion profile of the gain fibre needed to achieve phase matching [98] is what makes FOPO's much more complex systems than Raman lasers. One of the features of Raman lasers that makes them attractive is their simplicity. The only requirement for building an efficient oscillator based on Raman gain is having a pump with enough power and a fibre with sufficient non-linearity.

1.3 Raman fibre lasers

In non-linear effects such as SPM, XPM and FWM there is no energy exchange between the electromagnetic field and the dielectric medium where it is propagating. Nonetheless, there is a class of non-linear phenomena known as inelastic effects in which the dielectric medium plays an active role such as in stimulated Raman scattering (SRS) [99] and in stimulated Brillouin scattering (SBS) [100]. Both phenomena can be understood on a quantum-mechanical level as the annihilation of a photon from a pump field and the generation of a Stokes photon at a lower frequency (or higher wavelength) and a phonon. The main difference between them is that SRS is associated with optical phonons, whereas acoustic phonons participate in SBS.

Although in the quantum-mechanical picture the difference between them seems to be subtle, it leads to very dissimilar behaviour. For example, in silica fibres the

frequency shift between pump and Stokes beams associated with SRS is usually around 13.2 THz, whereas in SBS this value is much lower, lying between 10 GHz to 20 GHz. This difference in frequency shifts between both effects is due to the fact that SBS originates from light interaction with propagating acoustic waves, whereas SRS originates from light interaction with resonant modes of a molecular system, having the frequency shift determined by these discrete molecular resonances.

The long frequency shift allowed by SRS allied with the high non-linearities and long interaction lengths that can be found in optical fibres, makes Raman scattering a very efficient and simple tool for wavelength conversion, being already widely used in optical broadband amplification systems and tunable lasers [99]. Since all the experimental work presented in this thesis is about Raman lasers, the present section is dedicated only to SRS, deepening the understand about the physics involved in the Raman gain process and its usage in CW and pulsed fibre lasers. Further information about Brillouin scattering and Brillouin lasers can be found in ref. [100] and in references therein.

1.3.1 Stimulated Raman scattering

The Raman effect was discovered in 1928 by the Indian physicist C. V. Raman when he observed that a new type of down-shifted scattering was present when light was focused into sufficiently dense liquids and vapours [101, 102]. This led him to win two years latter the Nobel prize "for his work on the scattering of light and for the discovery of the effect named after him". The physics behind Raman scattering can be understood as an inelastic effect in which part of the incident beam energy is absorbed and maintained in the medium in the form of molecular vibrations, causing the light to be scattered back with less energy (or in a lower frequency) than previously. This is schematically shown in Fig. 1.9, where different molecular vibrational states and light scattering process related to these states are drawn.

When light that is propagating in a dielectric medium is absorbed, it can excite the molecules that are in a stable ground vibrational state E_0 to a higher unstable (sometimes called virtual) vibrational state E_v, where the difference E_v - E_0 equals the energy of the incident photon E_p. In a normal situation, since this new state is unstable, after a few femtoseconds the medium re-emits a photon with same

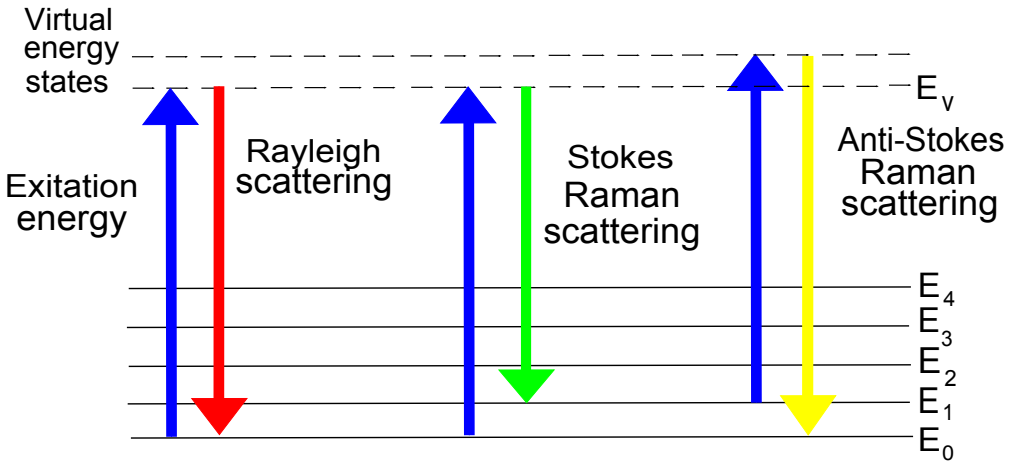

Figure 1.9: Schematic of Raman Scattering.

energy E_p and the molecule comes back to its original energy state E_0, in an elastic scattering process know as Rayleigh scattering. However, it can happen that after re-emitting back the absorbed photon the molecule instead of coming back to the ground state E_0 it stays in a higher but still stable vibrational state level E_1. In this case the re-emitted photon is going to have an energy E_s that equals to E_v - E_1, therefore being less energetic than the original absorbed photon E_p. From the Planck relation $E = h.\omega$ that defines the relation between the photon energy (E) and the frequency (ω) of its associated electromagnetic wave, where h is the Plank's constant, it can be seen that the new generated photon for this later case is going to be scattered in a lower frequency, or in a higher wavelength. This mechanism is called Stokes Raman scattering, or simply Raman scattering.

Although much less likely, a different situation, called anti-stokes Raman scattering can also occur. If a molecule that is already at the energy level E_1 absorbs a photon and re-emits it coming back to the ground level E_0, then the re-emitted photon is going to have more energy then the original photon that was absorbed. In this case the energy of the new photon equals $E_v + E_1$, therefore shifting the original frequency by the same amount as the Stokes case, however now to a higher frequency, or to lower wavelength.

Additionally, the existence of a previous signal at the Stokes frequency ω_s together with a beam at the pump frequency ω_p can stimulate the Raman scattering

process providing optical amplification to ω_s, which can be better understood in a wave picture. When the pump wave, and therefore also the scattered wave, have sufficient intensity they can both interact causing a non-linear enhancement of the medium excitation, which on its turn enhances the scattering. This positive feedback which is achieved above a critical incident intensity causes the scattered light to be exponentially amplified, characterizing the stimulated scattering regime.

Although for a given material, the shift in frequency is always the same, by changing the pump wavelength one can properly set the Stokes wavelength, allowing the generation of tunable optical amplifiers. This capacity of Raman amplifiers of extending the wavelength range in which one can obtain gain in optical fibres is very attractive to fibre lasers, in which the extensive use of rare-earth-doped fibre amplifiers restrain the usage of such lasers just to specific wavelength bands.

1.3.2 Raman gain in optical fibres

Despite an early report in 1970 of a Raman oscillator built using a liquid-core optical fibre waveguide structure [103], the first report of a Raman laser using a fibre waveguide made fully of glass came just two years later [104]. Since then the field increased immensely and Raman fibre lasers became an established reality used directly to efficiently achieve high-power at a number of wavelengths [105, 106, 107, 108] or used as a pump for other sources of wavelength conversion [109].

The Raman gain profile of optical fibres made of silica glass can be seen in Fig. 1.10. Its peak occurs at a frequency shift of around 13.2 THz (440 cm^{-1}) and its spectrum extends over about 40 THz, which allows the generation of broadband amplifiers [110] and widely tunable lasers [111]. For a pump at 1 μm co-polarized with the signal the peak of the Raman gain (g_r) is approximately 10^{-13} m/W. For un-polarized beams g_r is divided by a factor of 2, and for orthogonally polarized beams the Raman gain nearly vanishes. Its value also scales inversely with the pump wavelength.

Although the Raman gain in silica glass is not as high as the gain found in others optical amplifiers, doping the fibre with different materials or using different types of glass can dramatically change the intensity and the profile of the Raman gain, allowing the generation of strong amplification in just a few tens of meters of fibre. This possibility is further explained and explored in chapter 4 where a heavily doped

germanium fibre is used to build a Raman laser.

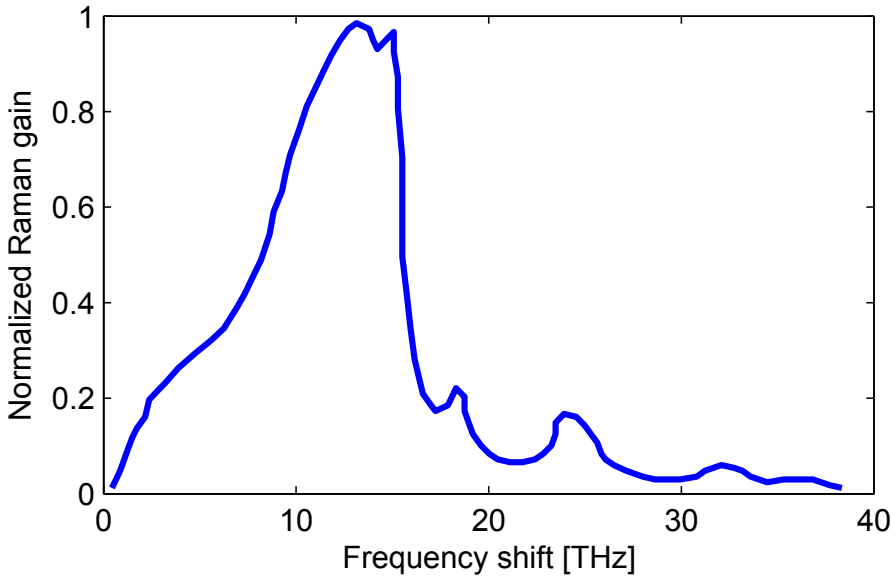

Figure 1.10: Normalized Raman gain profile in silica fibres for a pump at 1 μm.

The most interesting aspect about using Raman amplification in optical fibres is its capability of providing gain over the whole silica transparency window (300 nm - 2 μm), allowing the generation of coherent light in the gaps left in between the emission band of rare-earth doped elements. Although a strong pump laser is required for Raman amplification, usually at a Watt level for CW radiation, this is not necessarily a wavelength limitation, as the Raman process can be efficiently cascaded many times [112, 108].

To exemplify the wavelength versatility constraint found in typical fibre lasers, Fig. 1.11 shows the emission bands of ytterbium (Yb^{+3}), bismuth (Bi^{+3}), praseodymium (Pr^{+3}), erbium (Er^{+3}) and thulium (Tm^{+3}) doped-fibre amplifiers, which are some of the most used doped-elements in fibre lasers. Ytterbium- and erbium-doped fibres are already part of a mature technology that has been widely used over many years in fibre lasers [113]. More recently, a lot of interest has been placed in thulium-doped fibre lasers [114] providing gain for wavelengths around 2 μm. Other elements such as bismuth, praseodymium and neodymium can also be used in doped fibre lasers to fill the wavelength gap between the ytterbium and the erbium band, how-

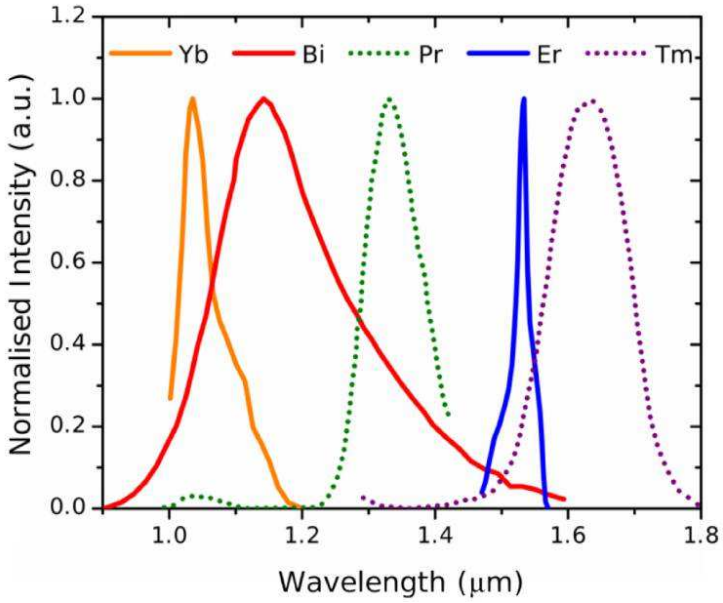

Figure 1.11: Typical emission bands of Yb^{+3}, Bi^{+3} and Er^{+3} doped-fibre amplifiers in silica hosts, and Pr^{+3} and Tm^{+3} doped-fibre amplifiers in fluoride hosts.

ever given the current technology their performance is far away from that of Erbium or Ytterbium fibre lasers and their use is not very practical in many applications. For that reason, it becomes evident that the development of fibre lasers based on Raman gain is interesting in order to fill these wavelength gaps and also to further extend optical amplification to the visible region of the spectrum. Moreover, mainly due to its distributed amplification nature, Raman amplifiers have become widely used in telecommunication systems over the last decades [99]. The possibility of combining pump lasers at different wavelengths allows the generation of broadband Raman amplifiers with flat gain [110, 115]. Adiabatic compression schemes can also take advantage of the distributed nature of Raman gain [116].

1.3.3 Mode-locked Raman fibre lasers

The wavelength versatility allowed by the use of Raman gain as an optical amplification source can be applied also to short-pulsed laser generation, where different applications often demand different operational wavelengths. There have been already a number of reports utilizing Raman gain in ultrafast sources [117, 118,

119, 120, 121]. However, to date, this field is still under development and none of these systems has reached a level of performance comparable with state-of-the-art rare-earth-based lasers. In Ref. [117], dissipative four-wave mixing was used for mode-locking, generating a pulsed laser with a very high repetition rate. While this is useful for some applications, the high repetition rate limits the delivered peak power. Nonlinear loop mirrors [118, 119] and nonlinear polarization evolution [121] have also been used to provide saturable absorption, but such systems suffer from instabilities due to fluctuations in ambient temperature, and often exhibit poor self-starting performance.

More recently, a Raman mode-locked laser using a semiconductor saturable absorber mirror (SESAM) was reported [120]. While the use of a SESAM improves self-starting and robustness against environmental perturbations, there is limited spectral operation from a single device. In addition, as already said before the fabrication cost of SESAMs at non-standard wavelengths is high. Availability of a broadband saturable absorber (SA) to achieve mode-locking at any desired wavelength across the transmission window of silica is an essential prerequisite to fully exploit the flexibility of Raman amplification in ultrafast sources across the visible and near-IR. Recent interest in the application of nano materials, in particular carbon nanotubes (CNTs) [122] and graphene [123, 124], as SAs in mode-locked lasers have moved the field a step closer to a fully universal device. The work shown in this thesis focuses mainly in this particular possibility of combining Raman gain and carbon-based saturable aborbers in an oscillator, contributing to move the field of short-pulsed lasers to a more universal laser source.

2 Raman laser mode-locked by carbon nanotubes

The rapid development of carbon nanotubes technology that has happened in the last decades, together with some of its unique optical, mechanical and electronic properties, have allowed its usage in a large number of applications in the most diverse areas such as medicine, electronics, chemistry, optics and as structural materials. One of its main applications in the laser sciences is its use as a saturable absorber. This is due to some interesting optical properties carbon nanotubes present, such as fast response time, broadband operation, low fabrication cost and easy incorporation in fibre devices.

The mode-locking of lasers using carbon nanotubes, and more recently also using graphene, have been extensively studied for the last decade in many different laser configurations generating short pulses at a number of different wavelengths and it is now becoming an alternative to SESAMs that are routinely used in commercial mode-locked lasers. Its broadband operation as a saturable absorber makes carbon nanotubes-based devices an ideal mode-locker to exploit the wavelength flexibility of Raman lasers, serving as a technique for the development of simple and compact ultrashort sources across the complete transparency window of silica fibres.

In this chapter first there is a brief introduction about carbon nanotubes highlighting some of its main optical properties that make them interesting devices in photonics sciences, then the experimental work done showing the use of carbon nanotubes as a saturable absorber to mode-lock Raman lasers is presented. In order to show the wavelength versatility allowed by the combination of CNT-based devices and Raman gain, two systems are built, one generating short pulses at 1120 nm and the other at 1660 nm. Conclusions are drawn in the end.

2.1 Introduction

Carbon is an element that can exist in nature under many different crystalline forms, such as diamonds, graphite, buckyballs, carbon nanotubes and graphene. Whereas graphite and diamond have been well known for more than a century, the discovery of carbon nanotubes is usually referenced to a work published by Ijima only in 1991 [125], and more recently was the discovery of graphene that, despite many early theoretical studies, was experimentally demonstrated only in 2005 by Novoselov et al. when a stable 2-D atom-thick layer of carbon was produced by mechanical exfoliation of graphite [126].

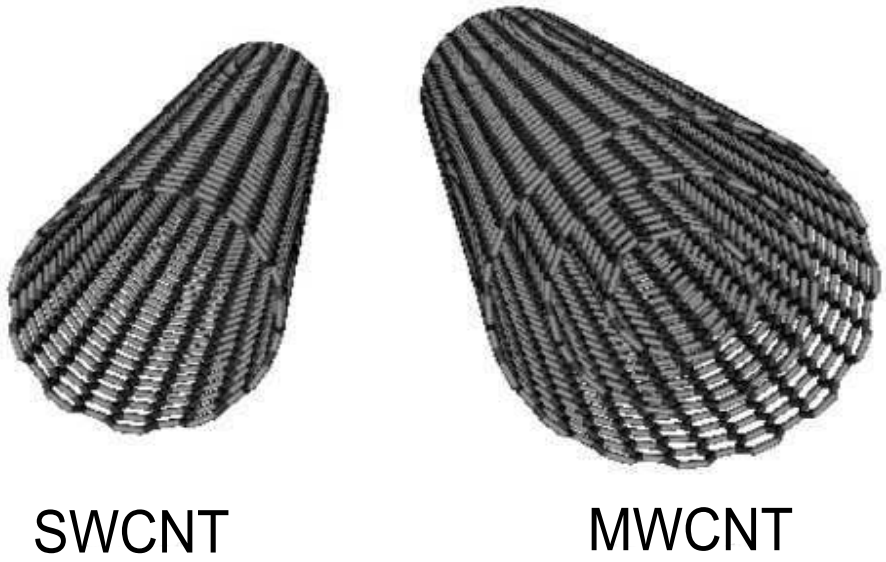

Figure 2.1: Single- and multi-wall carbon nanotubes. Adapted from [127]

Carbon nanotubes are essentially graphene wrapped in a 1-dimensional cylindrical tube format with diameter ranging from 0.5 nm to 100 nm and length ranging from micrometers to centimetres that can be either single-wall (SWCNT) or multi-wall (MWCNT) presenting a number of outer concentric shells as can be observed in Fig. 2.1. Its properties are defined mainly by the tube diameter and by the way the carbon layer is wrapped, what is called chirality, and depending on both factors they can be either metallic or semiconductors.

In general, CNT-based devices can be produced as follows: First an arc discharge, or a laser ablation procedure, is applied to a piece of graphite in order to generate carbon nanotubes and other allotropes of carbon. The result is then sonicated and centrifuged in a liquid in order to purify the samples and separate the nanotubes from other impurities. Finally, a host polymer is dispersed in the sample, which is then placed in a desiccator to evaporate the solvent leaving the CNTs embedded in polymer host matrix. Further detailed information about the fabrication procedures to produce CNT-samples can be found in Ref. [122].

The applications in science involving the use of carbon nanotubes are many and their number and variety keep increasing every year [128]. This is due to many of their unique properties that they can present such as very high electrical and thermal conductivity, tunable bandgap energy, optical absorption and photoluminescence, besides being amongst the hardest and stiffest materials in nature. Just to mention a few possible uses of carbon nanotubes, nanometer-sized electronic devices [129], optical gain devices [130], gas sensors [131] and saturable absorbers [122] built based on CNT have already been reported. In this section we focus on a brief description of carbon nanotubes structure, fabrication process, some of its properties and explain its use as a saturable absorber. The basic CNT constituent material, graphene, is studied in details in chapter 3.

2.1.1 CNT-structure and optical properties

To understand the structure of carbon nanotubes one has first to study the graphene lattice and how it can be wrapped-up in a cylindrical form. This schematic is shown in Fig. 2.2, illustrating each carbon atom connected by a covalent bond to other three carbons forming a hexagonal lattice. The primitive lattice vectors a_1 and a_2 are defined on a plane with unit vectors $\hat{x}$ and $\hat{y}$ by

$$a_1 = [\frac{\sqrt{3}a}{2}, \frac{a}{2}], a_2 = [\frac{\sqrt{3}a}{2}, -\frac{a}{2}] \tag{2.1}$$

where a is the lattice constant which is related to the carbon-carbon bond length a_{c-c} ($\sim$1.42 Å) by $a = \sqrt{3}a_{c-c}$. These parameters are important to calculate the nanotube chirality, which defines whether a CNT is metallic or semiconductor, and in the latter case also defines its band structure. The chiral vector C_h is defined as the vector connecting any two primitive lattice points of graphene such that when

folded into a nanotube these two points are coincidental, and is expressed in terms of a_1 and a_2 by

$$C_h = na_1 + ma_2 = (n, m) \tag{2.2}$$

where n and m are positive integers satisfying the condition $0 \leq \mathrm{m} \leq \mathrm{n}$. In the case shown in Fig. 2.2 folding the nanotube by conecting point A to point B would give $C_h = \overline{AB} = 3a_1 + 3a_2$, or in other words, that would be a (3,3) nanotube.

The diameter d_t of a carbon nanotube can then be calculated from is chirality by the expression

$$d_t = |C_h| = \sqrt{C_h.C_h} = \frac{a\sqrt{n^2 + nm + m^2}}{\pi} \tag{2.3}$$

where it can be observed that different chiralities can result in carbon nanotubes with same diameter, resulting that nanotubes with same diameter can present different properties.

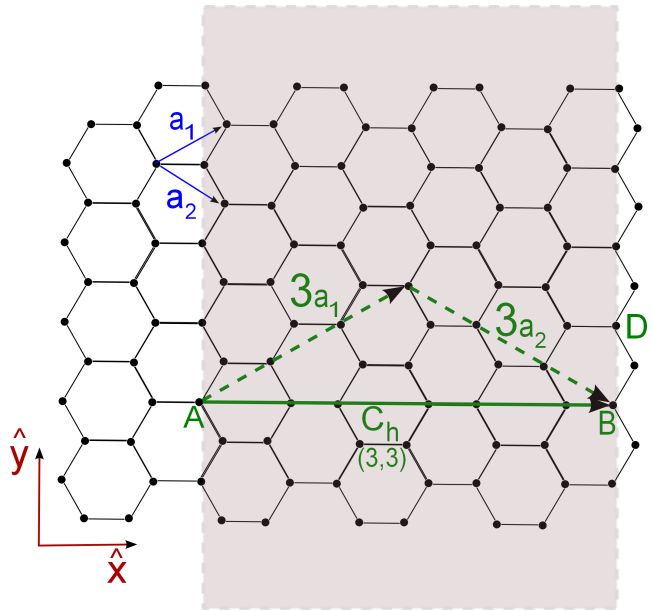

Figure 2.2: Conceptual construction of a CNT from a graphene lattice, rolling up point A to point B forming a nanotube with chiral vector (3,3).

As mention previously, the chirality is a unique signature of a nanotube that

defines many of its electrical and optical properties, and apart from the tube length, it is enough to completely describe its structure [132]. This is particularly important regarding its use as a mode-locker since the wavelength at which the nanotubes present saturable absorbance is defined by its bandgap energy which is defined by its chirality. Fig. 2.3 shows the 3 possible types of chirality in which carbon nanotubes can exist. If n = m then the nanotube is called armchair, when m = 0 then it is a zigzag type, otherwise it is simply a chiral nanotube. Armchair nanotubes are always metallic, while zigzag and chiral nanotubes can be either semiconductor or metallic. More precisely, for any integer q, if | n-m | = 3q, then the nanotube is metallic, for all others where | n-m | = 3q ± 1 we have a semiconductor.

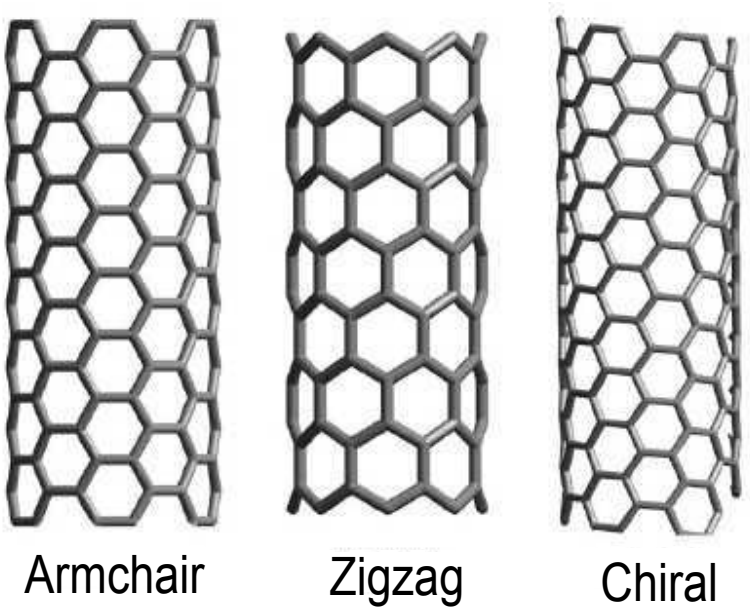

Figure 2.3: Different kinds of carbon nanotubes according to its chiralities. Adapted from [133]

The energy levels in a density of electronic states in a typical semiconductor carbon nanotube can be seen in Fig. 2.4. The only real bandgap is the E_{11} transition formed between the v_1 valence band and the conductance band c_1. The saturable absorbance in carbon nanotubes mainly appears when c_1 gets occupied with electrons that were excited from v_1 preventing further absorption. Another important trait about energy levels in carbon nanotubes, is the existence of interbands tran-

sitions, sometimes called pseudo-gaps, that appears due to the so-called Van Hove singularities, a typical signature of 1-dimensional materials. They are responsible for example for the E_{22} absorption transition that can cause electrons to excite from the valence band v_2 to the conductance band c_2 although the excitonic recombination always happens through the E_{11} gap. The E_{22} transition can also be used in mode-locking [134] by filling the conduction band through absorption from v_2. Since this transition is related to absorption of photons with higher energies, therefore higher frequencies acording to Planck relation $E = h.\omega$, this allows saturable absorption to happen for a given nanotube at shorter wavelengths in comparison with the traditional case when the excitation comes from absorption through the E_{11} transition, although in this case parameters such as the modulation depth and recovery time can vary significantly [134]. Since these transitions are dependent on the nanotube chirality and diameter they can be used for characterisation of the nanotubes through photoluminescence spectroscopy [132]. Moreover, the fact that in 1-dimensional materials the mechanical, elastic and thermal properties are strongly related to phonons makes Raman spectroscopy another useful technique for carbon nanotube characterisation [135].

2.1.2 Carbon nanotubes in mode-locked lasers

Although the discovery of carbon nanotubes happened in 1991 [125], the first demonstration of its use as an saturable absorber in a mode-locked laser came just in 2003 [136, 137], and since them, a vast number of fibre laser in different dispersion regimes and at different wavelengths were demonstrated to mode-lock by using single- or multi-wall carbon nanotubes [82, 94, 138, 139, 140, 141]. The interest of using CNT as a mode-locker for fibre lasers came not just due to its optical properties such as sub-picosecond transition time and high modulation-depths, but also due to the fact that thin films of carbon nanotubes can easily be made by dispersing them into a solvent and then embedding them into a polymer composite, creating in this manner a robust and environmentally stable device that can be easily handled and incorporated into fibre systems.

Another important feature of carbon nanotubes that make them very interesting devices for mode-locking and that differentiate them from SESAMs for example is the fact that is possible to achieve very broadband saturable absorption in a single

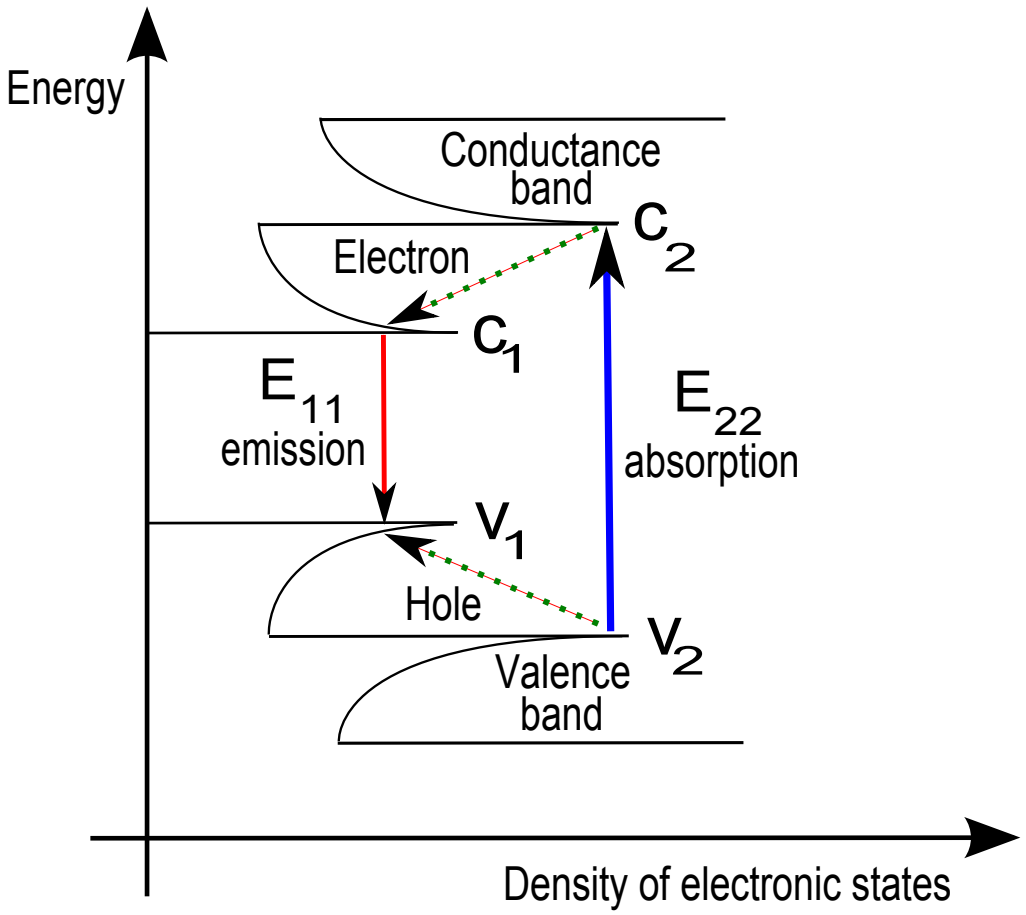

Figure 2.4: Typical density of electronic states diagram for a semiconductor carbon nanotubes.

CNT-device. Although this might sound counter-intuitive due to the fact that a given nanotubes with specific diameter and chirality presents specific optical bands and absorbs light just at these particular transitions, in real CNT samples usually there is a range of nanotubes with different diameters, permitting saturable absorbance over a broad range of wavelengths. An experimental demonstration of this fact can be seen for example in Ref. [82] where Kivistö et al. showed mode-locking from 1.06 μm to 1.9 μm using a single carbon nanotube sample. The drawback of this approach is the fact that the nanotubes that do not participate in the saturable absorption processes for a specific wavelength necessarily add non-saturable loss to the CNT-sample. A more purified sample in terms of tube diameter range distribution would present less non-saturable loss. However, that would drastically reduce the broadband operation capability of the CNT-based device.

In Raman lasers, the first demonstration of mode-locking using carbon nanotubes came in 2011 [94] and it is precisely the work described in this chapter. Later on, a few other papers describing similar systems at different wavelengths or using different fibres were published [142, 143, 144], confirming the versatility allowed by the combination of Raman gain and carbon nanotubes in mode-locking. Other results shown in these publications are also the subject of this or of later chapters in this thesis.

2.2 Erbium-pumped Raman laser mode-locked by DWCNT

Here we describe a passively mode-locked laser combining both Raman gain and a CNT-based saturable absorber in a normally dispersive cavity, showing the potential of this flexible approach. The oscillator generates highly chirped 500 ps pulses, that are then externally compressed to 2 ps, with 1.4 kW peak power, making it a simple wavelength-versatile source for various applications.

2.2.1 Experimental setup

The experimental setup used in this system is shown if Fig. 2.5. The all-fibre geometry consists of 100 m single-mode highly nonlinear fiber bought from Optical Fiber Solutions (OFS), commercially available as “OFS Raman Fiber”, with an enhanced germanium oxide (GeO_2) concentration for an increased Raman gain coefficient, counter-pumped through a wavelength division multiplexer (WDM),

that acts simply as an optical coupler, by a CW high power Er-doped fibre amplified spontaneous emission (ASE) source at 1555 nm that can provide up to 15 W of CW power. The expanded availability of high-power erbium-doped fibre lasers capable of delivering several Watts of optical power, makes them a very useful pump source for readily generate Raman gain from the 1.6 to 2 μm region of the electromagnetic spectrum.

Two WDM couplers were used after the gain fibre to extract the residual pump left that could otherwise damage other cavity elements. This is necessary because 100 m of fibre is not enough to efficiently deplete the pump and depending on the amount of power used even a few Watts could still remain after the amplification. An isolator was used to assure unidirectional lasing in the cavity, and a polarisation controller was used to allow fine control of the birefringence. Light was extracted from the cavity through a 5 % output coupler, and no synchronous pumping was necessary in this system. Moreover, to generate the pulses, a double-wall CNT-based saturable absorber was integrated into the cavity between a pair of fibre connectors.

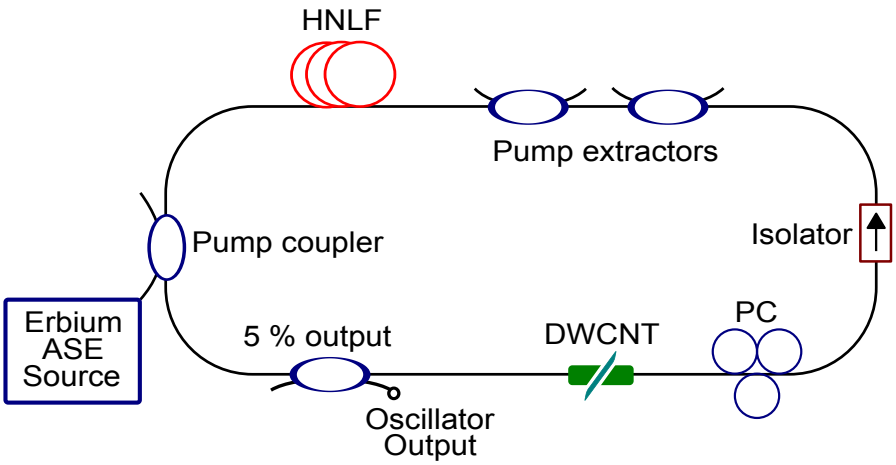

Figure 2.5: Experimental setup. HNLF, highly nonlinear fiber; PC, polarisation controller; DWCNT, double-wall carbon nanotubes.

The laser used to pump the gain fibre was a 4-stage cascade Erbium-doped ASE source containing two optical tunable filters that can be used to tune the output wavelength between 1550 nm to 1562 nm. The linewidth of the pump source is about 2.5 nm and it can give up to 15 W of CW power. According to the spec-

ifications the 100 m length single-mode HNLF used in the cavity has a Raman gain coefficient (G_r) of 2.51 $W^{-1}.km^{-1}$ at 1550 nm for an un-polirized pump and a effective area (A_{eff}) of 18.6 μm^2 at the same wavelength, which is ~4.5 times lower than the effective area of a STF fibre, which is approximately 85 μm^2 at 1550 nm. The dispersion is -20.5 $ps.nm^{-1}.km^{-1}$ at 1550 nm and from its slope of 0.031 $ps.nm^{-2}.km^{-1}$ it can be estimated to be about -17 $ps.nm^{-1}.km^{-1}$ at the Stokes wavelength at 1666 nm, which means that the laser operates in the normal dispersion regime at both pump and signal wavelengths. Losses are 0.33 dB/km at 1550 nm. The main reason for this fibre to be called highly non-linear is its reduced effective area, which at the same time is responsible for increasing the Raman gain by allowing higher pump intensities in the fibre core.

In order to compare the level of Raman amplification that can be obtained by the non-linear fibre used in this chapter and by a STF, one can simply analyse the Raman gain coefficient G_r that can be obtained in $W^{-1}.km^{-1}$ by

$$G_r = \frac{10^3.g_r}{2.A_{eff}.\lambda} \tag{2.4}$$

where g_r is the Raman gain at 1 μm in m/W, λ is the wavelength in microns, the factor of 10^3 is to convert meters to kilometres and the factor of 2 accounts for an un-polarized pump, which is the case of the experiment described in this chapter. In a STF, A_{eff}=85 μm^2 for λ=1.55 μm, and g_r=10^{-13} m/W, which gives G_r=0.38 $W^{-1}.km^{-1}$. This value is approximately 6.6 times lower than the G_r of the OFS Raman fibre used in this experiment. The concentration of GeO_2 in the fibre core was not given in the fibre specifications, however, it can also be estimated by applying Eq. 2.4. Considering G_r=2.51 $W^{-1}.km^{-1}$, A_{eff}=18.6 μm^2 and again λ=1.55 μm, that would give g_r = 1.45 m/W. According to measurements made in Ref. [145] this should correspond to a mol% of GeO_2 on the region of 12%.

The CNT-polymer used in the experiment was manufactured and initially characterised by collaborators from a research group based in the Electrical Engineering department at the University of Cambridge. The samples were prepared by solution processing [122], and they used carbon nanotubes grown by catalytic chemical vapor deposition [146]. After purification by air oxidation at 450 °C, followed by HCl washing, the remaining carbon-encapsulated catalytic nanoparticles were removed [147]. Analysis of the purified samples by transmission electron microscopy

(TEM) revealed the presence of ∼90% double-wall carbon nanotubes (DWNTs), ∼8% single-wall carbon nanotubes, and ∼2% triple-wall carbon nanotubes [147]. The diameter distribution for DWNTs is ∼0.8 - 1.2 nm for the inner and ∼1.6 - 1.9 nm for the outer diameters, as determined by Raman spectroscopy and TEM. This wide diameter distribution can potentially enable broadband operation, essential for the large wavelength coverage offered by Raman amplification. The purified nanotubes were then dispersed using a tip sonicator (Branson 450 A, 20 kHz) in water with sodium dodecylbenzene sulfonate surfactant, and mixed with aqueous polyvinyl alcohol (PVA) solution to obtain a homogeneous and stable dispersion free of aggregates. Slow evaporation of water from this mixture produced a CNT-PVA composite ∼50 μm thick. Optical microscopy revealed no CNT aggregation or defect in the composite, thus avoiding scattering losses.

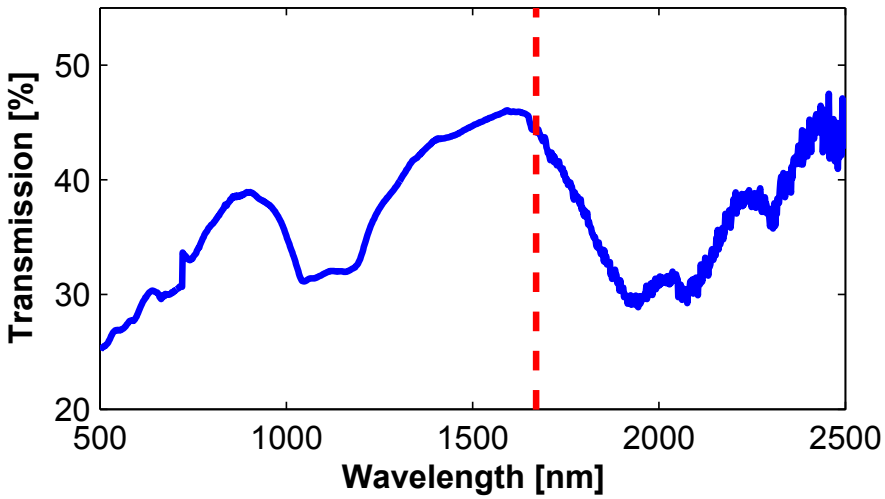

Figure 2.6: DWCNT transmission as a function of wavelength. The operational wavelength of the laser is marked in red.

The linear transmission of the DWCNT used in the experiment can be seen in Fig. 2.6. The two most significant troughs around 1.1 μm and 2 μm are due to the E_{22} and E_{11} transitions of the outer shells respectively. The E_{22} and E_{11} transitions of the inner shells should give rise to absorption peaks around 0.8 μm and 1.4 μm, which are not very prominent in this case, giving rise to the thought that the outer shells might play a dominant role in the saturable absorption mecha-

nisms for MWCNT. It is important, however, to notice that the variations in the transmission for the whole curve from 500 nm to 2500 nm are lower than 20%, which is an indication of a certain degree of distribution of different nanotubes, permitting saturable absorbance over a broad wavelength range. Nevertheless, it is also important to state that the transmission spectrum of a CNT-sample only serve as a first estimation of where saturable absorption might be present due to the observation of a absorption peak. For an better measurement and localization of saturable absorption the transmission should be measured against average power for a number of different wavelengths such as done in Ref. [123].

2.2.2 Results

Self-starting mode-locked operation was initiated as soon as the the pump power got to the threshold level of around 9.5 W. Stable operation was maintained over a range of pump powers above threshold, however increases higher than about 5 % tended to lead to spectral broadening and breakup of the single-pulse operation. The temporal pulse trace, the spectrum and the radio frequency (RF) trace at the output of the oscillator can be seen in Figs. 2.7, 2.8 and 2.9 respectively.

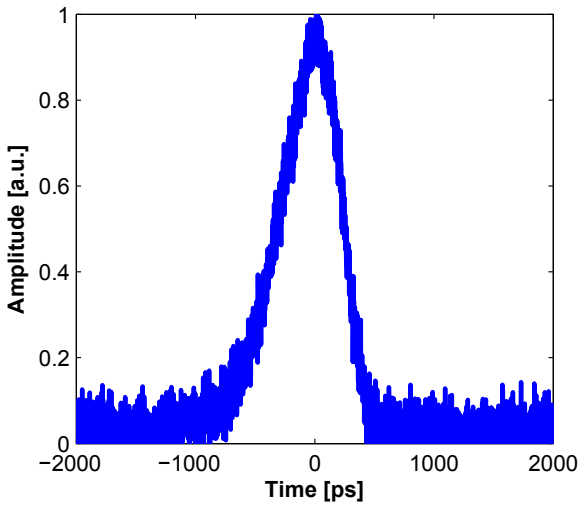

Figure 2.7: Normalized oscilloscope trace of pulse intensity profile at the output of the oscillator under 9.5 W of pump power.

The pulses were 500 ps long, and the average output power for stable mode-

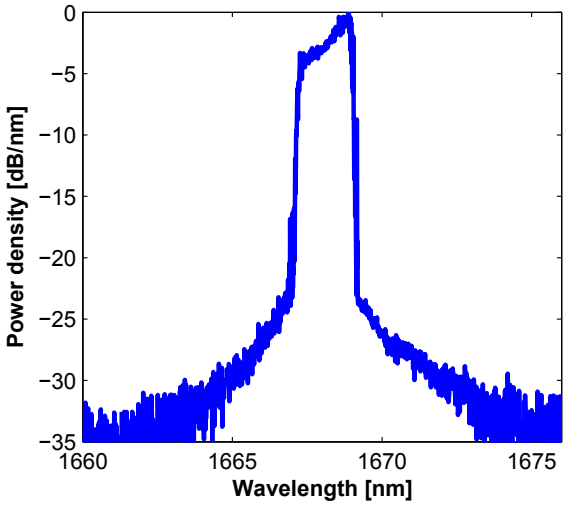

Figure 2.8: Normalized spectrum profile at the output of the oscillator under 9.5 W of pump power.

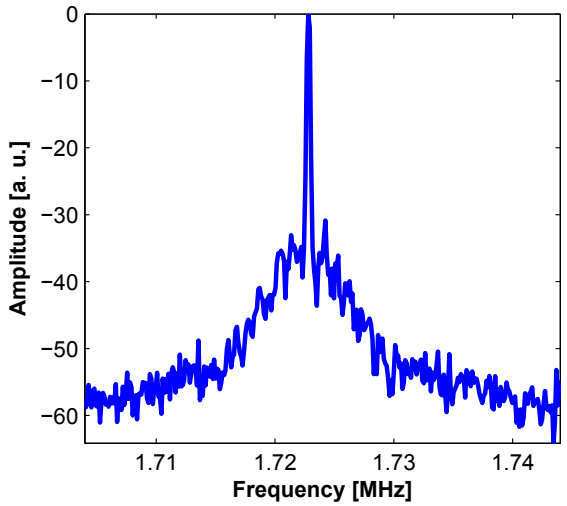

Figure 2.9: Normalized radio frequency trace at the output of the oscillator under 9.5 W of pump power.

locking was ∼0.08 mW, with a single pulse per round trip. The Raman laser operated at the first Stokes order at 1666 nm from a pump at 1555 nm. The low average power obtained can be attributed to the fact that the Raman gain is lower at higher wavelengths and also due to the fact that in order to maintain stable mode-locking we used a short length of fibre that is not enough to effectively deplete the pump resulting in several Watts of residual power after amplification. Moreover, the total cavity loss estimated in the order of 14 dB and the pump coupling loss of approximately 1 dB, which are mainly due to the splicing of fibres of different core sizes and also due to insertion loss of the cavity elements such as the isolator and the CNT-sample, also significantly contributed to scaling down the output power. By using output couplers with 10, 15 and 20%, slightly higher output powers could be obtained. However, the most stable pulse operation regime was found using the 5% output coupler.

The spectrum had a square shape, with a 6 dB bandwidth of ∼1.6 nm. The square-shaped spectrum and the long pulse duration are recognisable features of lasers operating in the dissipative soliton regime [88]. Such systems generate pulses carrying a large and predominantly linear chirp, and are suitable for compression. The RF trace showed a significant pedestal, containing 0.57% of the total energy, indicating that the cavity was prone to long-term temporal instabilities and fluctuations of the pulse-to-pulse energy. This relatively high noise contribution, compared to state-of-the-art rare-earth-based systems, is expected due to the high level of pump power and also due to the nearly instantaneous nature of the Raman gain. On the other hand, the narrow linewidth of the peak at 1.72 MHz, corresponding to the round-trip time of the cavity, is an indication of low pulse timing jitter.

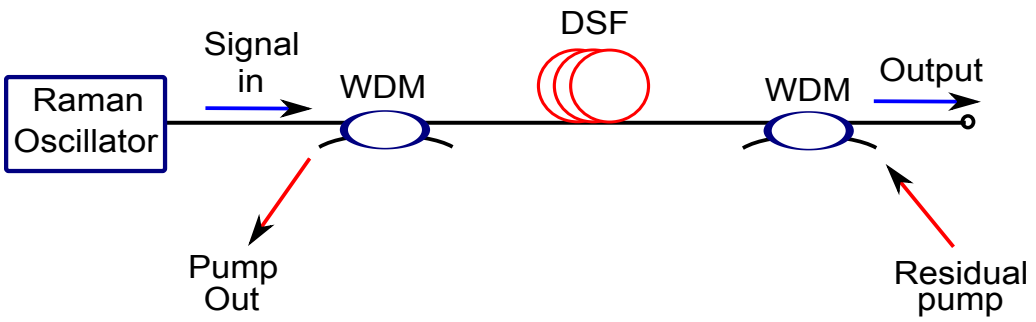

Figure 2.10: Schematic of the compressor/amplification stage after the oscillator.

In order to confirm the chirped nature of the pulse and to have a shorter pulse with higher peak power, after the oscillator, a second, 10 km Ge-doped fibre with a zero dispersion wavelength at 1320 nm was used as a combined amplifier and compressor in a chirped-pulse amplification scheme, as can be seen in Fig. 2.10. In particular, dissipative solitons have been proposed as a means of pre-chirping the pulse frequencies directly in the oscillator to simplify the chirped-pulse amplification design [88, 148]. The residual pump out of the seed oscillator was used to counter-pump the Ge-doped fibre.

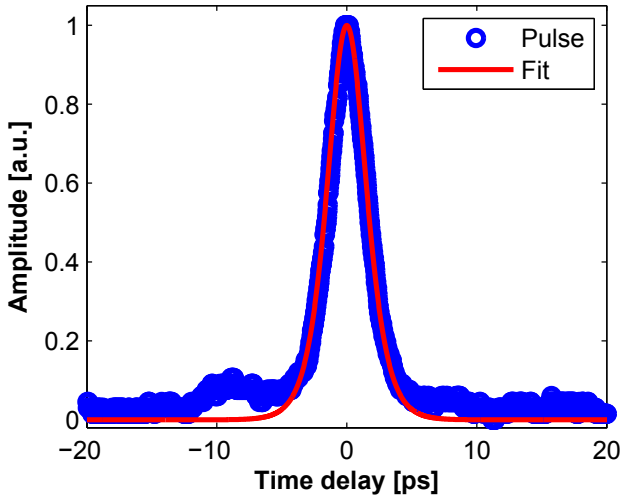

Figure 2.11: Normalized oscilloscope trace of pulse intensity profile at the output of the oscillator under 9.5 W of pump power.

The autocorrelation trace of the compressed and amplified pulse, its spectrum, and the RF trace of the fundamental cavity harmonic after compression are shown in Fig. 2.11, 2.12 and 2.13 respectively. The pulses were successfully compressed nearly 250 times from 500 to 2 ps, and no significant pedestal was observed on the autocorrelation traces. The average output power after amplification and compression was ∼5 mW, corresponding to the 18 dB gain provided by the amplifier, which required about 6 W supplied by the undepleted power from the oscillator stage. To use the residual pump from the master oscillator as a pump for external amplification is a practical way of recycling energy in a compact and simple way, enhancing the laser's overall conversion efficiency, however for a more precise con-

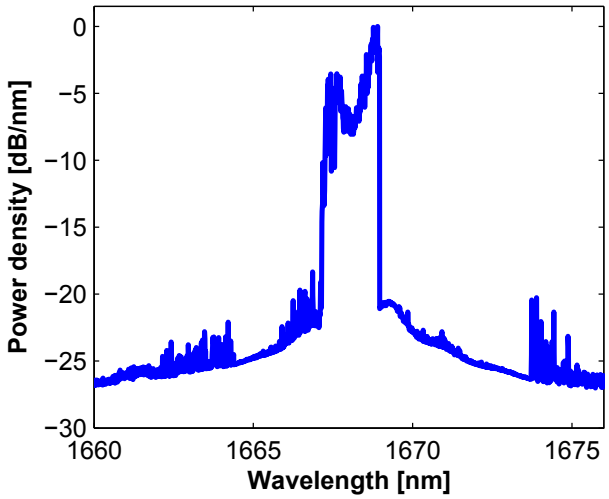

Figure 2.12: Normalized spectrum profile at the output of the oscillator under 9.5 W of pump power.

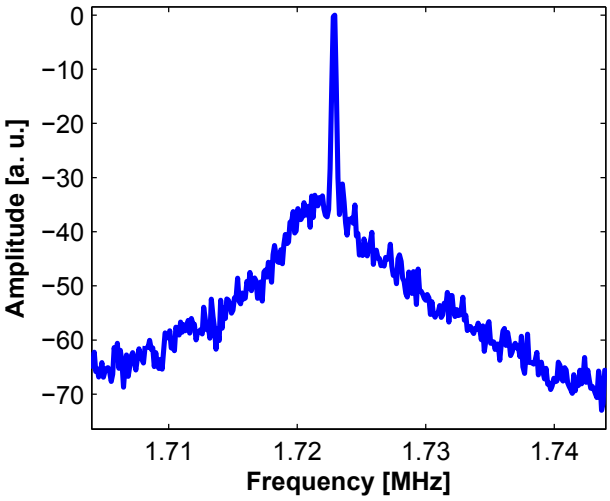

Figure 2.13: Normalized radio frequency trace at the output of the oscillator under 9.5 W of pump power.

trol of the amount of amplification, therefore of the output power, a separate pump with tunable power is necessary.

Importantly, as can be seen in Fig. 2.12, in spite of a small trough in the top of the spectrum caused by SPM, the spectral shape was mainly preserved, indicating linear compression. It can be noticed, however from Fig. 2.13 that noticeable degradation of the optical signal-to-noise ratio due to the amplified spontaneous signal in the amplifier fibre was apparent. The RF trace of the amplified and compressed signal was naturally centred at 1.72 MHz and shows a 6% increase of the noise pedestal when compared to the input signal. The pulse peak power after compression was ∼1.4 kW. Scalability of the peak power to higher levels should be possible by decoupling the amplifier from the compressor and by using a dedicated pump source for the external amplification.

2.3 Ytterbium-pumped Raman laser mode-locked by SWCNT

Since the main attractive feature of using Raman gain is its wavelength versatility, it is imperative to extend our previous results to other regions of the spectrum, where the difference in parameters, such as Raman gain and dispersion, could potentially lead to dissimilar behaviour. Here, we demonstrate a Raman oscillator pumped by a CW Yb-doped fibre laser, mode-locked by SWCNTs. An all-fibre configuration with all-normal dispersion is used, generating short-pulses at 1120 nm. The CW-pumping combined with the all fibre configuration reduces considerably the system complexity making it a simple and compact design. Moreover, the lasers operates in the normal dispersion regime, which has the potential of expanding the achievable pulse energy from mode-locked fibre lasers.

2.3.1 Experimental setup

The laser setup shown if Fig. 2.14, consisted of a high-power CW Yb-laser operating at 1070 nm that can provide up to 50 W average power coupled by a pump combiner into the cavity in a counter-propagating geometry. The active medium was a 60 m GeO_2-doped highly-nonlinear single-mode-fibre from OFS, the same used in the experiment shown in section 2.2. The fibre has normal dispersion at both pump

(1070 nm) and Stokes wavelength (1120 nm) and is still single mode since its cut-off wavelength is 988 nm. An isolator ensured unidirectional propagation. After the 60 m fibre, two wavelength division multiplexers (WDMs) extracted the undepleted pump light from the cavity to prevent damage to other passive optical components. A polarization controller allowed fine tuning of the birefringence. The SWCNT-saturable absorber was integrated into the cavity between a pair of fibre connectors. Light was extracted from the cavity by a 5% output coupler. The cavity output was then amplified in another Raman amplifier using 400 m of the same fibre used as the gain media inside the cavity. The residual pump power extracted from the cavity was used as a counter-pump for the external amplification, enhancing the overall conversion efficiency of the laser. A fused coupler beam splitter was used after the cavity output in order to have direct access to the pulse parameters before the amplification stage.

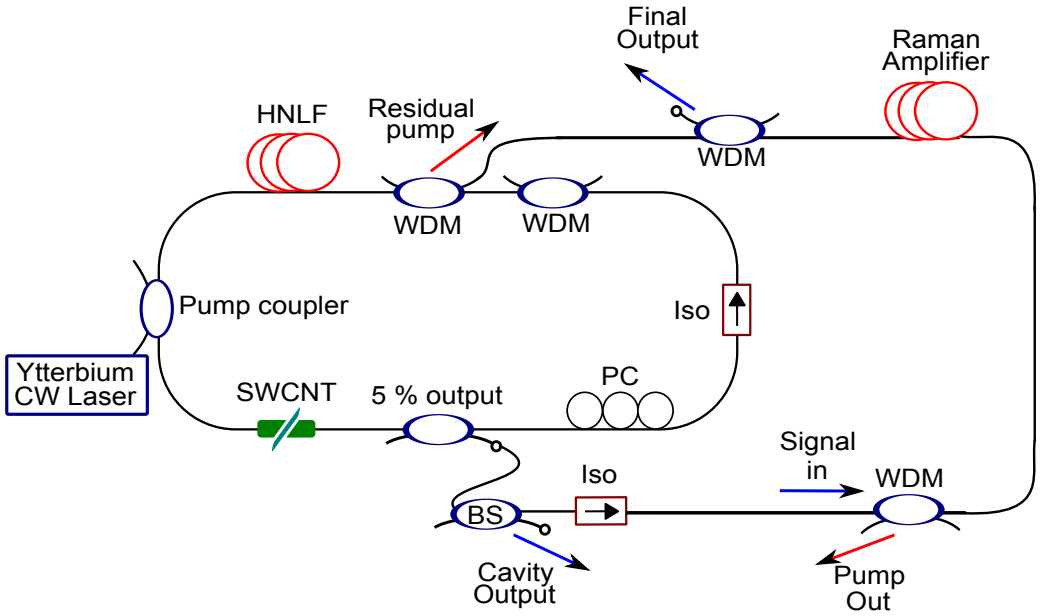

Figure 2.14: Experimental setup. HNLF, highly nonlinear fiber; SWCNT, Single-wall carbon nanotube saturable absorber; PC, polarization controler; Iso, Isolator; BS, Beam splitter.

To match the operation wavelength ($\sim$1.1 μm) of the Raman laser pumped with a Yb-doped fibre laser, requires CNTs whose lowest exciton transition energy (E_{11}) is $\sim$1.1 eV [122]. Thus, an absorption peak centered $\sim$ 1.1 μm, would maxi-

mize the change in absorption due to saturation [122]. Commercially available CoMoCAT CNTs (Southwest Nanotechnologies, Batch CAU-A002) with ∼0.75 - 0.8 nm diameter are ideal for this [149]. The CoMoCAT sample we used, which were produced by a catalytic method developed by Southwest Nanotechnologies, predominantly consisted of (6,5), (7,5) and (7,6) tubes, as determined by Raman spectroscopy [150], transmission electron microscopy [151] and photoluminescence excitation spectroscopy [152]. The diameter range for these chiralities is ∼0.75-0.9 nm, corresponding to a ∼1-1.3 eV gap [151]. The CNT saturable absorber was fabricated using solution processing [122]. 2 mg of CNTs were sonicated in 20 ml deionized water for 2 hr at 10-12 °C. The CNT dispersion was then centrifuged at 20,000 g using a MLA-80 fixed-angle rotor (Beckman) for 2 hr, and the top 70% decanted to obtain an aggregation-free CNT dispersion. This was then mixed with polyvinyl alcohol (PVA) in de-ionized water with a homogenizer and drop cast in a Petri dish. Slow evaporation at room temperature in a desiccator yielded a ∼ 50 μm CNT-PVA composite. Its absorbance is plotted in Fig. 2.15. This shows a peak ∼ 1170 nm, close to the desired operation wavelength of 1120 nm, corresponding to E_{11} of (7,6) tubes (∼0.895 nm diameter) [151]. Another peak ∼1028 nm is also seen, due to (6,5),(7,5) CNTs with 0.757 and 0.829 nm diameter [151]. The CNT based saturable absorber used in this section was again supplied and initially characterised by our collaborators from the University of Cambridge.

2.3.2 Results

Self-starting stable single pulse per round trip operation was achieved for pump power above the threshold value of 6.87 W. The presence of CNTs in the system was a necessary condition to obtain pulsed outputs. Their absence caused the laser to operate in the CW regime. It is important to notice that in comparison with the previous experiment presented in section 2.2 the threshold was achieved under ∼28% less pump power even using a fibre with 40% less length, stressing the fact that the Raman gain scales inversely with wavelength. Nevertheless, this is also attributed to the fact that the cavity losses were reduced in this experiment by a few dB's, mainly due to better splicing that could be achieved after a few months of practice in optimizing the splicing parameter to achieve lower losses.

Fig. 2.16, 2.17 and 2.18 plots the oscilloscope trace at the amplified output,

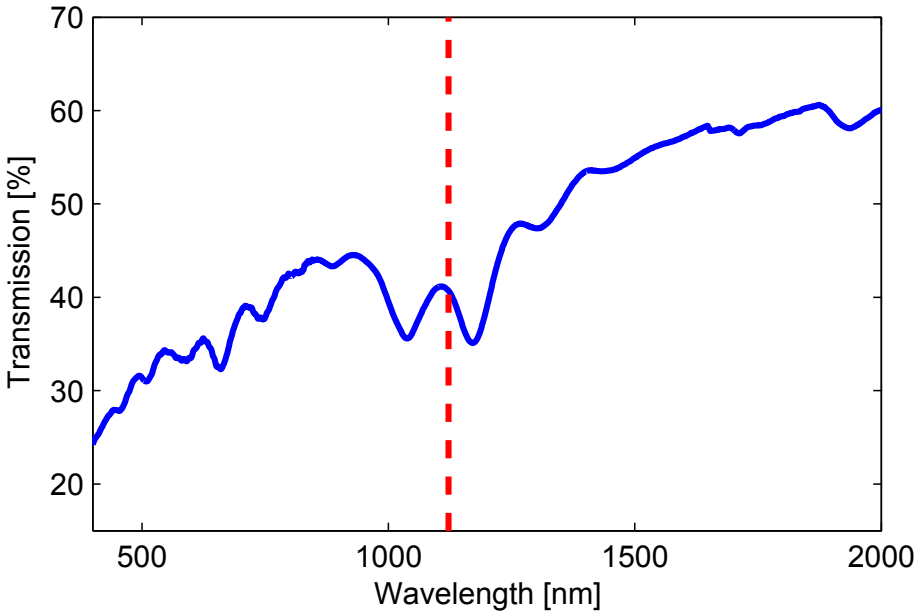

Figure 2.15: Transmission as a function of wavelength for the SWCNT used in the experiment. The operational wavelength of the laser is marked in red.

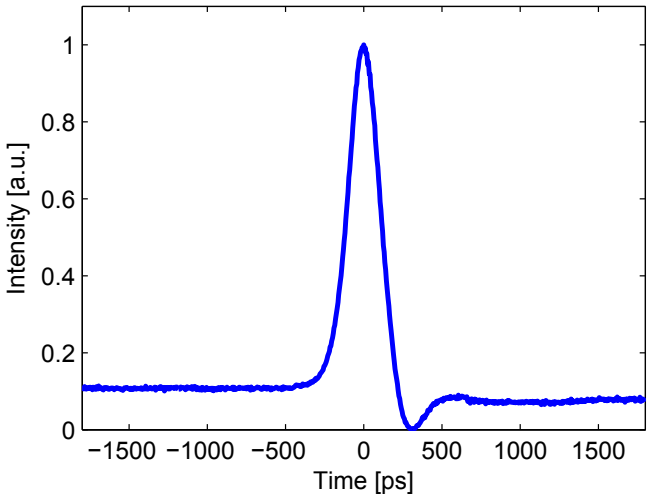

Figure 2.16: Normalized oscilloscope trace of pulse intensity profile after amplification for a under 6.87 W of pump power.

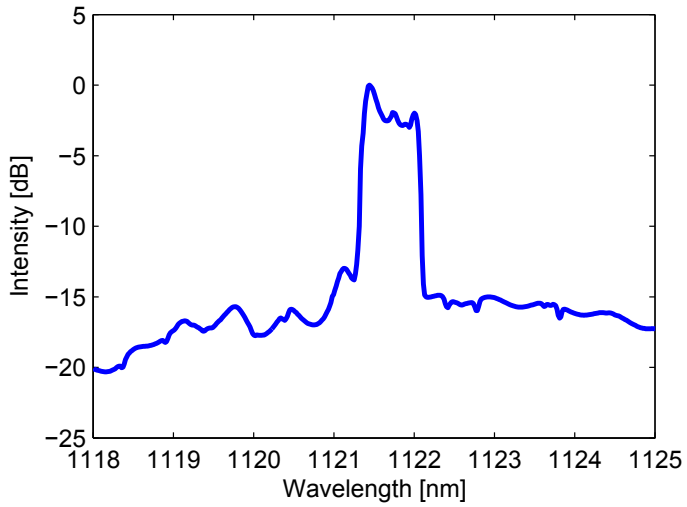

Figure 2.17: Normalized spectrum profile after amplification under 6.87 W of pump power.

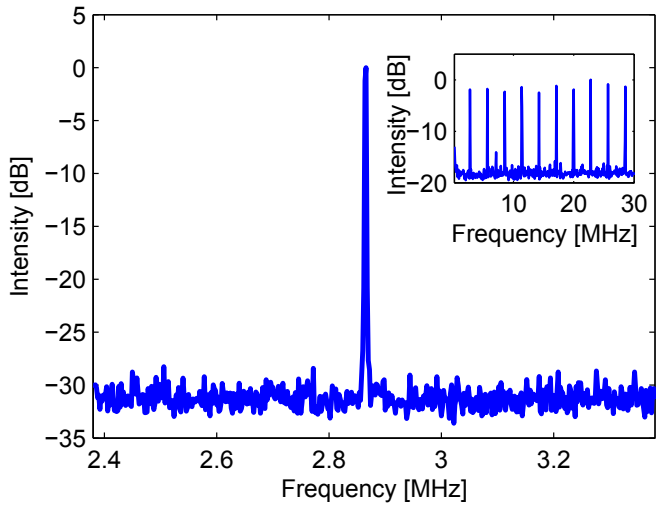

Figure 2.18: Normalized radio frequency trace after amplification under 6.87 W of pump power. The first 10 harmonics are shown as an inset.

its optical spectrum and its RF trace respectively. The pulse width was 236 ps, with an average power of 2.6 mW and a repetition rate of 2.87 MHz. The 6 dB bandwidth of the spectrum was 0.8 nm, as can be seen in Fig. 2.17, and again its square shape is a typical signature of dissipative solitons. The pulse and spectrum shape remained unchanged after amplification, the only main difference accounts for the optical power which was -13 dBm (0.05 mW) at the cavity output and 2.6 mW after amplification. In Fig. 2.18 the RF spectrum of the central peak and as an inset the first ten harmonics are shown. The trace centered at 2.87 MHz corresponds to one cavity round trip, and it presents no significant pedestal on a span of 1 MHz, with a noise floor $\sim$ 31 dB (a 10^3 contrast) down from the peak.

In order to show temporal coherence on the laser output, the autocorrelation trace of the pulses is shown on Fig. 2.19. If the envelope of a pulse shown on a oscilloscope trace is actually formed by a bunch of short-time amplitude fluctuations, then the autocorrelation trace would show a spike on the top of a pedestal, in which the height of the pedestal would be the same height as the spike and the duration of the spike would be the average duration of the small noise fluctuations. The 60 ps window of the autocorrelator did not permit to resolve the entire pulse, however the absence of a spike on the top of a pedestal was a clear indication that the laser was indeed mode-locked, and it was not a noise burst [18]. The natural technique to show coherence in dissipative soliton systems would be to temporally compress the pulse by means of anomalous dispersion, showing that the pulses are positively chirped [18], as it was done in the experiment in the previous section. However, there is no standard fibre with anomalous dispersion at 1120 nm. The pulse had a time-bandwidth product of 26.2, highlighting the larger chirp of the output pulses, therefore 8.4 km of a PCF with dispersion of 40 ps.nm^{-1}.km^{-1} at 1120 nm would be needed to fully compensate the chirp, assuming it was linear across the pulse, making this approach impractical given the current technology limitations.

Mode-locking was still achieved under a pump power of 7.52 W, which was the point when there was a break up of single pulses operation. After external amplification, both pulse duration and output power increased by increasing pump power, which is shown in Fig. 2.20. Under 7.52 W pumping, average powers of 59 mW could be achieved, giving pulse energies of approximately 20 nJ and peak powers of 13.8 W. The squared shape of the spectrum was maintained for the whole range of pump powers until 7.52, and no noise spike on the autocorrelation trace was found

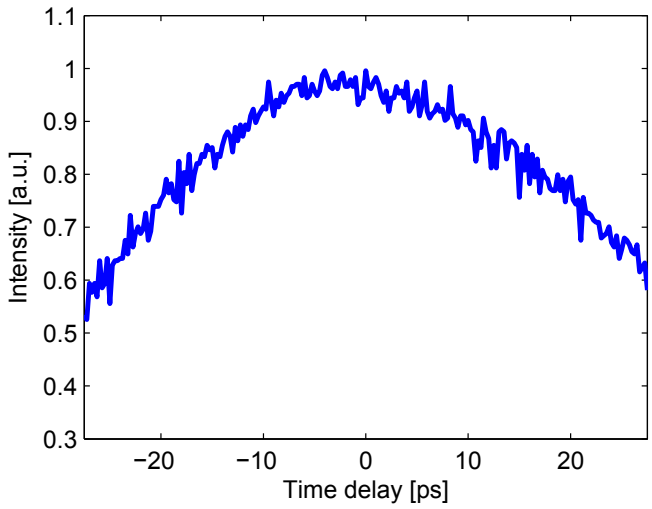

Figure 2.19: Autocorrelation trace of the pulse after amplification for a under 6.87 W of pump power.

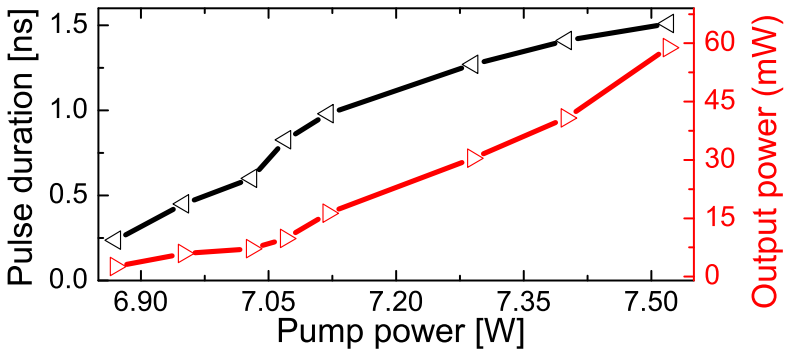

Figure 2.20: Pulse duration (black) and output power (red) on the amplified output against pump power.

within the same region.

2.4 Conclusion

In conclusion we have experimentally demonstrated that the combination of CNT-based saturable absorbers and Raman amplification can lead to the generation of short mode-locked pulses in all-fibre lasers. This combination is particularly interesting as a low-cost simple and compact technique for building pulsed lasers with high-peak power at wavelengths that are not covered by other more standard laser sources such as erbium- and ytterbium-doped fibre lasers, and it is a solution that could potentially be extended to the visible region of the spectrum. We have shown that both single wall and double wall CNTs can be used in the mode-locking of Raman lasers, by using them to generate short-pulses at 1120 and 1660 nm respectively. Both lasers use high-power rare-earth doped fibre lasers that are commercially available as a pump.

Firstly, an all-fibre passively mode-locked Raman laser utilising a broadband DWCNT-based saturable absorber was shown. The 500 ps pulses provided by the oscillator were amplified and simultaneously compressed to 2 ps with 1.4 kW peak power. The oscillator was implemented in a cavity with dominant normal dispersion, allowing generation of high energy pulses, up to $\sim$ 3 nJ, after amplification. Then, we demonstrated a passively mode-locked Raman laser using SWCNTs at 1120 nm. This again operates in the normal dispersion regime generating 236 ps pulses at the fundamental repetition frequency of the cavity. Our ultrafast laser at 1.1 μm, pumped with a CW-Yb fibre laser, confirms the flexibility in terms of wavelength of the combination of CNT based saturable absorbers and Raman amplification.

Nevertheless, it is important to stress that these results are preliminary, and that the performance of such lasers in terms of average power, noise levels and stability is still not comparable with standard mode-locked lasers based on rare-earth doped fibre. The high levels of pump power needed in those lasers is also a restriction in terms of simplicity and compactability of the system. This problem, however, can be minimized with the use of more exotic non-linear fibres, which is exactly the subject of the later experimental chapter of this thesis.

3 The universal laser - Raman and graphene

Graphene is a newly developed nano-material that due to many of its unique physical properties is causing a revolution in nano-sciences. The vast number of applications in which graphene can be involved makes it to be sometimes refereed as a "miracle material". Essentially, graphene is an one atom thick 2-dimensional layer of carbon atoms arranged in a honeycomb lattice, that serves as the basic building block of other carbon allotropes, such as carbon nanotubes, graphite and buckyballs. Different to carbon nanotubes, that can be either metallic or semiconducting, graphene is considered to be a zero band-gap semiconductor, or a semi-metal. These properties however, can be changed by doping graphene with other materials such as oxygen and hydrogen.

Amongst its unique properties, graphene is the strongest known material, it is a very good heat and electrical conductor, it is very stiff, yet very light and ductile. Graphene also presents remarkable optical and electronic properties such as inherent broadband saturable absorption due to the linear dispersion of the Dirac electrons, high non-linearities, near-ballistic electronic transport at room temperatures, and terahertz tunability of electrical properties.

The applications that involve the use of graphene or doped graphene-based devices are many, and can range from metamaterials, nano-electronic transistors, solar cells, flexible and nearly-transparent touch-screen displays to frequency multipliers, and light-emitting devices. Another important use of graphene is in laser sciences as a broadband saturable absorber. Although being a nearly transparent material, a graphene layer can absorb $\sim$2.3% of the incident light at any wavelength, which can be saturated under high optical intensities, allowing a compact, simple and cost-efficient mode-locker for ultrafast lasers. Conversely to carbon nanotubes where broadband saturable absorption can be achieve by a mix of tubes with dif-

ferent diameters, the broadband nature of saturable absorption in graphene is an intrinsic property of the material, making graphene an ideal "universal" mode-locker avoiding unnecessary non-saturated losses that could be detrimental to pulse generation.

In this chapter first there is a brief introduction about graphene highlighting some of its main optical and electronic properties as well as how they differ from carbon nanotubes. Then the experimental work done showing the use of graphene as a mode-locker for a Raman laser is presented. Due to the broadband nature of both phenomena, the combination of Raman gain and a graphene-based saturable absorber is an ideal technique towards a simple and compact universal short-pulsed laser source.

3.1 Introduction

Despite theoretical works from the early days of the last century arguing that 2-dimensional (2D) crystals could not physically exist because they would be thermodynamically unstable [153, 154], theoretical studies on graphene, or on one layer graphite, nevertheless has attracted considerable attention for more than sixty years [155, 156]. After many decades of theoretical works, in 2004 Novoselov et al. finally managed to experimentally produce stable single layer and few layer graphene by mechanical exfoliation of graphite [126]. One year later, in a work published by the same author, other stable 2D atomic layer crystals were experimentally produced again by mechanical exfoliation, such as boron nitride, several dichalcogenides, and complex oxides [157]. The reason why they claim such 2D crystals are stable under ambient conditions is that they are quenched in a metastable state because they are extracted from a 3D material, and moreover due to the strong inter-atomic bonds that ensure that thermal fluctuations do not cause defects on the crystal. The discovery of graphene by Novoselov et al. in 2004 would 6 years later in 2010 grant to him and his co-worker A. K. Geim the nobel prize in physics "for groundbreaking experiments regarding the two-dimensional material graphene".

Graphene can be produced by a number of different methods [124]. The most common technique is mechanical exfolitaion of graphite, such as shown by Noveselov et al. in the first experimental demonstration of graphene [126]. This is usually done by peeling off a piece of graphite by adhesive tape, and is still one of the easiest

and most used techniques for fundamental research capable of producing single layer graphene up to millimetres in size. Nevertheless, its main limitation is the fact that this method is not very practical for large-scale production. Alternative approaches to this issue can be to produce graphene by chemical vapor deposition (CVD) [158, 159], or liquid phase exfoliation [160]. Both techniques allow large-scale production of graphene.

Although graphene is essentially a one layer material, bi-layer graphene and few-layer graphene (3 to 10 layers) are sometimes also referred as graphene because they present very similar characteristics for certain applications such as its use as a saturable absorber. Nevertheless, other properties can change significantly with number of layers. More than 10 layers of stacked graphene is considered graphite. Characterization of graphene is easier than carbon nanotubes due to its more simple structure, and can be mainly done by Raman spectroscopy [161, 162], where the number and the orientation of layers, the quality and types of edge, and some effects of perturbations can be detected. It is also worth mentioning that in spite of being just a single atom thick, graphene can be visualized by optical microscopy if prepared on top of Si wafers [163].

3.1.1 Structure and electronic properties of graphene

The chemical structure of graphene is very similar to a carbon nanotube as was shown in Fig. 2.2. Essentially graphene is an unrolled carbon nanotube, which structurally is a layer of carbon atoms connected by a covalent bond to each other in a honeycomb lattice with atomic space equals to $\sim$1.42 Å. As mentioned previously, although graphene is ideally a single layer material, a few layers can be stacked on the top of each other being maintained by weak van der Waals forces forming what is called few layer graphene (FLG), which is illustrated in Fig. 3.1. The material is considered to be graphite if the numbers of layers is higher than 10 [164].

To properly understand graphene and its properties is important to take a look first at the carbon atom. Carbon is the chemical element with atomic number 6, therefore it has 6 electrons orbiting its nucleus of which 4 are on its valence band and consequently can form covalent bonds to other atoms. The arrangement of such electrons in a carbon atom and in graphene can be seen in Fig. 3.2. In elemental carbon the $1s$ and the $2s$ orbitals have both two electrons, and the $2p_x$ and $2p_y$

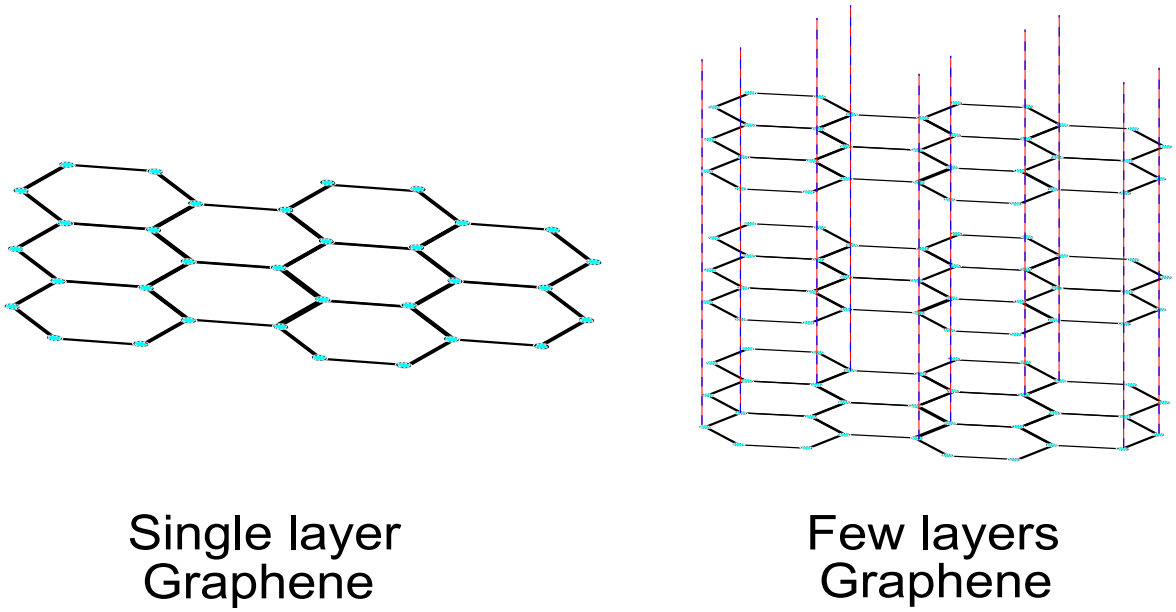

Figure 3.1: Honeycomb structure of single layer graphene (SLG) and few layers graphene (FLG).

have both one. In graphene the $2s$ orbital interacts with the $2p_x$ and $2p_y$ forming three hybrid sp^2 orbitals. The covalent bonds created by the interaction of the sp^2 orbitals are called σ-bonds, which are the strongest type of covalent bonds [165]. What makes graphene the strongest know material [166] is exactly the fact that each carbon has three σ-bonds localised along the same plane. The electron from the valence band that does not form a σ-bond occupies the orbital $2p_z$ that is perpendicular to the graphene plane. This electron is called a π-electron and is weakly bonded to the nuclei, therefore being relatively delocalised and presenting high mobility. These π-electrons are the ones responsible for the electronic properties of graphene [167].

One of the most important features of graphene electronic properties is the fact that its charge carriers behave as massless Dirac fermions [168]. In condensed matter physics, usually the Schrödinger equation is enough to fully calculate the electronic properties of materials. Nonetheless, although electrons around a carbon atom do not behave relativistically, the honeycomb lattice of graphene gives rise to a periodic potential that makes electrons behave as if massless quasi-particles,

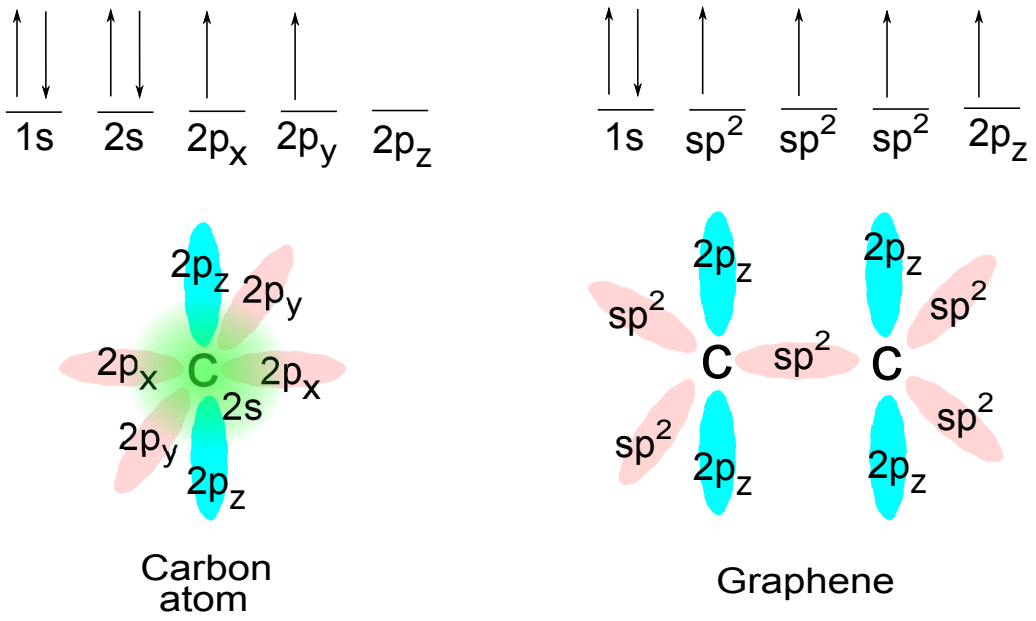

Figure 3.2: The arrangement of electrons and their relative spin in orbitals for elemental carbon atom and graphene.

which therefore needs to be treated by a relativistic wave equation, also known as the Dirac equation [83, 165]. For this reason, these quasi-particles are also known as massless Dirac fermions. This characteristic of graphene makes it a very useful tool for the study of quantum electrodynamics [169].

The band structure of graphene can be seen in Fig. 3.3. The most interesting feature about it, that gives rise to many of graphenes properties, such as broad-band saturable absorption, is the fact that around the carbon atoms, or in the so-called the Dirac points [165], the energy dispersion is linear. In 3 dimensions this is represented by a cone, known as the Dirac cone, in which the upper part is the conduction band and the lower part is the valence band. Under equilibrium conditions both bands touch each other at the Fermi level ($E_f = 0$ eV) but do not overlap, making graphene into a zero band-gap semiconductor with zero density of states at the Fermi level [83].

The electronic properties of graphene and its carrier densities, therefore its conductivity can, nonetheless, be changed by an applied voltage, which is the so-called field effect [170, 126] that is typical of semi-conductors. This can potentially lead

to the use of graphene as nano-scale transistors, which is one of its most promising applications. Similar use of graphene can be obtained also by chemical doping with elements such as bismuth and gold [171].

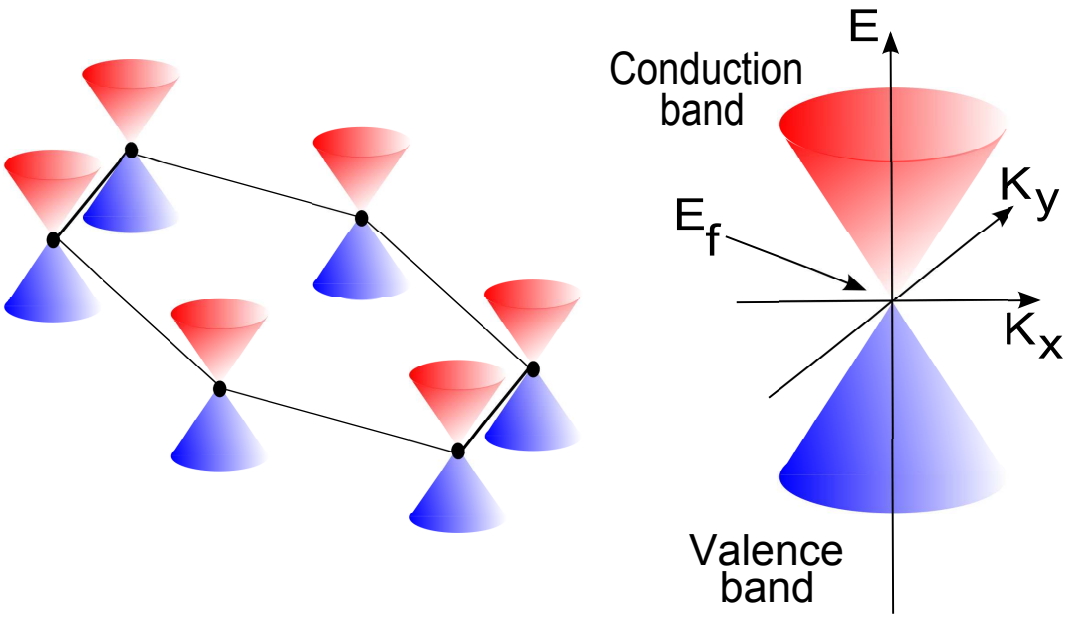

Figure 3.3: Band structure of graphene and its linear dispersion, also know as Dirac cone, around each carbon atom (Dirac points). E_f is the Fermi level, E is energy and K_x and K_x are the momentum in both x and y axis.

It is worth mentioning that the band structure of graphene shown in Fig. 3.3 is valid only for single layer graphene. In bi-layer graphene the dispersion relation is similar, however it becomes parabolic around the Fermi energy, with a band overlap of 0.16 meV, which is very small. In three or more layers, this gap overlap between the valence and the conduction band becomes bigger and the FLG starts behaving as a semi-metal. For eleven or more layers the difference between the electronic band structure of graphene and graphite becomes smaller than 10% [164]. Graphene can also be turned into a semiconductor or an insulator [172] by chemical modifications such as by partial oxidation or fluorination [173], or by building it as a nanoribbon [174], which broadens even more the possibilities in which graphene can be used as nano-scale electronic devices.

3.1.2 Optical properties of graphene

Although the recent interest in graphene both in academia and industry is mainly due to its many possible applications in electronics, graphene also has some interesting optical properties that makes it a candidate for many photonic devices, such as in ultrafast lasers or in far-infrared light generation, amplification and detection [124]. Despite being of only atom-layer thickness, single layer graphene absorbs ∼2.3% of incident light [175]. Optically speaking, in FLG the individual adjacent layers very weakly interact with each other, and can be considered for practical purposes as independent layers [176]. Therefore, the optical absorption increases nearly linearly with the number of layers, rising for example to ∼20% for ten layers. This linear absorption profile can be used as a quick estimation of the number of layers involved in the absorption process. Moreover, another important trait of optical absorption in graphene is the fact that it is basically flat from 400 to 2500 nm [123, 124].

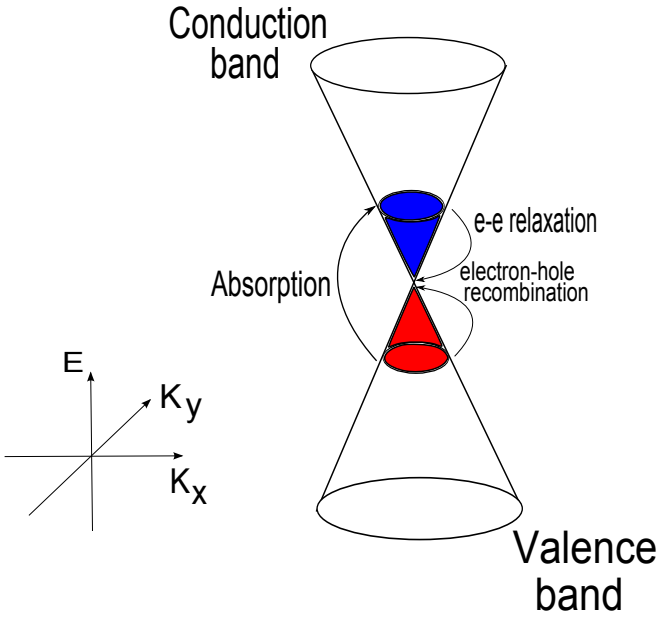

Figure 3.4: Saturable absorption process in graphene, where $e - e$ is electron-electron, E is energy and K_x and K_x are the momentum in both x and y axis.

The saturable absorption mechanism in graphene is illustrated in Fig. 3.4. Although the energy band structure of graphene and carbon nanotubes are very dif-

ferent, there are some similarities with the process described in section 2.1.2. The main difference is the fact that the linear dispersion relation in graphene and the lack of a bandgap allows photons with any energy, therefore at any wavelength, to excite electrons from the valence band to the conduction band. This is the key point which precisely gives rise to the broadband operation in graphene. The electron-hole recombination occurs on a picosecond scale due to interband relaxation [123]. As in any other saturable absorber, under strong incident pump the conduction band can be filled with electrons decreasing the quantity of electrons that can be absorbed, therefore saturating the loss.

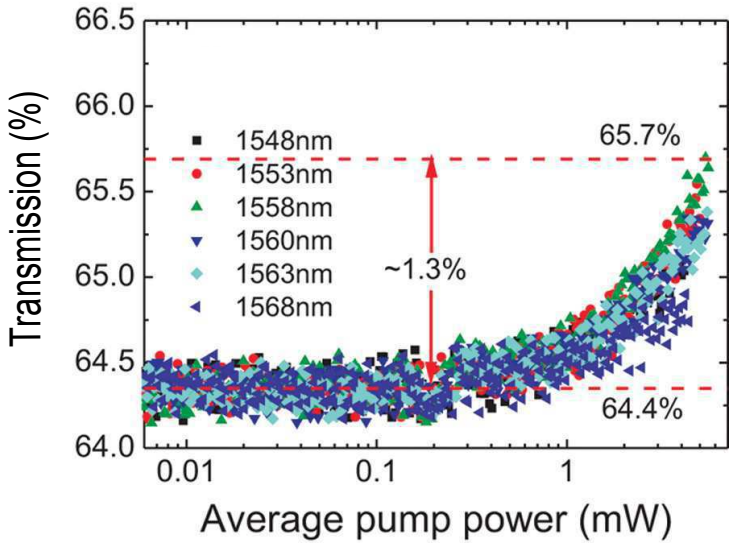

Figure 3.5: Saturable absorption in graphene from 1548 to 1568 nm. Courtesy of the University of Cambridge, adapted from [123].

A measure of the saturable absorption in graphene can be seen in Fig. 3.5, where the transmission is shown against input average power coming from a pulsed fibre laser with pulse durations of 580 fs. The experiment was carried out by our collaborators from Cambridge University and it was published and described in detail in [123]. As it can be seen, at low average powers, the transmission remains practically constant, however when the average power is increased to 5.35 mW, corresponding to an intensity of 266 MW/cm^2, the corresponding transmitted

power increases by ∼1.3% at 1558 nm. Proper characterization of the modulation depth and saturation intensity could not be performed in [123] due to limitations of the pump. A more complete measurement of the saturation properties was later reported by D. Popa et al. [177] where a modulation depth of ∼2% was measured. Nevertheless, it is worth mentioning that since the modulation depth of SLG can not exceed 2.3% which is the maximum absorption per layer in graphene, often in mode-locked lasers usually FLG or at least few independent samples of single-layer graphene has to be used.

A final remark about graphene's optical properties is that SLG ideally does not present luminesence due to the lack of a band-gap. Nonetheless, as mentioned in the previous section, a band-gap can be induced by chemical modifications [172, 173], or by building it as a nanoribbon [174], which could potentially make graphene-based devices useful tools for infra-red light generation, amplification and detection.

3.1.3 Graphene as a saturable absorber

In photonics, one of the most important uses of graphene is as a saturable absorber in mode-locked lasers. Such as carbon nanotubes, the most attractive feature of graphene as a saturable absorber is the capability of operating in a broad operation range in terms of wavelength. This broadband operation, however, arises in graphene and in carbon nanotubes from very different mechanisms. As mentioned previously, a range of tubes with different diameters in a single CNT-based device is what is responsible for saturable absorption to be available at a number of different wavelengths, however when operating at a specific wavelength, the other nanotubes that are not in resonance end up adding loss to the process, which can be detrimental to the mode-locking. Graphene appears exactly as a perfect solution for this problem. As described in the previous section saturable absorption in graphene is an intrinsic feature caused by its unique electronic band properties. Therefore, any graphene sample can be used as a mode-locker for fibre lasers at any wavelength, without the need of any special engineering fabrication process to change its properties. That is the reason why graphene is sometimes referred as a "universal mode-locker".

The first demonstration of the use of graphene as a saturable absorber in a mode-locked laser was reported by Hasan et al. [122] where 800 fs pulses where produced

at 1557 nm from an erbium-doped fibre laser operating in the solitonic regime. This was five years after the first experimental demonstration of graphene by Novoselov et al. in 2004 [126]. Since Ref. [122], there were many reports of the use of graphene as a mode-locker at a number of wavelengths [178, 179, 180], in a number of different laser configurations [181, 182, 183]. Amongst the most highly cited results, it is important to highlight the report of: a dispersion-managed erbium-doped fibre laser mode-locked by graphene generating 174 fs pulses [177], a dissipative soliton fibre laser generating 50 ps pulses [181], and a thulium-doped fibre laser mode-locked by graphene generating 3.6 ps pulses at 1.94 μm [179].

The first experimental demonstration of a mode-locked Raman laser using as a saturable absorber graphene was shown in [184], which is precisely the subject of this present chapter described in detail in the next section. One year later, there was another report of a Raman laser mode-locked by graphene at a different wavelength [180], being so far the only two demonstrations of such lasers.

3.2 Harmonic and single pulse operation of a mode-locked Raman laser using graphene

Here an all-fibre passively mode-locked Raman laser using graphene as a saturable absorber is presented. Different lengths of a highly non-linear fibre presenting normal dispersion at both pump and signal wavelengths are used in the cavity to provide Raman amplification. The cavity is pumped by a continuous wave Raman laser at 1450 nm, and generates short pulses around 1550 nm, which depending on polarization and filtering parameters can be either at the repetition rate of the cavity or at higher harmonics of it. The combination of the broadband nature of Raman gain and graphene in a single laser is a contribution to move the field of ultrafast laser towards a universal source.

3.2.1 Experimental setup

The laser setup was very similar to the one used in the experiments shown earlier in this thesis in chapter 2, and it can be seen in Fig. 3.6. It consisted of an all-fibre optical cavity pumped by a high power continuous wave (CW) Raman laser at 1450 nm in a counter-propagating configuration. The optical fibre used as the

Raman gain medium was different lengths of the same fibre described in the previous experiments detailed in chapter 2, which is a single-mode speciality optical fibre (OFS Raman Fibre), with an enhanced germanium oxide (GeO_2) concentration for an increased Raman gain coefficient (2.5 $W^{-1}km^{-1}$). The fibre dispersion at 1550 nm is -20.5 $ps.nm^{-1}.km^{-1}$ with a slope of 0.031 $ps.nm^{-2}.km^{-1}$ and effective core area of 18.6 μm^2. The overall loss at 1550 nm is ~0.33 dB/km. Two wavelength division multiplexing (WDM) couplers were used after the fibre in order to dump the residual pump power out of the cavity, which otherwise could have damaged the optical components of the oscillator. A polarization insensitive optical isolator was employed to ensure unidirectional propagation and a 15% output coupler was used. Furthermore, an optical filter with variable bandwidth was used to assist the intra-cavity pulse shaping dynamics and an intra-cavity polarization controller was used to allow fine adjustment of the cavity birefringence.

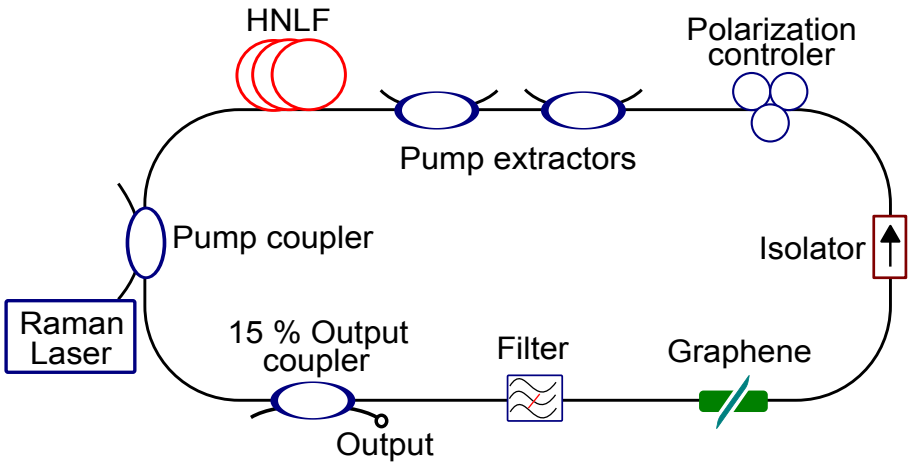

Figure 3.6: Raman oscillator configuration. HNLF Highly nonlinear fibre.

The graphene sample used in this experiment was a 5-6 layer graphene that was fabricated by collaborators from the School of Electrical and Electronic Engineering at Nanyang Technological University, Singapore. Differently from the previous experiments using carbon nanotubes described in chapter 2 where the samples were embedded in a polymer structure and placed between a pair of fibre connectors, the graphene saturable absorber used in this case was introduced into the cavity through transferring a piece of free standing few layers graphene film onto the end

facet of a fiber pigtail via the Van der Waals force [185, 186]. The transmission loss of the graphene sample against wavelength can be seen in Fig. 3.7. This was measured by using a CW tunable laser from 1520 to 1580 nm with 1 mW of average power, not showing any significant peak in the absorption. The insertion loss to the system of the graphene sample was ∼1.5 dB (or 29% absorption) in the whole range from 1520 nm to 1580 nm, which is lower than what was obtained with the CNT-samples used previously, indeed confirming the argument that graphene can avoid unwanted insertion losses caused due to the large distribution of CNTs that do not participate in the mode-locking for a given wavelength.

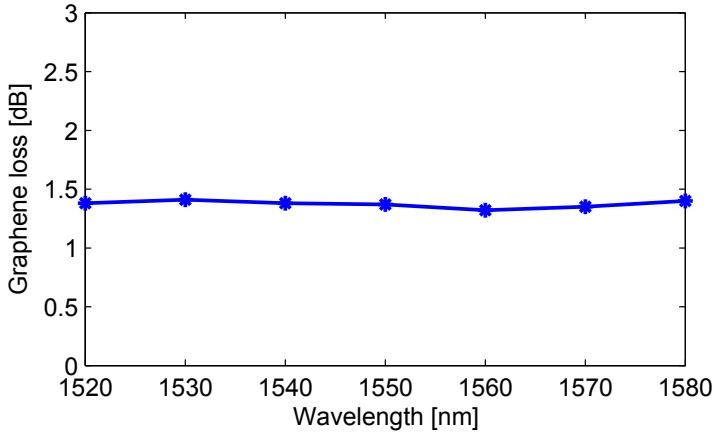

Figure 3.7: Transmission loss of the 5 to 6 layers graphene used in the experiment.

3.2.2 Results

Harmonic mode-locking

The initial results were obtained using a length of 100 m non-linear fibre. In this configuration no optical filter was employed in the cavity since the fibre gain length was insufficient to overcome the filter insertion loss of ∼3 dB. The mode-locking threshold was achieved under 4.4 W pump power, and pulsed operation was maintained up to the maximum power of the pump source of 4.8 W. For pumping with 4.8 W, the oscilloscope trace, the optical spectrum and the RF spectrum at the cavity output are shown in Fig. 3.8, 3.9 and 3.10 respectively.

The generated pulses were 750 ps long with an average power of 8.3 mW. The

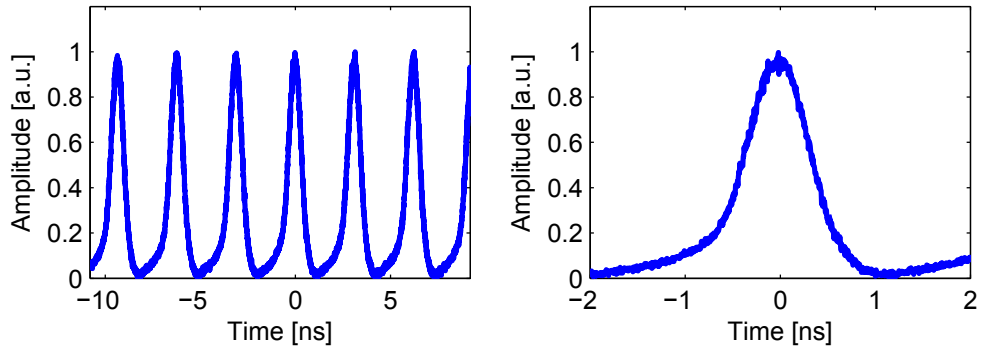

Figure 3.8: (a) Oscilloscope temporal trace of the high harmonic mode-locked 750 ps pulses from the cavity without filter and with 100 m of non-linear fibre at 2 different time scales.

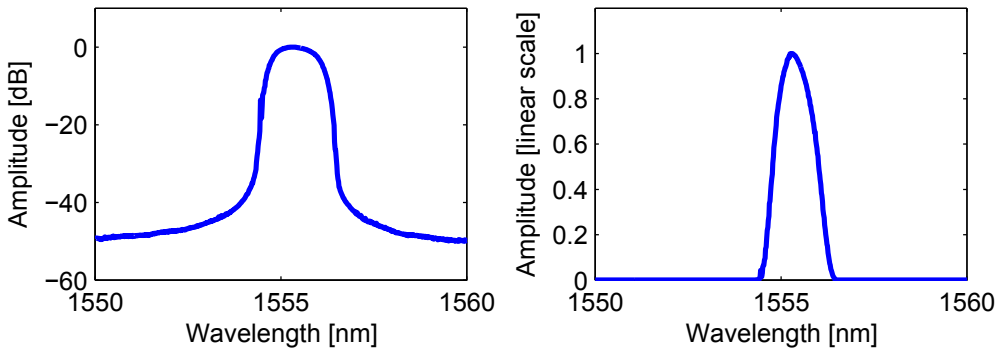

Figure 3.9: Normalized spectrum of the high harmonic mode-locked 750 ps pulses from the cavity without filter and with 100 m of non-linear fibre in a dB (a) and in a linear (b) scale.

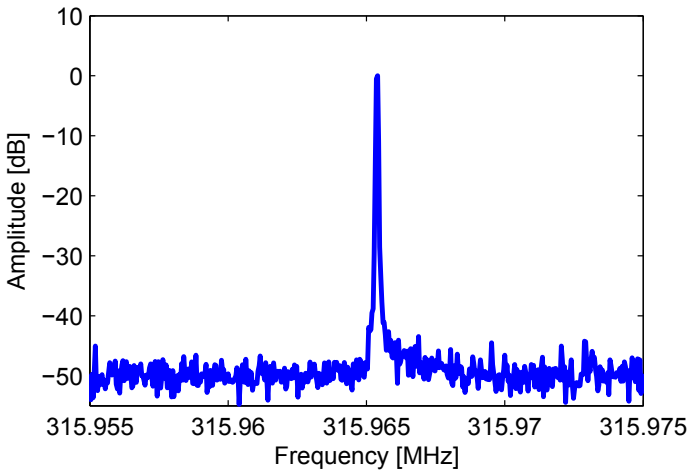

Figure 3.10: Normalized radio frequency trace of the high harmonic mode-locked 750 ps pulses from the cavity without filter and with 100 m of non-linear fibre.

spectrum has a linewidth of 1.6 nm at 6 dB and a square shape typical of lasers operating in the dissipative soliton regime. The pulses were generated at a repetition rate of 315.96 MHz, which is approximately 160 times the repetition rate of a single pulse operation in a 100 m long optical cavity. This is attributed to the fact that harmonic mode-locking is likely to happen when a saturable absorber with weak absorption is used, which normally should be the case for a few layer graphene interface [123]. Moreover, since Raman amplification is effectively instantaneous, no energy can be stored, therefore gain is available all the time making pulses likely to build up more than once per round trip. The RF trace, however, has a 50 dB extinction ratio, and no significant pedestal is present, indicating that the pulse-to-pulse energy fluctuation instabilities are not very high. The high repetition rate obtained, although can be useful for applications such as high speed optical sampling and frequency metrology, causes considerably reduction of the peak power levels, which in this case remains approximately 0.035 W.

By changing the polarization and the pump power, strong long-term modulations could be observed in the pulse train as well as changes in the spectral and temporal pulse shape. However, the associated change in the repetition rate was no more than 10%. We believe the absence of a wavelength restrictive filter together with the low modulation depth of graphene meant the pulse train could not remain stable over

a period of time greater than 15-20 minutes. Using a 100 m length fibre, operation with a single pulse per round trip was not achieved.

Increasing the fibre length to 200 m decreased the threshold level to 2.6 W, and again pulsed output was obtained over the available pump power range. Using the maximum pump power of 4.8 W and a 4.8 nm bandwidth filter centred at 1550 nm resulted in a train of 600 ps pulses with 332.5 MHz repetition rate and 8.5 mW average power as can be seen in Fig. 3.11.

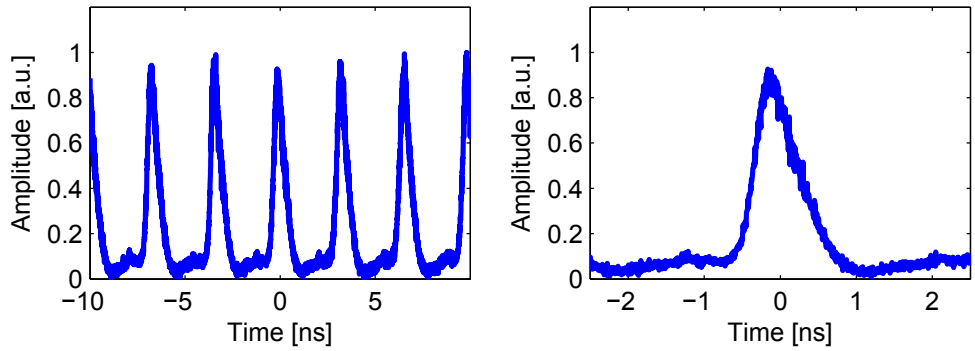

Figure 3.11: (a) Oscilloscope temporal trace of the high harmonic mode-locked 600 ps pulses from the cavity with a 4.8 bandwidth filter and with 200 m of non-linear fibre at 2 different time scales.

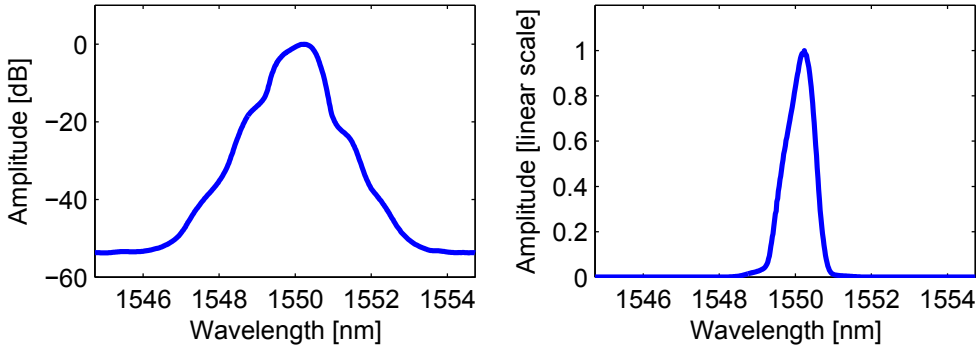

Figure 3.12: Normalized spectrum of the high harmonic mode-locked 600 ps pulses from the cavity with a 4.8 bandwidth filter and with 200 m of non-linear fibre in a dB (a) and in a linear (b) scale.

The spectrum, shown in Fig. 3.12, has a 6 dB level bandwidth of 1.2 nm, however a substantial pedestal component was present. In this configuration the laser was

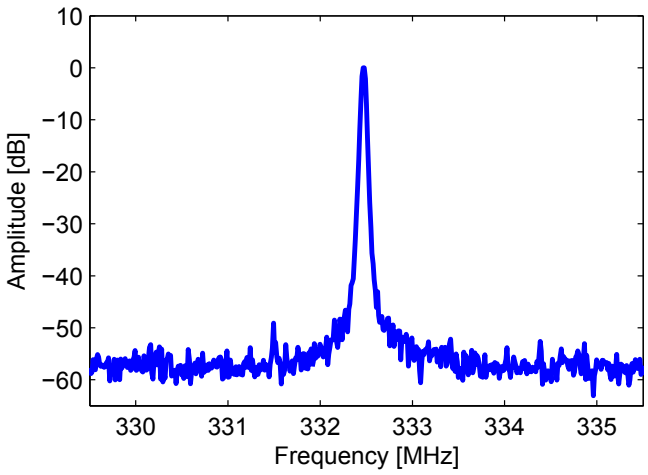

Figure 3.13: Normalized radio frequency trace of the high harmonic mode-locked 600 ps pulses from the cavity with a 4.8 bandwidth filter and with 200 m of non-linear fibre.

not strongly affected by changes of polarization and pump power, and the pulses and spectral shapes remained unchanged over a period of hours of operation. We attribute this higher stability to the use of the optical filter in the cavity, which is necessary for mode-locking in the dissipative soliton regime when the other elements of the cavity do not provide sufficient spectral filtering. The repetition rate exhibited some variation, however remaining within a few discrete values between 310 and 340 MHz. Moreover, as can be seen from the pulse trace (Fig. 3.11) and from the RF trace (Fig. 3.13) in this case the pulse-to-pulse fluctuations are much higher, which can be attributed to the longer length of fibre used. Furthermore, the broader peak found in Fig. 3.13 compared to the one shown in Fig. 3.10 is an indication of higher timing-jitter.

Other filters with 12.8, 2.3, and 1 nm bandwidths were also tested with the center wavelength varying in the range from 1540 nm to 1560 nm, which was the maximum tunability permitted by the used optical filter. Apart from changes in the spectral shape, single pulse per round trip mode-locking was not observed and pulsed output was always in high harmonics of the cavity with insignificant variations of the pulse parameters and repetition rate. Again, due to the high repetition-rate, the peak power of the pulse train was very low, remaining approximately 0.042 W.

Single-pulse operation and pulse compression

Although the most common and by far the most stable operation regime obtained in this laser was pulses in high harmonics of the cavities, under specific conditions single pulse per round-trip could be observed. Still using 200 m of gain fibre, but removing the filter, single pulse per round trip operation could be achieved, which is shown in Fig. 3.14, 3.15 and 3.16. This operational regime was obtained for pump powers just above the threshold. Further increase of the pump power caused pulse break down and higher harmonic mode-locking.

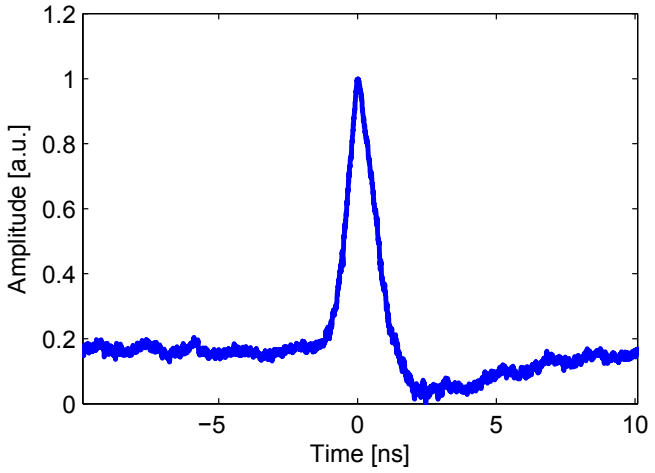

Figure 3.14: (a) Oscilloscope temporal trace of the high harmonic mode-locked 600 ps pulses from the cavity with a 4.8 bandwidth filter and with 200 m of non-linear fibre at 2 different time scales.

The mode-locked pulses were 1.25 ns long, with an output average power of 4.9 mW at 0.9 MHz repetition rate, corresponding precisely to the round trip time of the cavity. The longer pulse duration was mainly due to the absence of an optical filter and the longer length of fibre, which were also sources of instability, making the single pulse operation difficult to maintain for more than a few minutes. The spectrum had a Gaussian-like shape on the top of a small pedestal with a 6 dB bandwidth of 0.8 nm and the RF trace had a contrast of approximately 50 dB against the noise floor. The low repetition-rate allowed a substantially higher peak power to be obtained, which was about 4.3 W, giving pulse energies of $\sim$ 5.4 nJ.

Increasing the fiber length to 400 m again led to harmonic mode-locking with

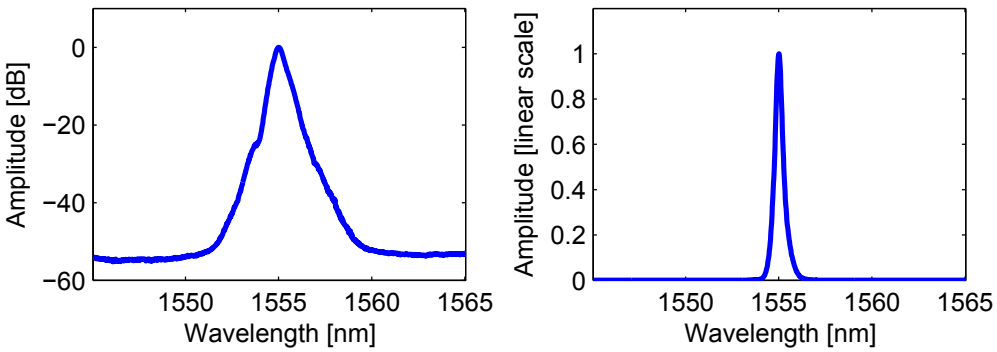

Figure 3.15: Normalized spectrum of the high harmonic mode-locked 600 ps pulses from the cavity with a 4.8 bandwidth filter and with 200 m of non-linear fibre in a dB (a) and in a linear (b) scale.

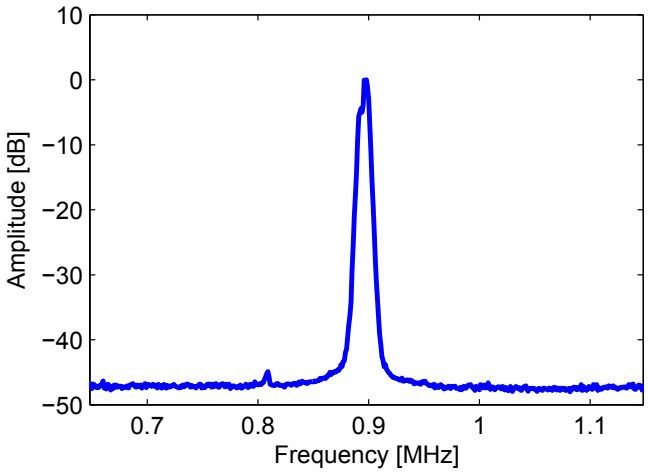

Figure 3.16: Normalized radio frequency trace of the high harmonic mode-locked 600 ps pulses from the cavity with a 4.8 bandwidth filter and with 200 m of non-linear fibre.

pulse durations from 600 to 700 ps and repetition rates from 310 to 340 MHz, depending on pump power, filter bandwidth, central wavelength and polarization adjustment. However, single pulse operation could once again be achieved when a filter with a bandwidth of 12.8 nm was used. This time the pulse duration was 600 ps and the average power 3.3 mW, achieved when the cavity was pumped with 2.8 W power. The repetition rate of 500 kHz, matched exactly the cavity round trip, and the spectral 6 dB level bandwidth was 0.6 nm. Within the pump powers from threshold to approximately 25% higher, the single pulse regime could be maintained and exhibited significantly higher stability than that obtained with the previous setup, without an optical filter. Nonetheless, stability in the pulse parameters for more then tens of minutes could only be achieved when the laser was in the harmonic mode-locking regime.

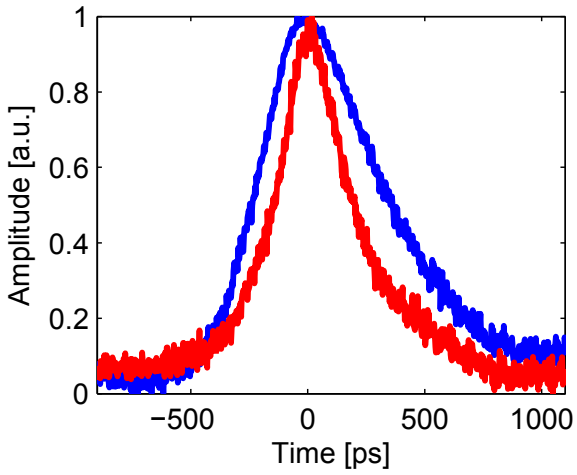

Figure 3.17: Normalised oscilloscope trace of the 600 ps pulses from the cavity output (blue line) using 400 m of non-linear fibre and a 12.8 nm filter, and pulse compressed to 350 ps in 21 km of STF (red line)

In order to confirm the chirped nature of the pulse, a signature of dissipative solitons, a 21 km length of standard Telecom fiber (STF) was spliced to the cavity output providing anomalous dispersion to compensate the expected positive chirp on the pulses. Given the narrow spectral bandwidth (0.6 nm) and the large duration (600 ps), the pulse was expected to possess a large chirp, indicated by the large time-bandwidth product of 29.8, requiring about 60 km of STF to reach full com-

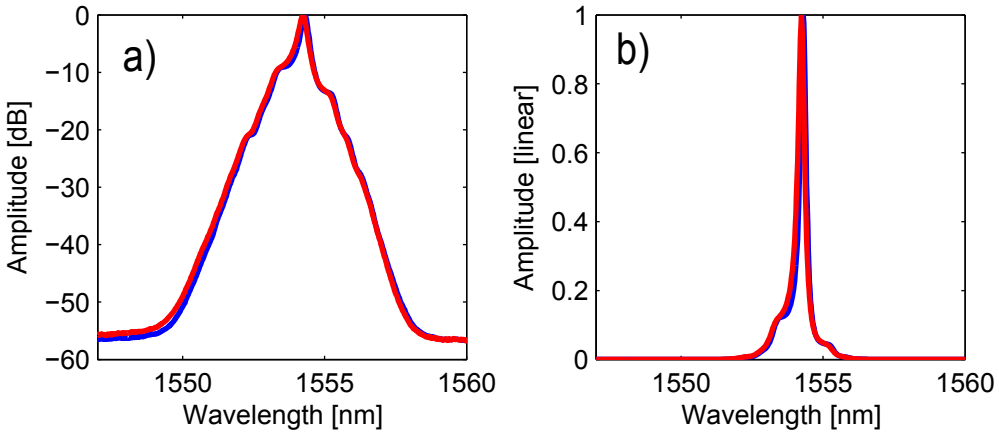

Figure 3.18: Normalized spectrum of the compressed (red line) and uncompressed (blue line) mode-locked pulses from the cavity using 400 m of non-linear fibre and a 12.8 nm filter in a dB (a) and in a linear (b)

pression in the ideal situation, assuming a fully linear chirp. Using 21 km of STF with an estimated dispersion of 17 ps.nm^{-1}.km^{-1} the pulse should be compressible to 385 ps, which is close to the obtained value of 350 ps, with the discrepancy allowed for the uncertainty on the value of dispersion. Temporal envelopes of both uncompressed and compressed pulses and their optical spectra are shown in Fig. 3.17 and Fig. 3.18 respectively. Due to no significant changes in the optical spectra it is typical to assume that compression because of the negative chirp of the STF took place in the absence of significant nonlinear contributions.

Moreover, it is important to mention that a higher degree of compression could not be achieved not only due to the long lengths required but also mainly due to the lack of stability of the pulse parameters. This was problematic because changes in the spectral width, or in the pulse duration, also lead to changes in the amount of dispersion needed to apply to the pulse in order to achieve compression close to transform-limit values. Therefore, also leading to different length requirements to achieve a transform-limited pulse. The 21 km STF was chosen mainly because it was the longest fibre readily available in the laboratory. Still, the 1.7 times compression was a good indication that the pulse was indeed chirped.

3.3 Conclusion

To summarize, harmonic mode-locking of a Raman laser was demonstrated in several configurations with the use of a few layers graphene as a saturable absorber. Different pulse durations and pulse shapes, as well as variable repetition rates were obtained depending on polarization, pump power adjustments, filter bandwidth and length of the gain fibre. Not all of these changes were quantitatively controlled and further studies are still necessary to understand more completely the dynamics of this Raman laser. Single pulse per round-trip operation could also be achieved when the longer lengths of fibre were used and a 600 ps pulse was compressed to 350 ps by 21 km of a STF. The use of an optical filter was shown to be essential to make mode-locking stable.

Although the demonstrated approach of combining Raman gain and graphene saturable absorption for mode-locking is a potential technique towards the development of wavelength versatile ultra-short pulsed sources, it is important to stress that these are still preliminary results. A lot of laser and material engineering are still needed in order to make the current performance level, specially in terms of stability, useful for applications. The low modulation depth of graphene of about 2%, or even of a few layers graphene, is still an obstacle towards stable mode-locking of Raman lasers. Carbon nanotubes, for example, usually present modulation depths in the range of 12 to 20%. This issue should possibly be addressed by stacking together a few graphene samples, which was not possible in our configuration due to the fact that we were not using a polymer film with graphene embedded on it, but graphene directly deposited on the outer face of an optical patch-cord.

Is also important to mention that current performance of CNT-based saturable absorber in mode-locking, specially of Raman lasers, are much closer to practical applications, as demonstrated in chapter 2, than graphene-based saturable absorbers. Nonetheless, this is still ongoing research, and further development of graphene technology together with the use of fibres with higher Raman gain, therefore allowing shorter cavities, can potentially be a way towards better performance in order to realize the huge potential of the combination of Raman amplification and graphene in mode-locking.

4 Ultrafast Raman lasers in highly doped germanium fibre

As discussed in previous chapters, Raman amplification is a very useful technique to generate laser sources at non-conventional wavelengths that are not covered by the emission band of rare-earth-doped elements. Nonetheless, the fact that Raman lasers usually need very long fibre lengths (hundreds of meters) and/or very high pump powers, is still a hindrance to a more widespread use of Raman laser in practical systems.

This is true because long fibre lengths can reduce the compactness of the source, which is exactly one of the advantages of fibre lasers. However, more importantly, in pulsed systems long lengths do not allow single-pulse per round trip at high-repetition rates, and moreover it can also be problematic to the mode-locking dynamics. To use short lengths in Raman laser is possible if one uses very high pump powers (Watts or tens of Watts), however that creates an even more dramatic situation.

High-power pump sources tend to be very expensive, and to insert them in all-fibre systems, other elements in the cavity, such as couplers and isolators, also have to be able to handle such powers which again increases the overall costs. Not to mention that such high power devices are sometimes difficult to be commercially obtained for unconventional wavelengths. The complexibility of the system also increases since new elements, for example couplers to remove the residual pump from the cavity, are needed. Furthermore, the dynamics of mode-locking can also suffer from the use of high optical power levels, specially in what concerns ASE noise contributions.

The only practical way to overcome such a situation in all-fibre systems is to use as the Raman gain medium, optical fibres with very high non-linearity, and hence high-Raman gain. High non-linearity can be achieved through two methods, either

by using PCFs with reduced effective area, that can be also filled with gases or liquids, or to simply use solid core single-mode fibres that are made or that are heavily doped with different materials, such as germanium oxide or phosphorus oxide. Both approaches can lead to high Raman gain, and therefore reduced fibre lengths and pump power requirements. Nevertheless, heavily doped fibres presents the advantage of being easier to incorporate in all-fibre configuration due to the low splicing losses that can be achieved.

In this chapter we present a Raman laser mode-locked by nanotubes using a silica fibre heavily doped with germanium oxide. Again, the dissipative soliton regime was used to generate long pulses that were compressed by an external fibre with anomalous dispersion. More importantly, reduced lengths of gain fibre were needed without the necessity of enhancing the levels of pump power used in the experiments shown in previous chapters.

The results presented in this chapter, which include the shortest (in terms of length) mode-locked Raman fibre laser ever reported using only 25 m of gain fibre, highlight the fact that this approach of using highly non-linear fibres can be used not only in CW Raman systems but also in short-pulsed Raman lasers, contributing to make them more simple and compact wavelength versatile laser sources.

4.1 Introduction

Silica single mode optical fibres have been extensively used as a medium to generate Raman amplification for both CW and pulsed signals at a number of wavelengths [110, 187, 188, 189], for various applications [190]. Nevertheless, the low Raman gain coefficient found in silica fibres ($g_r = 1.10^{-13}$ m/W at 1 μm) means that long lengths of fibre or pump lasers with very high powers have to be used, which is the main hindrance to a more extensive use of Raman amplification in practical and compact systems.

Initially other glasses, specially other oxide-based glasses, were proposed as an alternative to silica, such as GeO_2, B_2O_3, and P_2O_5 [191, 192]. It was shown in 1978 by F. L. Galeener et al. [191] that the Raman cross section in vitreous GeO_2 is nearly an order of magnitude greater than that of SiO_2. This concept was further explored in a later publication in 1981 by Shibata et al. [192], where enhancement of Raman gain was also confirmed for silica glasses doped with moderate concen-

trations (< 30 mol.%) of GeO_2, B_2O_3, and P_2O_5.

From these 3 elements that were initially proposed, GeO_2 was by far the most extensively used for Raman amplification in optical fibres [105, 193, 194] for the simple reason that it has a higher Raman gain [191]. Furthermore, the fact that GeO_2 was already routinely used in the fabrication process of STFs in order to enhance the fibre core refractive index [8], and also the fact that the peak of the main Raman shift in GeO_2 glass (420 cm^{-1}) is very close to the Raman shift in silica (440 cm^{-1}) also contributed to its preferred use as the doping element. Nevertheless, although much less used, there were also a considerable number of publications reporting Raman amplification in P_2O_5 doped fibres [194, 195, 196, 197].

In the last two decades, the rapid development of PCF technology has allowed fibres with very reduced effective areas [50] to be fabricated, leading to silica-based fibres with effective nonlinearity 40 times higher than STFs [106]. In this case, the increase in the Raman gain is due to the increase in non-linearity that arise because of the higher power density concentrated in a small effective area. In solid-core PCFs, this value can be further enhanced by doping the reduced core with elements such as germanium oxide [198]. Another candidate for low-threshold Raman generation in optical fibre is gas-filled hollow-core PCFs [199, 200, 201], specially using hydrogen, which has allowed single-pass Raman generation in less than 3 meters of fibre [201]. The main drawback of the use of such highly non-linear PCFs is the fact their integration into all-fibre configuration is not as straight-forward as it is with solid-core silica fibres doped with germanium oxide and fibre splices might suffer from excessive losses of several dBs. This is particularly problematic for Raman lasers since the high pump power levels required to achieve lasing could potentially lead to fibre fuses [202]. Therefore the light in such systems is usually bulk-coupled to the gain fibre, losing the benefits associated with an all-fibre configuration.

More recently, over the last ten years, the increase in the number of applications for lasers in the wavelength region over 2 μm [203], specially for medical applications due to fundamental vibrational peaks of the O-H bond in water at 1.94 and 2.95 μm [204], has lead to an increase interest in the development of laser sources in the mid-infrared. For wavelengths around 2 μm the easiest solution is to use thulium-doped, or even holmium-doped (Ho^{3+}) silica fibres. Nevertheless, silica fibres become very lossy for wavelengths above 2 μm, and therefore other glasses have to be used. Fluoride fibres [14], or more precisely ZBLAN glasses (ZrF_4-BaF_2-LaF_3-AlF_3-NaF),

are amongst the most used hosts for laser generation between 2 to 4 μm, not only because they present moderate losses for such wavelengths ($<$ 10 dB/km for wavelengths lower than 3.2 μm) but also due to the fact that they can be doped with elements such as thulium, erbium and holmium that are able through different electronic transitions to generate and amplify light at a number of wavelengths in that region [203].

Despite the fact that the Raman gain scales inversely with wavelength, the broadband nature of Raman amplification can still be used for wavelengths above 2 μm. The use of silica fibres heavily doped with germanium as the gain medium in Raman fibre lasers was already reported for wavelengths slightly higher than 2 μm [105, 205]. Other non-silica glasses that have been used to fabricate Raman fibre lasers towards the mid-infrared are chalcogenide [206, 207], and fluoride glasses [208]. Tellurite glasses can also potentially be used for this purpose [209], however up to date the only reports of Raman fibre lasers based on tellurite fibres were carried out at wavelengths around 1.55 μm [210]. The possibilities of making Raman lasers to operate beyond the 2 μm region is further explored in subsection 4.1.3.

In this section we describe the physics involved in enhancing the Raman gain in optical glasses, first in silica doped fibres and later in other non-silica-based fibres, and explain how this can potentially pave the way towards the fabrication of very compact and efficient Raman fibre lasers. Issues concerning the fabrication process of such fibres are also covered in this section.

4.1.1 Raman gain in heavily doped silica fibres

As mentioned previously, the first relative measurement of the Raman spectra of different oxide glasses usually used to generate Raman gain was done in 1978 by F. L. Galeener et al. [191], from where Fig. 4.1 was taken. The plot was normalized as a function of the peak Raman intensity for SiO_2, and it was found that GeO_2, P_2O_5 and B_2O_3 have respectively a Raman cross section 9.2, 5.7 and 4.7 times that of silica. Moreover, P_2O_5 has a second peak at a higher shift that is still 3.1 times higher than silica. These materials were strong candidates for the gain medium for Raman amplification both because they were already widely used in optical fibre technology [211] and also because they are glasses that have low optical losses [192].

Fig. 4.1 is also good to illustrate the fact that different materials present different

Raman shifts. It can be observed that the peak shift for maximum Raman gain in GeO_2 (420 cm^{-1}) is very close to the shift in SiO_2 (440 cm^{-1}), which brings the immediate advantage of allowing the usage of germanium-based Raman amplifiers using the same devices, such as couplers and filters, that are currently used in Raman amplifiers based on silica fibre. On the other hand, materials such as P_2O_5 and B_2O_3, which have a main peak at the shift of 640 and 808 cm^{-1} respectively, can be used to achieve different gain bands from a same pump wavelength, highlighting the broadband wavelength versatility of Raman gain. Moreover, such materials with larger frequency shifts can also be used to achieve the same gain bands obtained when using SiO_2 fibres, however using less cascaded shifts [196], reducing the system complexity.

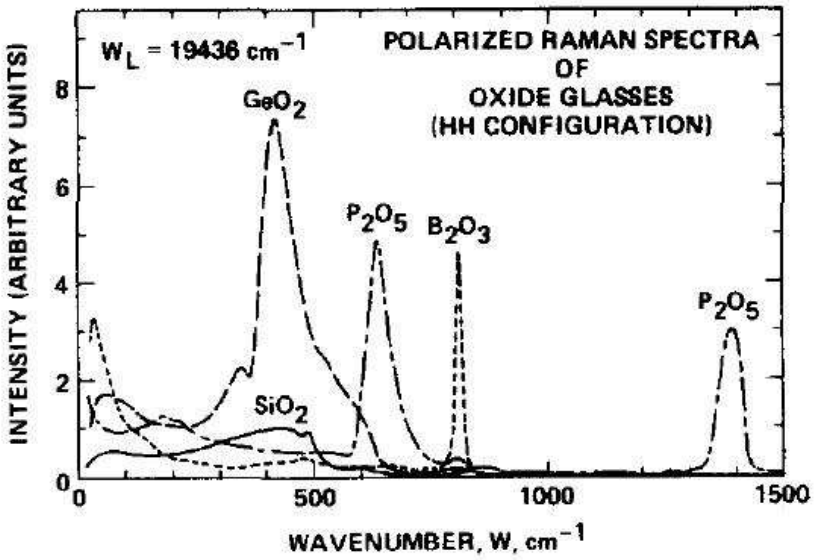

Figure 4.1: The relative Raman spectra of vitreous GeO_2, B_2O_3, SiO_2 and P_2O_5, taken from Ref. [191].

This possibility of using different materials to obtain optical amplification at different wavelengths can be clearly seen in Fig. 4.2, where it is shown the Stokes wavelength obtained from a pump at 532 nm and 1060 nm, for a shift of 440 cm^{-1} from SiO_2, 420 cm^{-1} from GeO_2, 808 cm^{-1} from B_2O_3, and 650 and 1390 cm^{-1} from P_2O_5 glasses. Fig. 4.2 was generated by a MATLAB code that was simply starting

from an initial wavelength in nm, converting it to frequency, subtracting from it the correspondent frequency shift in THz of the given material, and then again converting it back to wavelength. The same operation was realized successively for the higher stokes orders.

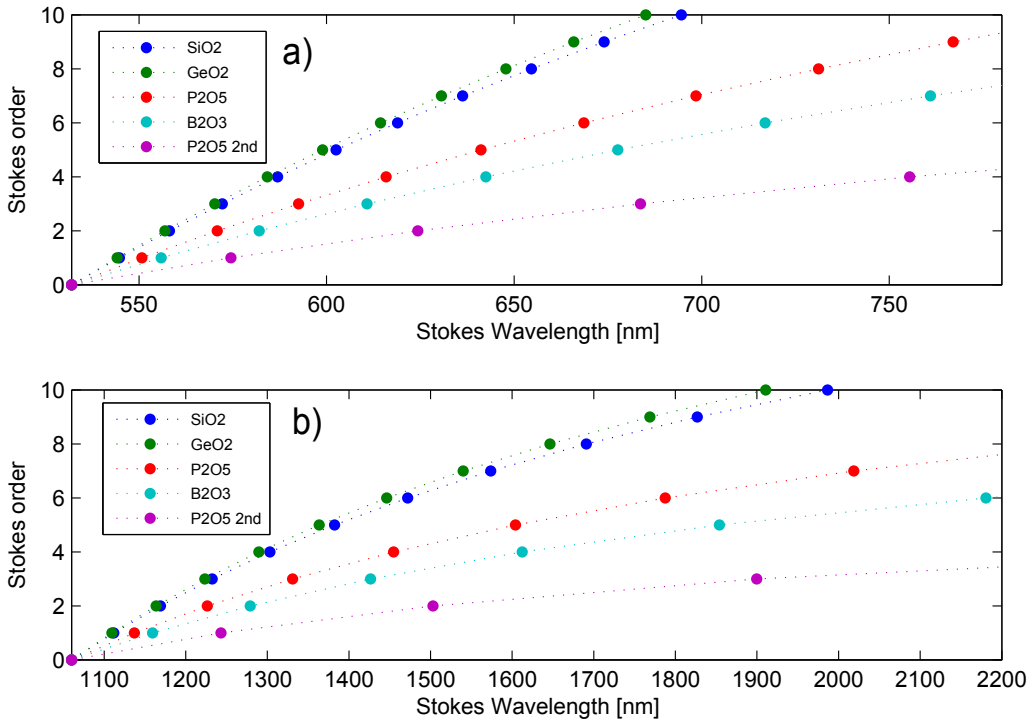

Figure 4.2: Frequency shift of n-th order from a pump at 532 nm (figure (a)) and from a pump at 1060 nm (figure (b)) for GeO_2, B_2O_3, SiO_2 and P_2O_5 glasses. For the case of P_2O_5 it is shown the Stokes shift for both peaks at 650 and 1390 cm^{-1}.

It can be observed that for both cases the wavelengths obtained from Raman shifts from SiO_2 and GeO_2 are very close to each other, especially for the first 4 or 5 Stokes order. Raman lasers that are cascaded to Stokes orders higher than 4 or 5 are more rare because after each shift they become less efficient, therefore needing higher pump powers. Nonetheless, if a very highly non-linear fibre is used, such lasers can be built even presenting moderate efficiencies. In Ref. [212], for example, a 7-th order cascaded Raman fibre laser is built from an ytterbium fibre laser at 1.07 μm using only 3 meters of a silica fibre heavily doped with germanium

showing 70 % conversion efficiency.

The most important feature of Fig. 4.2, however, is the fact that other glasses can be used to fill the gaps left from the discrete nature of the Raman shifts, which stress the wavelength versatility of the Raman gain, even when the pump wavelength cannot be changed. This wavelength versatility is further enhanced by the fact that the Raman gain not only in silica but also in P_2O_5 and in GeO_2 glasses is also relatively broad (> 25 THz), which can be used in systems to tune the amplification band from its peak position.

The possibility of achieving higher wavelengths using less cascaded Raman orders is also an important benefit that can arise from the use of other glasses, because it allows to reduce, for example, the amount of fibre gratings needed in the system, helping to reduce costs and enhancing simplicity. This is particularly true if the second peak of a P_2O_5 at 1390 cm^{-1} is used to provide the optical amplification. This is the case, for example, in Ref. [196] where a silica fibre doped with P_2O_5 was used to built a Raman fibre laser at 1.48 μm from a Nd:YAG laser at 1.06 μm using only 2 Raman shifts. Such lasers can serve as a pump for Erbium-doped amplifiers.

A study similar to the work published by F. L. Galeener et al. [191] was reported 3 years later in 1981 by N. Shibata et al. [192] where they measured the Raman spectra for silica fibre doped with the same glasses studied previously, namely GeO_2, P_2O_5 and B_2O_3. The doping concentration of the fibres studied in [192] were maintained between 10 and 30 mol.%, mainly due to the fact that that were many technological limitations at that time about the fabrication of doped optical fibres and higher concentrations were very difficult to achieve [205]. Nonetheless, the results showed by N. Shibata et al. can shed light about some of the reasons why later some glasses were more used in doped fibres than others.

It was shown in [192] that the shape of the Raman spectrum of GeO_2 doped fibre is virtually the same as the vitrous GeO_2 spectrum, with the main peak at a shift of 425 cm^{-1} instead of at 420 cm^{-1}. The main differences, however, were observed for P_2O_5 and B_2O_3 doped fibres. It was shown that the peak at 808 cm^{-1} is drastically reduced when B_2O_3 is incorporated in SiO_2 glass, and no other stronger peak due to B_2O_3 molecular vibration is observed, which basically discards the possibility of efficiently using boron-doped fibres as the Raman gain medium at least for moderate concentrations of B_2O_3. A similar situation is found in P_2O_5 silica doped fibres,

where the main peak at 650 cm^{-1} is also greatly reduced, however, the second peak at 1390 cm^{-1}, although slightly shifted to 1320 cm^{-1}, is maintained and it increases linearly with the doping concentration. Indeed, this is also confirmed by the fact that later publications of Raman fibre lasers using P_2O_5 doped silica fibres were basically all using a Raman shift around 1320 cm^{-1} [194, 196, 197].

Although the Raman cross section of the 1320 cm^{-1} Raman shift in phosphorus-doped silica fibre is not much higher than the Raman cross section of pure silica (it would be needed for example 60 mol.% for a twice fold increase), P_2O_5 doped fibres are still very useful due to their capability of achieving higher wavelengths with less cascaded orders, which as mentioned previously reduces costs and enhances the laser efficiency. In addition, Bragg gratings can be directly written in phosphosilicate fibres by using 193 nm radiation [196], which can make the system even more compact.

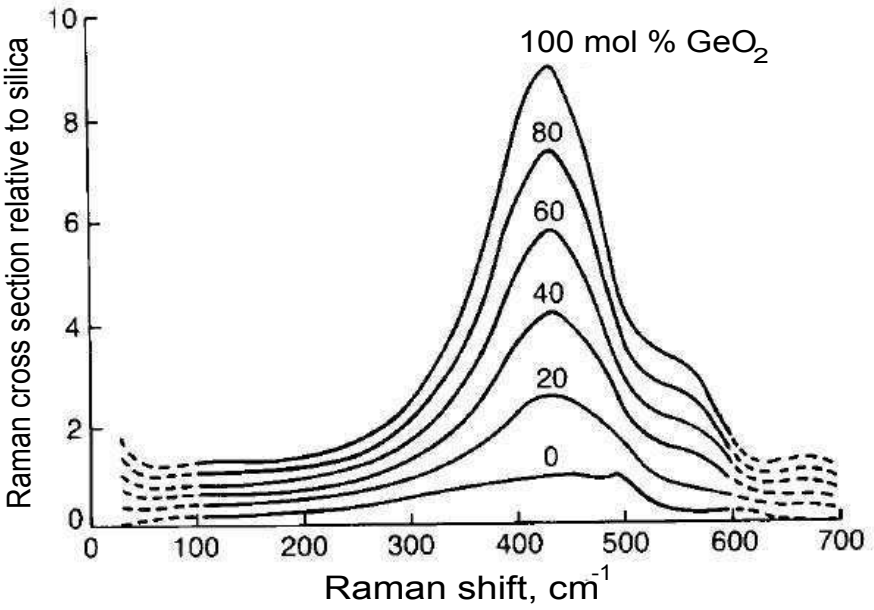

Figure 4.3: Calculated Raman cross section relative to silica for different GeO_2 doping concentrations, adapted from [145].

From the studies published previously on oxide-doped optical glasses [191, 192] it becomes evident that GeO_2 is the element that can provide higher levels of

Raman gain enhancement in comparison to the other elements studied. This was indeed confirmed by the large amount of reports on Raman fiber lasers based on germanium doped-fibres [105, 144, 193, 194, 205, 212]. The Raman cross section of germanium doped fibre increases proportionally to the doping concentration. This was experimentally measured in Ref. [145] for germanium concentrations up to 65 mol.%, and it is illustrated at Fig. 4.3 (also taken from [145]), where numerical calculations of the Raman spectra is shown for different GeO_2 doping levels. It is important to highlight from Fig. 4.3 the fact that the peak of the Raman cross section for the case of 100 mol.% doping shows good agreement to the value obtained in Ref. [191] for vitreous GeO_2. Moreover, it can also be observed that the concentration of GeO_2 does not have significant effect on the Raman shift for maximum gain.

Very high Raman gains were initially prevented due to the fact that fibres with levels of doping of more than 30 to 40 mol.% were difficult to manufacture [205] mainly because of the mismatch of the thermal expansion coefficients of GeO_2 and SiO_2 [105]. Nevertheless, in 2004 it was reported for the first time [205, 212] the fabrication of single mode fibres with core concentrations of 51 to 97 mol.% of GeO_2. These new levels of doping concentrations opened up the possibility of unprecedented high levels of Raman gain to be obtained from GeO_2 doped fibre. In Ref. [205], for example, a silica fibre with 75 mol.% concentration of GeO_2, which is exactly the same fibre used in the experiments shown in this chapter, was demonstrated to possess a Raman gain coefficient at least an order of magnitude higher than previous GeO_2 doped fibres used as highly non-linear Raman gain medium. In order to stress the capability of such fibre to provide a large amount of Raman gain over short lengths of fibre, still in Ref. [205] a 10 W Raman laser at 1.12 μm was built using only 3 meters of this fibre from a 13 W pump at 1.06 μm.

In addition, it is also important to mention that such high Raman gains found in GeO_2 doped fibres are not only due to the gain provided by the material in itself, as demonstrated in Fig. 4.1 and 4.3, but is also due to the fact that high concentrations of germanium in the core result in a higher refractive index difference (Δn) between the core and the cladding, which allows reduced effective areas, as a result increasing even more the gain. This fact can be observed, for example, about the fibre used in the experiments that are shown later in this chapter, that presents an effective area of only 5 μm^2 at 1.55 μm, which is about 15 times lower

then STFs and still approximately 3.5 times lower than the highly non-linear fibre used in the previous experiments shown in this thesis. This helps to confirm the well-established fact that silica fibres heavily doped with GeO_2 are ideal hosts for compact Raman gain generation in all-fibre configurations.

4.1.2 Raman lasers beyond 2 μm

Although this is not explored in the experiments reported in this chapter, it is also important to briefly discuss another possibility that the usage of different glasses can bring to Raman fibre lasers, which is the capability of providing optical amplification in fibres for wavelengths over 2 μm towards the mid-infrared. As mentioned previously in the introduction of this chapter, the prime driver in such wavelength ranges is mainly due to the interest for optical sources to be used in medical and military applications [203].

Dopant(s)	Host glass	Pump λ (μm)	Laser λ (μm)	Transition
Er^{3+}, Yb^{3+}	Silicate	0.975	1.5	$^4I_{13/2} \rightarrow {}^4I_{15/2}$
Tm^{3+}, Ho^{3+}	ZBLAN	0.792	1.94	$^3F_4 \rightarrow {}^3H_6$
Tm^{3+}	Silicate	0.793	2.05	$^3F_4 \rightarrow {}^3H_6$
Tm^{3+}, Ho^{3+}	Silicate	0.793	2.1	$^5I_7 \rightarrow {}^5I_8$
Ho^{3+}	Silicate	1.950	2.14	$^5I_7 \rightarrow {}^5I_8$
Tm^{3+}	ZBLAN	1.064	2.31	$^3H_4 \rightarrow {}^3H_5$
Er^{3+}	ZBLAN	0.975	2.8	$^4I_{11/2} \rightarrow {}^4I_{13/2}$
Ho^{3+}, Pr^{3+}	ZBLAN	1.1	2.86	$^5I_6 \rightarrow {}^5I_7$
Dy^{3+}	ZBLAN	1.1	2.9	$^6H_{13/2} \rightarrow {}^6H_{15/2}$
Ho^{3+}	ZBLAN	1.15	3.002	$^5I_6 \rightarrow {}^5I_7$
Ho^{3+}	ZBLAN	0.532	3.22	$^5S_2 \rightarrow {}^5F_5$
Er^{3+}	ZBLAN	0.653	3.45	$^4F_{9/2} \rightarrow {}^4I_{9/2}$
Ho^{3+}	ZBLAN	0.89	3.95	$^5I_5 \rightarrow {}^5I_6$

Figure 4.4: Characteristic of infrared rare-earth doped fibre lasers with emission wavelengths above 1.55 μm, adapted from [203].

A summary of the main fibre laser sources used from 1.5 to 4 μm can be seen in Fig.4.4, which was adapted from [203]. For wavelengths around 1.9 to 2 μm

the easy solution is to use thulium doped fibre lasers based on silica. Nevertheless, silica glass poses a limit for light generation above 2 μm due to the fact that at longer wavelengths ($\lambda > 2$ μm), infrared absorption related to vibrational resonances increase exponentially, being for example approximately 110 dB/km at 2.1 μm [105]. Different glasses that present lower losses towards the mid-infrared then have to be used for such purposes, and a few possibilities are chalcogenide [16, 213], fluoride [14] or telluride glasses [209]. It also important to mention, that tellurium is actually also a chalcogenide element [213], however in the recent literature about optical fibres academics are tending to treat them as a separate category on its own [209, 210]. Thulium doped ZBLAN, which is a type of fluoride fibre [214], can extend the wavelength reach slightly further until ~2.3 μm, and above that there are still other wavelength ranges that can be reached by ZBLAN doped with other rare earth ions such as erbium or holmium.

Here we come to a similar problem faced by rare-earth doped fibre lasers from 1 to 2 μm, which are the wavelength gaps that are not covered by the emission bands of such elements. And again, one of the possible solutions to this problem is to use Raman amplification instead. Nevertheless, it is important to mention that from 2 to 4 μm the technical challenges involved in Raman generation are many, such as high loss and the inverse wavelength dependence of the Raman gain, and this is still a current research field with few experimental demonstrations.

For wavelengths slightly higher than 2 μm, heavily doped GeO_2 fibres suits well for Raman generation, both due to its high Raman gain and also because the infrared absorption in germanium oxide is slighty up-shifted in comparison with silica. This was already demonstrated for example in Ref.[105] where a 1.15 W average power Raman laser at 2.1 μm was built from a 16 W thulium doped fibre laser pump at 1.94 μm. In the same experiment, in a single pass configuration, for a pump power of 20 W, a second Stokes shift were obtained at 2.32 μm, however with very reduced optical power. In Ref. [205] a fourth-order cascaded Raman laser was build lasing at 2.2 μm with 250 mW average power from a pump power of 1.1 W at 1.6 μm provided by a Erbium doped fibre laser. In both cases [105, 205], the fibre used was heavily doped GeO_2 fibre with 75 mol.% concentration.

For longer wavelengths the main candidates for the Raman gain media are chalchogenide, telluride and fluoride glasses. With the current technology fluoride fibres can present losses of approximately 0.65 dB/km at 2.6 μm and <20 dB/km at 2.9

μm [203]. In terms of loss, fluoride fibres suit well for Raman generation using as pump a high power thulium doped laser at around 2 μm. The Raman shift in such fibres is $\sim$ 579 cm^{-1} (or 17.37 THz) [215], which allows first order Stokes generation around 2.2 μm direct from a pump at 2 μm. Indeed, a Raman fibre laser was reported generating 3.7 W at 2231 nm using 29 m of a fluoride fibre as the Raman gain and as a pump a thulium doped fibre laser pumped by a 36 W diode at 791 nm [208]. The Raman gain (g_0) in such fibres was measured to be around 3.52*10^{-14} m/W for an unpolarized pump at the wavelength of 2 μm, which is slightly higher than the Raman gain for silica at such wavelengths ($\sim$2.5*10^{-14} m/W). Longer lengths of fibre and higher pump powers should allow Raman cascaded lasers in such fibres at longer wavelengths around 2.5 or even at 3 μm.

Telluride fibres present a wide transmission window (0.35 to 5 μm) and fibres with losses of 20 dB/km at 2 μm have already been fabricated [216]. The Raman shift in this type of fibres is $\sim$ 743 cm^{-1} (or 22.3 THz) and the Raman gain is estimated to be $\sim$16 times higher than in silica [210]. Nevertheless, the losses beyond the 2 μm region for usual telluride fibres are often still very high [217] for efficient Raman generation, which together with the fact that they are difficult fibres to be commercially obtained [206] have still not allowed any experimental report of a Raman fibre laser beyond 2 μm in such glasses.

The most promising glass for Raman generation over 2 μm are chalcogenide glasses based on As_2S_3 and As_2Se_3, which have Raman gain coefficients approximately 50 and 350 times larger then typical fluoride glasses, respectively [207]. Indeed, this possibility was already experimentally confirmed twice [206, 207]. In Ref. [206] a 0.5 m As_2Se_3 fibre was used to generate 0.64 W at 2.06 μm from a thulium doped pump at 2.05 μm, which represents a shift of only 28 cm^{-1} (or 0.84 THz). A second order Stokes shift could also be observed at 2.07 μm when the length was extended. To avoid such short Raman shifts, an As_2S_3 can be used instead, which shows a 340 cm^{-1} or (10.2 THz) as shown in Ref.[207] where a 0.6 W peak power Raman laser at 3.34 μm in 3 m of fibre was experimentally demonstrated using as a pump an erbium-doped fluoride glass lasing at 3 μm.

Lastly, it is important to mention that this possibility of using other glasses to build Raman lasers beyond the 2μm is a very recent research topic, being more a future perspective than a established reality. The experimental work show in this chapter is fully focused at shorter wavelengths, with the intent to demonstrate that

the concept of using heavily doped GeO_2 fibres can be used in pulsed systems in order to reduce pump power or fibre length requirements.

4.2 Short cavity length Raman pulsed laser using DWCNT

In this section a mode-locked Raman laser using 25 m of a GeO_2 doped fibre as the gain medium is introduced employing double wall carbon nanotubes as the saturable absorber. The oscillator generates long chirped pulses in the dissipative soliton regime, which are externally compressed in a STF. This result confirms the capability of applying to short-pulsed lasers the same benefits offered by highly doped fibres that were so far mainly applied to CW systems. The laser here presented is so far the mode-locked Raman laser using the shortest length of gain fibre ever reported. This result was published in Ref.[144].

4.2.1 Experimental setup

The all-fibre geometry used in this experiment, illustrated in Fig. 4.5, was similar to the one used for the results shown in chapter 3 (Fig. 3.6), with only a few changes. Here the Raman gain fibre was replaced by a 25 m length heavily doped GeO_2 with 75 mol.% core-doping concentration, which is the same fibre utilized in Ref. [105, 205, 218]. The gain fibre was core pumped through a wavelength-division multiplexer (WDM) by the same CW Raman laser at 1455 nm used in chapter 3, again with no need for synchronous pumping. The saturable absorber used was the same DWCNT polymer composite described in section 2.2 integrated into the cavity between a pair of fibre connectors. The only difference is the fact that this time the laser was operating at 1550 nm and not at 1660 nm, which is not a problem to the absorber due to its broadband operation range. Again, the absence of an absorber caused the laser to operate in a CW regime. A polarization insensitive in-line optical isolator and a fibre-based polarization controller were used to stabilize the mode-locking. Light is extracted from the unidirectional cavity through a 15% output coupler. In order to prevent high-levels of un-depleted pump power damaging the passive cavity components, two WDM couplers were again needed to extract the residual pump light after the gain fibre. Another difference from the previous setup used in chapter 3 is the fact that an optical filter was not necessary to achieve mode-locking.

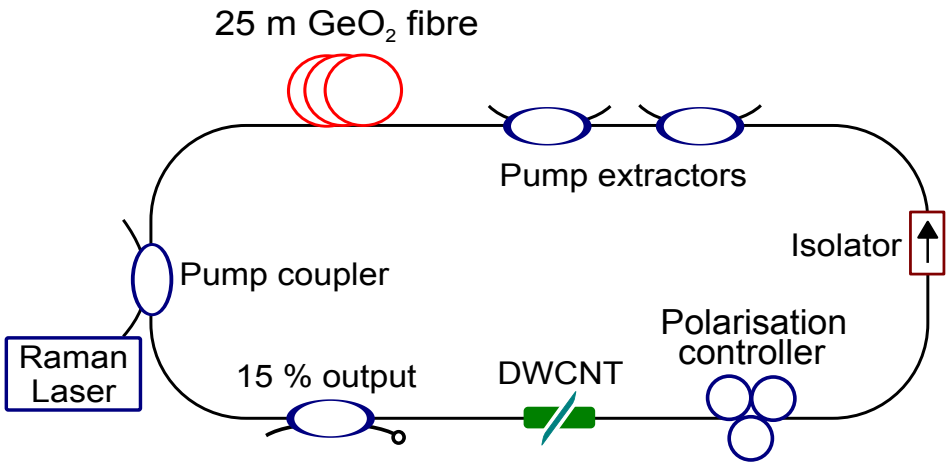

Figure 4.5: Experimental setup of the mode-locked Raman laser using 25 m of GeO_2 doped fibre. DWCNT: Double wall carbon nanotube-based saturable absorber.

The GeO_2 doped fibre was obtained from a collaboration with the Fiber Optics Research Center in Moscow, where it was originally fabricated [194]. The zero dispersion wavelength of this fibre is expected to be in the 1.8 to 1.9 μm range [218], which means that for this experiment both pump (1455 nm) and signal (1555 nm) were propagating under normal dispersion. The losses are around 40 dB/km at 1550 nm, which is much higher than the losses of STFs for the same wavelength, however since we are using only 25 m of fibre, the overall loss is kept to approximately 1dB. The cut-off wavelength is around 1.4 μm and the core diameter is $\sim$2 μm. The refractive index difference between the core and the cladding (Δn) is 0.11, which allows very reduced effective areas, and therefore very high non-linearities and Raman gain. The effective area of the fibre was not given. However, calculations of the Raman gain coefficient of this fibre based on the net gain obtained experimentally are made in the end of this section in order to compare the performance of this fibre with the OFS Raman fibre used in the experiments shown in the previous chapters. Nevertheless, the 75 mol.% concentration of GeO_2 doping in the core in comparison with the estimation of 12 mol.% calculated for the previous fibre is already a good indication of a much higher Raman gain. Other parameters of the fibre are described in more detail in [205].

4.2.2 Results

Mode-locking

Self-starting mode-locking is achieved for pump powers from 4.2 W up to 4.8 W, which is the maximum power available from our CW pump source. It is important to notice here, that in comparison, for example, with the oscillator used in the previous chapter (100 m case), there was a slight reduction of the threshold from 4.4 W to 4.2 W even using a gain fibre 4 times shorter, which highlights the extremely high non-linear properties of this GeO_2 doped fibre. The same is valid if we compare this threshold condition with the result showed in section 2.3 where 6.87 W of pump power were needed in a 60 m oscillator at 1.06 μm. Here, even operating at a higher wavelength where the Raman gain is smaller and using less than half of the length previously used, the threshold power was still reduced by ∼40%.

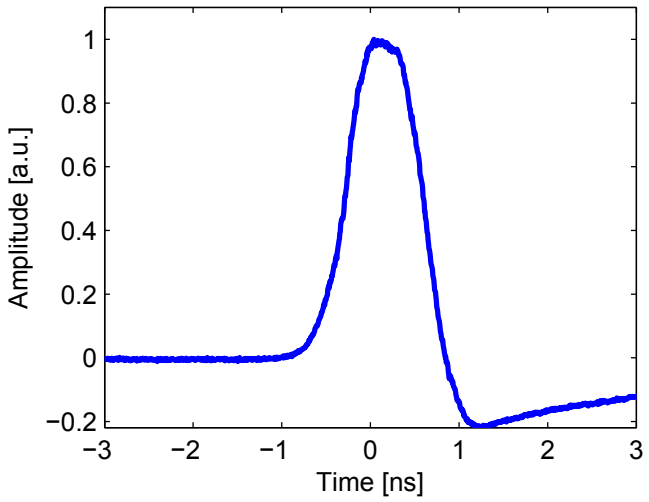

Figure 4.6: Normalised oscilloscope trace of the pulse at the output of the mode-locked cavity.

Fig. 4.6 and Fig. 4.7 show the oscilloscope pulse trace and the spectrum obtained at the output cavity for laser operation just above threshold. The pulses are 850 ps long with 0.4 mW average power. The long pulse duration again is due to the fact that the laser is operating in the dissipative soliton regime. The spectrum centred at 1552.5 nm has a 3 nm 6-dB bandwidth and a squared shaped, a typical signature of lasers operating in the dissipative soliton regime.

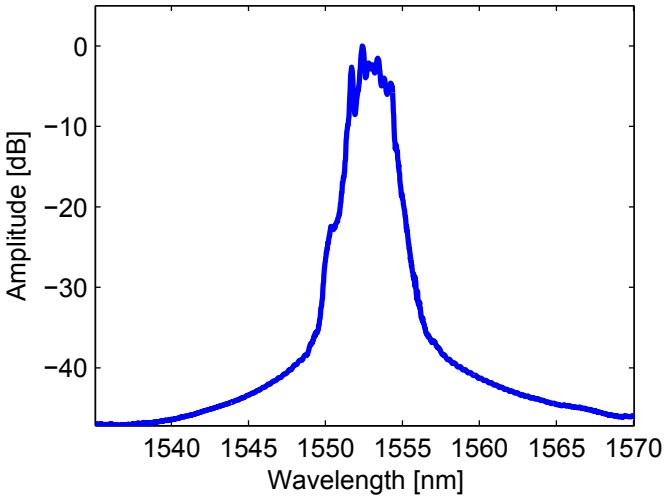

Figure 4.7: Normalized optical spectrum of the pulse at the output of the mode-locked cavity.

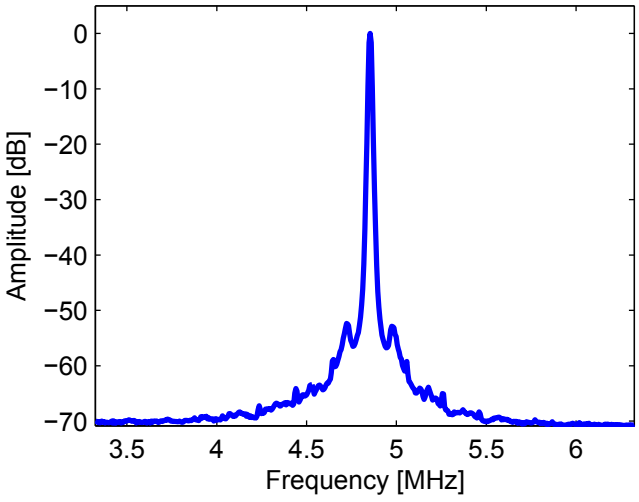

Figure 4.8: Normalized RF trace of the fundamental frequency of the pulse at the output of the mode-locked cavity.

The RF trace of the fundamental harmonic of the cavity, shown in Fig. 4.8 confirms the single pulse per round trip operation at a repetition rate of 4.85 MHz in the approximately 42 m cavity. In terms of Raman lasers operating at the fundamental frequency of the cavity, this is much higher than many previous reports of, for example, 64 KHz in Ref.[119], 205 KHz in Ref.[120] and 300 KHz in Ref. [121], and still higher than the previous reports shown in this thesis of 1.72 MHz in section 2.2, 2.87 MHz in section 2.3 and 0.9 MHz in section 3.2.

Still in Fig. 4.8, it can be observed that the extinction ratio between the peak and the noise floor is around 70 dB. Nevertheless, there is a fairly large pedestal 50 dB below the peak, which indicates that the laser operates with a fairly high noise jitter and pulse-to-pulse amplitude fluctuations, as it is usual observed in mode-locked Raman fibre lasers. The extended RF trace showing the first 7 harmonics can be observed in Fig. 4.9, which shows a small noise contribution at half the fundamental frequency of the cavity, which is a sign of a regular amplitude modulation at such frequency. The modest average power, together with long pulse duration and the MHz repetition rate, results in a pulse peak power of 0.1 W, and a pulse energy of 0.08 nJ.

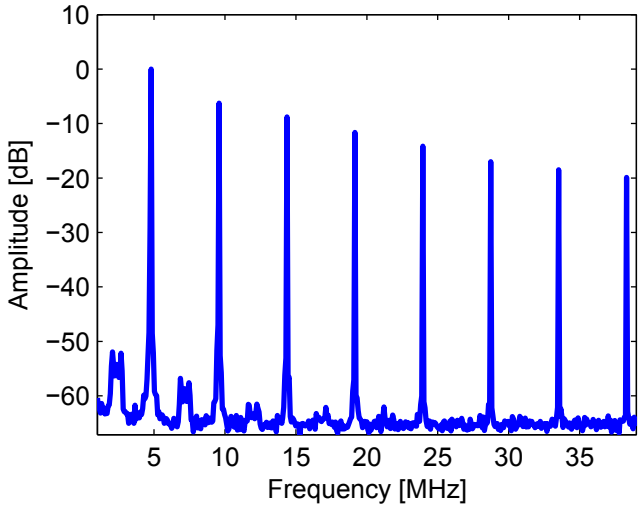

Figure 4.9: Normalized extended RF trace showing the fundamental frequency and its first 7 harmonics.

Pulse compression

In order to verify the chirped nature of the pulses, as expected for a mode-locked laser operating in the normal dispersion regime, 12.7 km of STF was spliced to the output of the laser providing anomalous group-velocity dispersion. The oscilloscope pulse trace and the spectrum after the STF are shown in Fig. 4.10 and 4.11 respectively. Given the initial 850 ps pulse duration and the 3 nm bandwidth centred at around 1552.5 nm, the pulse is approximately 317 times transform limited, and considering a dispersion value of -17 ps/nm/km in the STF, it should be compressed to about 202 ps after 12.7 km of fibre. The obtained pulse, shown in Fig. 4.10 is 185 ps long, which is within 10% of its expected value, showing a compression of ∼4.6 times.

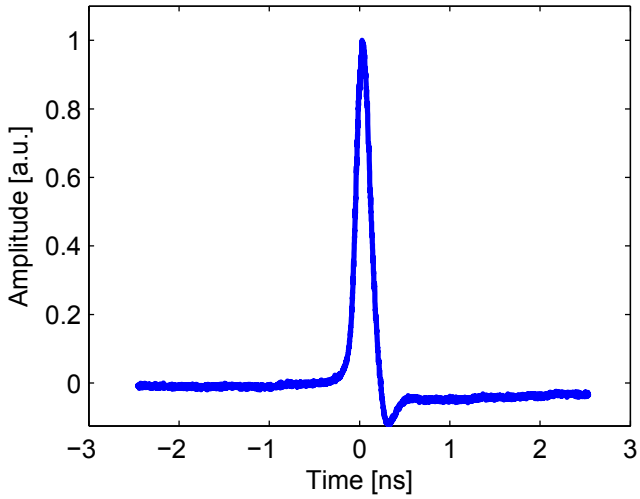

Figure 4.10: Normalised oscilloscope trace of the compressed pulse after 12.7 km of STF.

The spectrum, which can be seen in Fig. 4.11, still has a 6-dB bandwidth of 3 nm and it was again centred at 1552.5 nm. It shape remained without any significant change, which is a clear indication that no non-linear effect took part during the compression. The average power after compression was reduced to 0.2 mW, however the shorter pulse duration enhanced the peak power to 0.22 W.

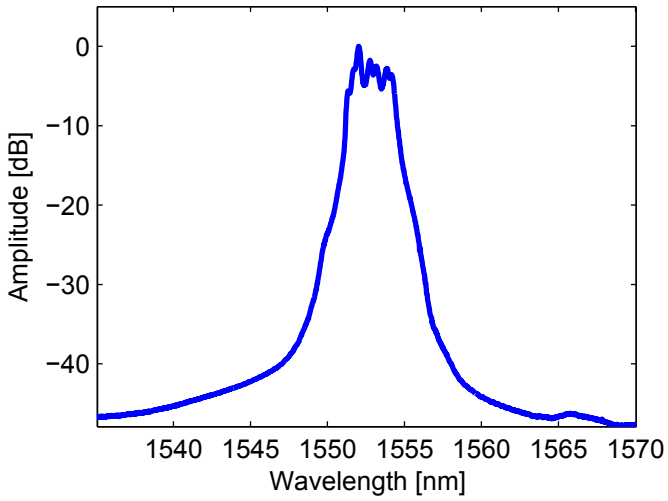

Figure 4.11: Normalised optical spectrum of the compressed pulse after 12.7 km of STF.

Gain and threshold analysis

The overall loss of the cavity was measured to be around 8.7 dB, which means that from the threshold condition, where loss equals gain, that the Raman gain provided by the fibre under 4.2 W of pump power was also 8.75 dB. The Raman gain can be expressed in dB by Eq. 4.1 [8], where G_r is the Raman gain in $W^{-1}.km^{-1}$, P_t is the threshold pump power and L_{eff} is the effective length which can be calculated by Eq. 4.2 where L is the fibre length and α_p is the pump loss, which in our case was 50 dB/km [212]. Calculating the Raman gain from Eq. 4.1 we obtain G_r = 18.1 $W^{-1}.km^{-1}$ at 1550 nm for an un-polarised pump, which is approximately 7.2 times higher than the G_r of the OFS Raman fibre used in the experiments shown in chapters 2 and 3. This is in accordance with the predictions made in Ref. [212] where it was stated that this fibre possesses a Raman gain coefficient an order of magnitude higher than usual high-gain non-linear fibres used for Raman amplification. Moreover, the G_r of this fibre at 1.5 μm is approximately 47.5 higher than the G_r of an STF at the same wavelength.

$$G_{dB} = \exp(2G_r P_t L_{eff}) \tag{4.1}$$

$$L_{eff} = \frac{1 - \exp(-\alpha_p L)}{\alpha_p} \tag{4.2}$$

In order to estimate how much the fibre length could be reduced by increasing the pump power, and also how much the pump power could be reduced by increasing the fibre length, we can use the G_r calculated above and reshape Eq. 4.1 and 4.2 into Eq. 4.3 and 4.4 so that we obtain the fibre length as a function of pump power for threshold condition (loss = gain). The result is plot in Fig. 4.12 where the gain fibre length needed to achieve 8.7 dB of gain (threshold) is estimated for pump powers from 3.2 to 30 W.

$$L = \frac{-\ln(1 - \alpha_p L_{eff})}{\alpha_p} \tag{4.3}$$

$$L_{eff} = \frac{\ln(G_{dB})}{2 G_r P_t} \tag{4.4}$$

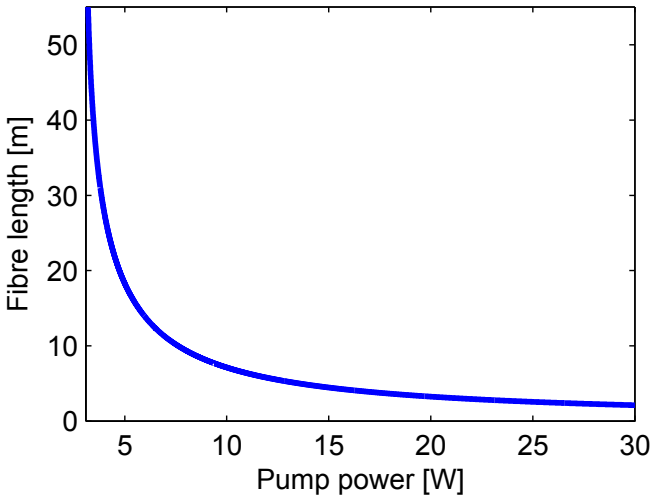

Figure 4.12: Estimation of fibre length needed to achieve threshold condition as a function of pump power.

From Fig. 4.12 it can be seen that short lengths of fibre can be used if we increase the pump power a few times. Using 5 W for example, should already allow to reduce the fibre length to ∼18 m, whereas only 7 m of this GeO_2 fibre would be needed

for a 10 W pump. Using a 20 W pump, which is a reasonable value to be obtained with fibre lasers, one could potentially build the same oscillator using only 3.2 m of gain fibre. In a more extreme case, increasing the pump to 30 W only 2.1 m of fibre would be necessary in order to achieve threshold.

Looking at the lower pump power side of Fig. 4.12, it can be seen that even by increasing significantly the fibre length, the pump power necessary to achieve threshold for this fibre can not be reduced considerably. This happens due to the fact that this fibre has a very large loss at 1450 nm (50 dB/km) which becomes a real hindrance to the Raman gain if we use long lengths of fibre. From Eq. 4.1 and 4.2, for example, it can be calculated that for pump powers lower than ∼3 W, no length of fibre can satisfy threshold condition. Nevertheless, a modest reduction of pump power could still be achieved for slightly longer fibre lengths. For example, 40 m of this gain fibre should allow only 3.5 W of pump power to be used, whereas if 55 m is used, threshold could be obtained under only 3.1 W.

There are however a few possible routes that could lead to a further reduction of pump power requirements even using this same fibre. The first one would be to reduce the overall losses of the oscillator (current 8.7 dB), which could be done for example by optimizing the splice losses and also by using a more purified (in terms of diameter range) CNT-sample that could present less losses, which in our case, according to Fig. 2.6 is ∼3dB. Again according to Eq. 4.3 and 4.4, by reducing the threshold requirement by only 2.5 dB, an oscillator with 70 m of gain fibre and 2.6 W of pump should be achievable. Another possible route could be to build a Raman laser for a pump at this fibre loss-minima, which is around 1.9 μm [212] where the loss is ∼20 dB/km. For this case, although the Raman gain would be reduced to approximately 13.1 W.km^{-1} due to its inverse wavelength dependence, we can estimate that the pump power could be reduced to 2 W for a 85 m length of gain fibre.

It is also important to mention that although these gain calculations can give good insights into how to use this fibre to reduce length or power requirements, every change on either fibre length or pump power would certainly affect the mode-locking dynamics of the laser due to differences of dispersion, self-phase modulation and gain levels, which could lead to temporal and spectral parameters of the pulse to diverge from the results presented in Figs. 4.6, 4.7 and 4.8.

Noise calculations

As could be observed in many of the Raman lasers reported in this thesis, the RF spectrum of such lasers in terms of both extinction ratio and pedestal components are much noisier than state-of-the-art rare-earth doped mode-locked fibre lasers. As mentioned previously, this is expected to be due to the high levels of pump power, which generate ASE, that are needed and also due to the nearly instantaneous nature of the Raman gain which immediately transfers any noise from the pump direct to the amplified signal. Here we present a quantitative study of the energy fluctuation and the timing jitter of the GeO_2-based Raman oscillator, following a methodology described in Ref. [219]. A comparison with other previously reported mode-locked Raman fibre lasers is difficult to undertake since the RF traces tend to be omitted from such publications [117, 118, 119, 120, 121, 142].

The pulse-to-pulse energy fluctuations and the timing jitter can be calculated from parameters obtained from the RF trace of the fundamental frequency and a higher order harmonic on a long and a short span [219]. This is plotted in Fig. 4.13 where the RF trace of the fundamental (b) and of the 30th harmonic (d) are shown on a long range span (3 MHz), with 300 Hz resolution, and also on a short range span (100 kHz), with 100 Hz resolution (a) and (c). The pulse-to-pulse energy fluctuations can be expressed by Eq. 4.5 where ΔP is the power ratio between the central spike at the fundamental frequency and the peak of the noise floor (Fig. 4.13(b)), Δf (Hz) is the frequency width of the noise component (Fig. 4.13(a)), and Δf_{Res} (Hz) is the resolution bandwidth of the spectrum analyser. In our case, $\Delta P = 1.58{*}10^{-7}$ (-68 dB), $\Delta f = 300$ kHz, and $\Delta f_{Res} = 100$ Hz, which gives a $\Delta E = 0.0218$ or 2.18%, which is not much higher than other published results found in literature. In Ref.[218] for example the ΔE obtained for a mode-locked thulium-doped fibre laser using the same calculation was 0.5%.

$$\Delta E = \sqrt{\frac{\Delta P \Delta f}{\Delta f_{Res}}} \tag{4.5}$$

The timing jitter can be calculated by Eq. 4.6 [219] using parameters from the RF trace of a higher harmonic, where T is the cavity period and n is the harmonic order. From Fig. 4.13(c) and (d), we obtain $\Delta P = 1.26{*}10^{-4}$ (-39 dB), $\Delta f = 15$ kHz, and $\Delta f_{Res} = 100$ Hz, which for $n = 30$ and $T = 206.1$ nm gives $\Delta T = 150$ ps.

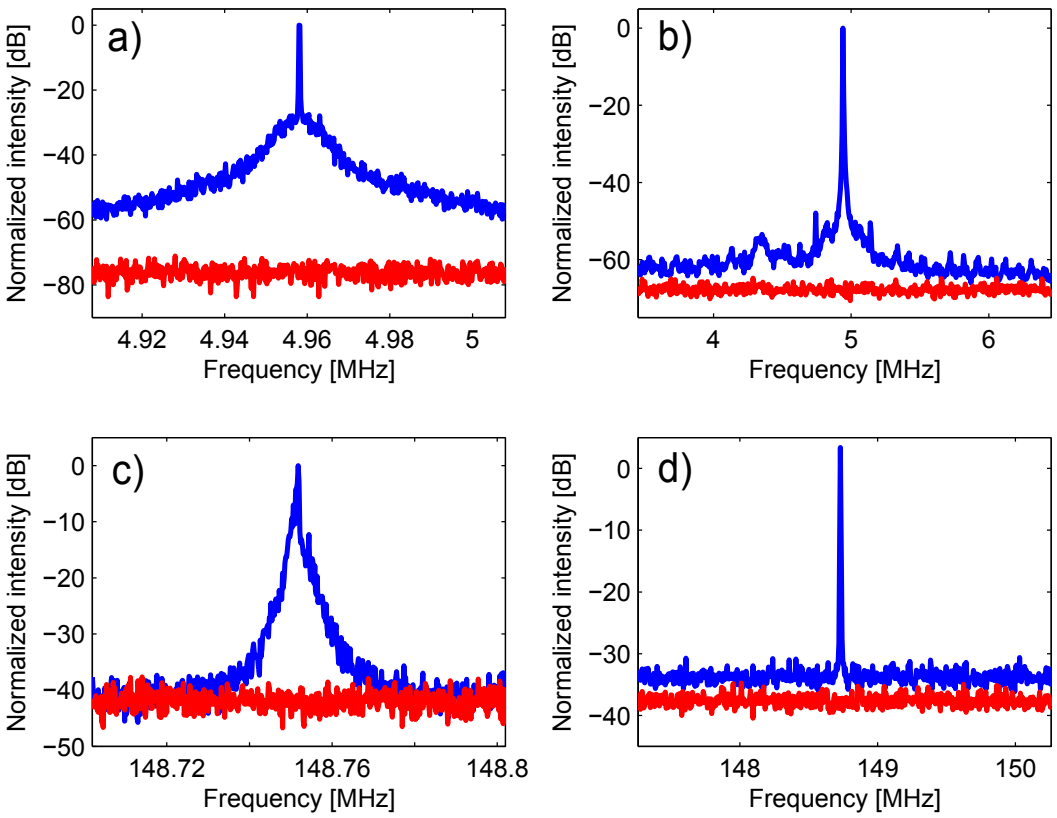

Figure 4.13: RF spectra. (b) Fundamental, and (d) 30th harmonic on a long range span (3MHz), with 300Hz resolution; (a) Fundamental, and (c) 30th harmonic on a short range span (100kHz), with 100Hz resolution. The noise floor is shown in red.

In comparison to the pulse duration obtained of 850 ps, the timing jitter is 17.6%, which can be considered to be a high value, indicating that this specific laser would not suit for applications that require low levels of jitter-noise, which nonetheless do not invalidate that fact that the concept of using heavily doped GeO_2 fibres can lead towards better performance in Raman lasers.

$$\Delta T = \frac{T}{2\pi n}\sqrt{\frac{\Delta P \Delta f}{\Delta f_{res}}} \tag{4.6}$$

4.3 Conclusion

In this chapter it was reiterated and discussed how different types of glasses can be used in order to reduce length and power requirements in Raman lasers, allowing such laser sources to be more simple, efficient, and produced with lower costs, which is usually difficult to achieve in Raman lasers due to the relatively low Raman gain provided by standard silica fibres. The main focus was on optical fibres highly doped with GeO_2, since this is by far the most often used material which is currently used to enhance the Raman gain of silica and that can even be used for Raman generation beyond the 2 μm region.

In this chapter we reported a passively mode-locked Raman laser using as the gain medium only 25 meters of a highly doped GeO_2 fiber (75 mol.%) in an all-fiber configuration, which is so far the mode-locked Raman oscillator using the shortest gain fibre ever reported. The mode-locking was achieved by employing double-wall carbon nanotubes as the saturable absorber, which are ideal to be used together with Raman gain in order to exploit the broadband nature of both, providing a solid technique to produce wavelength versatile short pulsed sources. The fundamental frequency of 4.85 MHz shows that ultrafast Raman lasers can move towards repetition rates that are comparable with rare-earth doped fibre systems. The net-normal dispersion cavity generated 850 ps long pulses at 1552.5 nm that were externally compressed by 12.7 km of STF to 185 ps, showing the chirped nature of the output pulses.

Gain calculations based on the GeO_2 fibre used in the experiment suggests that by using a moderately high pump power, in the range of a few tens of Watts, the fibre length of the gain fibre in the oscillator could be reduced to only a few

meters. By increasing the fibre length or by slightly reducing the cavity losses it is suggested that the pump power could be reduced to ∼3 W. Further reduction of pump power could happens if the laser operates at a wavelength in which the fibre present less losses (around 1.9 μm for example). Noise properties of this laser were also calculated, showing that the pulse-to-pulse energy fluctuations, in the region of a few percent, are not much higher than other previous reported mode-locked fibre lasers. The same can not be said about the pulse jitter, which was calculated to be of around 17% of the pulse duration, stressing that this is an issue that has to be treated if one is interested in applications where high levels of jitter can not be tolerated. A possible route towards a less noisier laser could be to considerably reduce the pump power.

5 Conclusion

The intent of this thesis was to make a contribution towards increasing the versatility in terms of wavelength for short-pulsed fibre lasers, so that the wavelength gaps between the emission band of usual rare-earth doped fibre amplifiers can be fulfilled by low-cost, simple, and compact laser sources. The approach chosen here was to use Raman amplification as the optical gain source and newly developed nanomaterials, such as carbon nanotubes and graphene, as the saturable absorber to generate the short-pulses through mode-locking.

Raman gain together with carbon nanotubes or graphene is an ideal combination as a simple technique to allow short pulse generation at theoretically any wavelength from the visible to at least the 2 μm region of the spectrum. Different to rare-earth doped fibres, the amplification due to stimulated Raman scattering does not rely on any electronic transition of an active ion, and provided that a suitable pump source is available it can be obtained virtually at any wavelength over the silica transparency window (0.4 - 2 μm). This broadband capability to provide gain in Raman amplifiers can be further extended towards the mid-infrared by using other glasses different from silica. This possibility is discussed briefly in chapter 4. Moreover, Raman amplification is intrinsically a very simple technique, which needs only an optical fibre with enough non-linearity and a pump with enough power, avoiding issues such as phase-matching which have to be taken into account in other wavelength tunable amplification schemes, such as in optical parametric amplification.

Carbon nanotubes and graphene, nano-materials developed approximately over the last two decades, both present saturable absorption over a broad wavelength range. Whereas in graphene this is an intrinsic property of the material due to its linear dispersion relation near the Dirac point, in carbon nanotubes this can easily be achieved by embedding in a single sample tubes with different diameters. This broadband capability of both materials is exactly what makes their combination

with Raman gain to be an innovative concept and a simple technique towards a more universal wavelength versatile short-pulsed source.

In chapter 2 we reported what was the first experimental demonstration of a Raman laser mode-locked by a carbon nanotube-based saturable absorber. A double-wall carbon nanotube sample was used in a erbium-pumped oscillator operating in the dissipative soliton regime generating 500 ps chirped pulses at 1660 nm that were externally compressed to 2 ps in 10 km of a fibre with anomalous dispersion. Additionally, in order to experimentally show the same technique at a different wavelength, we reported a ytterbium-pumped Raman laser operating at 1120 nm mode-locked by single-wall carbon nanotubes. The laser operating again in the dissipative soliton regime, generated 236 ps pulses with no short-time fluctuations shown on the autocorrelation trace.

The performance of both lasers in terms of noise and peak powers reported in chapter 2 can not be compared with state-of-the-art mode-locked lasers based on rare-earth doped amplifiers. The high noise levels are attributed mainly to the nearly instantaneous nature of the Raman gain, that specially under such very high levels of pump power can generate a lot of ASE and transfer any noise fluctuation from the pump direct to the signal. Nevertheless, these sources could still be used as a simple technique to generate short pulses at unconventional wavelengths for applications where low coherence levels are not problematic. Moreover, using optical fibres with even higher levels of non-linearity would allow lower pump powers and shorter lengths to be used, which should potentially allow these noise levels to be reduced. Additionally, the output power levels could easily be scaled up by using external Raman amplification, which would however enhance the noise levels of the laser. Lastly, it is important to mention that both, single-wall and double-wall carbon nanotubes did work effectively as the saturable absorber, always allowing a self-starting laser with single-pulse per round trip operation. Fine tuning of pulse parameters was possible by tuning the polarisation controllers.

In chapter 3, we demonstrated for the first time a Raman laser mode-locked by graphene. This time a cascaded Raman laser at 1450 nm was used as a pump source, generating the pulses at 1550 nm, extending the results again to a different wavelength range. Hundreds of picosecond pulses were obtained for different configurations using different lengths of a highly non-linear fibre and also for different intra-cavity filter bandwidth. Harmonic mode-locking and single pulse per

round trip operation were observed in this laser. Nevertheless, the performance of the laser was poorer in relation to both lasers reported in chapter 2, specially in terms of stability. This was attributed mainly due to the weak absorption found in graphene saturable absorbers.

Although graphene has this unique intrinsic property of presenting saturable absorption over a very broad wavelength range, which makes it in theory an ideal "universal" mode-locker, carbon nanotube-based saturable absorbers as it was confirmed by the lasers reported in this thesis still offers a more reliable solution for self-starting and stable single-pulse operation. Moreover, saturable absorbers based on carbon nanotubes can also offer broad wavelength range coverage ($\sim$1 μm) by using in the same device a broad range of tubes with different diameters. Nevertheless, it is important to mention that this broadband operation in carbon nanotubes are not as broad as in graphene and it comes of the expense of enhancing non-saturated losses. Therefore, it is plausible to imagine that there is still going to be research interest into engineering more robust and efficient Raman lasers mode-locked by graphene. The current ongoing research in graphene technology and also the development of optical fibres with enhanced non-linearities can pave the way towards such laser sources.

In chapter 3 we discuss the possibility of using silica fibres heavily-doped with GeO_2 (75 mo.%) that present extremely highly non-linearities in order to reduce pump power and fibre length requirements which are the main hindrances to a more extensive practical use of Raman lasers. Here we bring this concept also to pulsed lasers systems, reporting the experimental demonstration of a very short (25 m of gain fibre) Raman laser mode-locked by nanotubes and using $\sim$ 4.2 W of pump power. The oscillator generates 850 ps pulses that are externally compressed to 185 ps by a 12.7 km of a STF. This result highlights the fact that Raman lasers can with current technology move a step closer to the performance and size of lasers based on rare-earth doped materials, at least in terms of repetition rate and fibre length requirements. Further development of fibre technology should allow a further reduction of pump power and fibre length requirements.

Summarising, we have investigated the possibility of using Raman gain to create wavelength versatile simple and compact pulsed sources. It is clear from the results that the current development of mode-locked Raman lasers are still steps behind the performance of state-of-the-art rare-earth-doped fibre lasers, however they can be

used for applications that require laser radiation at non-conventional wavelengths. Moreover, although the results are only preliminary and still a lot of engineering has to be done in order to achieve better laser performances, the wavelength versatile concept of using carbon nanotubes and graphene together with Raman gain in a fibre oscillator was demonstrated to work. It is also clear that given the current technology carbon nanotubes perform much better than graphene as a mode-locker for Raman lasers, being a reliable source for self-starting single pulse operation.

As a future perspective, it is expected that the ongoing research on nano-materials could produce CNT-based or graphene samples with more absorption and less loss, which can still bring benefits towards better performance for Raman lasers. Another important issue is the technological development of low-loss optical fibres with different glasses that can allow higher Raman gains to be obtained in shorter lengths, which from the 1 to 2 μm region has GeO_2 doped fibre as the main candidate. A new trend that has recently arisen in the laser field, is the possibility of building Raman lasers for the spectral region beyond 2 μm. The development of high power thulium doped fibre laser to be used as a pump together with the development of low-loss and highly non-linear chalchogenide fibres are amongst the main candidates towards such sources. Graphene and some carbon nanotubes can also potentially be used for mode-locking at such wavelengths.

List of publications

Journal papers

C. E. S. Castellani, E. J. R. Kelleher, J. C. Travers, D. Popa, T. Hasan, Z. Sun, E. Flahaut, A. C. Ferrari, S. V. Popov, J. R. Taylor, *"Ultrafast Raman laser mode-locked by nanotubes"*, Optics Letters **36**, pp.3996 (2011).

C. E. S. Castellani, E. J. R. Kelleher, Z. Luo, K. Wu, C. Ouyang, P. P. Shum, Z. Shen, S. V. Popov, J. R. Taylor, *"Harmonic and single pulse operation of a Raman laser using graphene"*, Laser Physics Letters **9**, pp. 223 (2012).

C. E. S. Castellani, E. J. R. Kelleher, D. Popa, T. Hasan, Z. Sun, A. C. Ferrari, S. V. Popov, J. R. Taylor, *"CW-pumped short pulsed 1.12 μm Raman laser using carbon nanotubes"*, Laser Physics Letters **10**, pp. 015101 (2013).

Conference papers

C. E. S. Castellani, E. J. R. Kelleher, D. Popa, Z. Sun, T. Hasan, A. C. Ferrari, S. V. Popov, J. R. Taylor, *"Nanotube-based passively mode-locked Raman laser"*, Conference on Lasers and Electro-Optics (CLEO), Baltimore, USA (2011).

E. J. R. Kelleher, C. E. S. Castellani, J. C. Travers, Z. Sun, A. C. Ferrari, S. V. Popov, J. R. Taylor, *"On the Study of Giant Chirp Oscillators"*, Progress In Electromagnetics Research Symposium (PIERS), Marrakesh, Morocco (2011).

C. E. S. Castellani, E. J. R. Kelleher, D. Popa, Z. Sun, T. Hasan, A. C. Ferrari, S. V. Popov, J. R. Taylor, *"Nanotube-based passively mode-locked Ytterbium-pumped Raman laser"*, Conference on Lasers and Electro-Optics Europe (CLEO EUROPE), Munich, Germany (2011).

C. E. S. Castellani, E. J. R. Kelleher, D. Popa, Z. Sun, T. Hasan, A. C. Ferrari, O. I. Medvedkov, S. A. Vasiliev, E. M. Dianov, S. V. Popov, J. R. Taylor, "Mode-locking by nanotubes of a Raman laser based on a highly doped GeO_2 Fiber", Conference on Lasers and Electro-Optics (CLEO), San Jose, USA (2012).

Bibliography

[1] G. P. Agrawal, *Fiber-Optic Communications Systems*, 3rd Edition John Wiley & Sons (2002).

[2] J. Hecht, *City of light: the history of fiber optics*, Oxford: Oxford University Press (1999).

[3] C. W. Hansell, US Patent 1,751,584, "Picture transmission," filed 13 Aug. 1927, issued 25 March 1930.

[4] F. P. Kapron, D. B. Keck, and R. D. Mauer, *"Radiation losses in glass optical waveguides"*, Appl. Phys. Lett., **17** pp. 423 (1970).

[5] M. Kawachi, A. Kawana, and T. Miyashita, *"Low-loss singlemode fibre at the material-dispersion-free wavelength of 1-27 μm"*, Electron. Lett., **13** pp. 442 (1977).

[6] M. Horiguchi, and H. Osanai, *"Spectral losses of low-OH-content optical fibres"*, Electron. Lett., **12** pp. 310 (1976).

[7] T. Miya, Y. Terunuma, T. Hosaka, and T. Miyashita, *"Ultimate low-loss single-mode fiber at 1.55 μm "*, Electron. Lett., **15** pp. 106 (1979).

[8] G. P. Agrawal, *Nonlinear Fiber Optics*, 4th Edition Academic Press (2010).

[9] J. B. MacChesney and D. J. DiGiovanni, *"Materials development of optical fiber"*, J. Am. Ceram. Soc. **73**, pp. 3537 (1990).

[10] K. Tsujikawa, K. Tajima, and M. Ohashi, *"Rayleigh Scattering Reduction Method for Silica-Based Optical Fiber"*, J. Lightwave Technol. **18**, pp. 1528 (2000).

[11] K. Tsujikawa and M. Ohashi, *"Rayleigh Scattering in K_2O-MgO-SiO_2 and Na_2O-B_2O_3-SiO_2 Glasses"*, Opt. Fiber Technol. **6**, pp. 74 (2000).

[12] G. A. Thomas, B. L. Shraiman, P. F. Glodis and M. J. Stephan, *"Towards the clarity limit in optical fibre"*, Nature **404**, pp. 262 (2000).

[13] M. J. Yuen, *"Ultraviolet absorption studies of germanium silicate glasses"*, Appl Opt. **21**, pp. 136 (1982).

[14] D. C. Tran, G. H. Sigel, B. Bendow, *"Heavy metal fluoride glasses and fibers: A review"*, J. Lightwave Technol. **2**, pp.566 (1984).

[15] H. Takahashi, I. Sugimoto, *"A germanium-oxide glass optical fiber prepared by a VAD method"*, J. Lightwave Technol. **2**, pp.613 (1984).

[16] T .Kanamori, Y. Terunuma, S. Takahashi, T. Miyashita, *"Chalcogenide glass fibers for mid-infrared transmission"*, J. Lightwave Technol. **2**, pp.607 (1984).

[17] J. R. Taylor, *Optical Solitons - Theory and Experiment*, 1st Edition Cambridge University Press (1992).

[18] J. C. Diels and W. Rudolph, *Ultrashort Laser Pulse Phenomena*, 2nd Edition Academic press (2006).

[19] M. E. Marhic, *Fiber Optical Parametric Amplifiers, Oscillators and Related Devices*, 1st Edition, Cambridge University Press (2007).

[20] T. Li, *Optical Fiber Communications: Vol. 1 Fiber Fabrication*, Academic Press (1985).

[21] J. D. Kafka, T. Baer, and D. W. Hall, *"Mode-locked erbium-doped fiber laser with soliton pulse shaping"*, Opt. Lett. **14**, pp.1269 (1989).

[22] A. Fernandez, T. Fuji, A. Poppe, A. Fürbach, F. Krausz, and A. Apolonski, *"Chirped-pulse oscillators: a route to high-power femtosecond pulses without external amplification"*, Opt. Lett. **29**, pp.1366 (2004).

[23] E. J. R. Kelleher, J. C. Travers, E. P. Ippen, Z. Sun, A. C. Ferrari, S. V. Popov, and J. R. Taylor, *"Generation and direct measurement of giant chirp in a passively mode-locked laser"*, Opt. Lett. **34**, pp.3526 (2009).

[24] G. P. Agrawal and M. J. Potasek, *"Nonlinear pulse distortion in single-mode optical fibers at the zero-dispersion wavelength"*, Phys. Rev. A **3**, pp.1765 (1986).

[25] V. A. Bogatyrjov, M. M. Bubnov, E. M. Dianov, and A. A. Sysoliatin, *"Advanced fibres for soliton systems"*, Pure Appl. Opt. **4**, pp.345 (1995).

[26] S. V. Chernikov and P. V. Mamyshev, *"Femtosecond soliton propagation in fibers with slowly decreasing dispersion"*, J. Opt. Soc. Am. B **8**, pp.1633 (1991).

[27] S. V. Chernikov, D. J. Richardson, E. M. Dianov and D. N. Payne, *"Picosecond soliton pulse compressor based on dispersion decreasing fiber"*, Electron. Lett. **28**, pp.1842 (1992).

[28] R. W. Boyd, *Nonlinear Optics*, 2nd Edition Academic press (2003).

[29] G. P. Agrawal, *"Nonlinear fiber optics: its history and recent progress"*, J. Opt. Soc. Am. B **28**, pp.A1 (2011).

[30] R. H. Stolen, *"The Early Years of Fiber Nonlinear Optics"*, J. Lightwave Technol. **26**, pp. 1021 (2008).

[31] R. H. Stolen and C. Lin, *"Self-phase-modulation in silica optical fibers"*, Phys. Rev. A **17**, pp. 1448 (1978).

[32] M. N. Islam, L. F. Mollenauer, R. H. Stolen, J. R. Simpson, and H. T. Shang, *"Cross-phase modulation in optical fibers"*, Opt. Lett. **12**, pp. 625 (1987).

[33] A. Hasegawa and F. Tappert, *"Transmission of stationary nonlinear optical pulses in dispersive dielectric fibers. I. Anomalous dispersion"*, Appl. Phys. Lett. **23**, pp. 142 (1973).

[34] P. Grelu and N. Akhmediev, *"Dissipative solitons for mode-locked lasers"*, Nature Photonics **6**, pp. 84 (2012).

[35] A. Chen, G. Wong, S. Murdoch, R. Leonhardt, J. Harvey, J. Knight, W. Wadsworth, and P. Russell, *"Widely tunable optical parametric generation in a photonic crystal fiber"*, Opt. Lett. **30**, pp. 762 (2005).

[36] F. Forghieri, R. Tkach, A. Chraplyvy, and D. Marcuse, *"Reduction of four-wave mixing crosstalk in WDM systems using unequally spaced channels"*, IEEE Photon. Technol. Lett. **6**, pp.754 (1994).

[37] K. Tai, A. Hasegawa, and A. Tomita, *"Observation of modulational instability in optical fibers"*, Phys. Rev. Lett. **56**, pp. 135 (1986).

[38] E. Brainis, D. Amans, and S. Massar, *"Scalar and vector modulation instabilities induced by vacuum fluctuations in fibers: Numerical study"*, Phys. Rev. A **71**, pp. 023808 (2005).

[39] P. Franco, F. Fontana, I. Cristiani, M. Midrio, and M. Romagnoli, *"Self-induced modulational-instability laser"*, Opt. Lett. **20**, pp. 2009 (1995).

[40] C. J. S. de Matos, D. A. Chestnut, and J. R. Taylor, *"Low-threshold self-induced modulational instability ring laser in highly nonlinear fiber yielding a continuous-wave 262-GHz soliton train"*, Opt. Lett. **27**, pp. 915 (2002).

[41] E. J. Greer, D. M. Partick, P. G. J. Wigley and J. R. Taylor, *"Generation of 2 THz repetition rate pulse trains through induced modulational instability"*, Electron. Lett. **25**, pp.1246 (1989).

[42] J. M. Dudley, J. R. Taylor, *Supercontinuum Generation in Optical Fibers*, 1st Edition Cambridge University Press (2010).

[43] L. F. Mollenauer, R. H. Stolen, J. P. Gordon, and W. J. Tomlinson, *"Extreme picosecond pulse narrowing by means of soliton effect in single-mode optical fibers"*, Opt. Lett. **8**, pp.289 (1983).

[44] F. M. Mitschke and L. F. Mollenauer, *"Ultrashort pulses from the soliton laser"*, Opt. Lett. **12**, pp.407 (1987).

[45] J. C. Knight, T. A. Birks, P. St. J. Russell, and D. M. Atkin, *"All-silica single-mode optical fiber with photonic crystal cladding"* Opt. Lett. **21**, pp.1547 (1996).

[46] R. F. Cregan, B. J. Mangan, J. C. Knight, T. A. Birks, P. St. J. Russell, P. J. Roberts, D. C. Allan, *"Single-Mode Photonic Band Gap Guidance of Light in Air"*, Science **285**, pp.1537 (1999).

[47] J. C. Knight, T. A. Birks, P. St. J. Russell, and J. P. de Sandro, *"Properties of photonic crystal fiber and the effective index model"*, J. Opt. Soc. Am. A **15**, pp.748 (1998).

[48] J. C. Knight, J. Arriaga, T. A. Birks, A. Ortigosa-Blanch,W. J.Wadsworth and P. S. J. Russell. *"Anomalous dispersion in photonic crystal fiber"*, IEEE Photonic. Tech. Lett. **12** pp. 807 (2000).

[49] T. A. Birks, J. C. Knight, and P. St.J. Russell, *"Endlessly single-mode photonic crystal fiber"*, Opt. Lett. **22**, pp.961 (1997).

[50] V. Finazzi, T. M. Monro, and D. J. Richardson, *"Small-core silica holey fibers: nonlinearity and confinement loss trade-offs"*, J. Opt. Soc. Am. B **20**, pp.1427 (2003).

[51] A. Ferrando, E. Silvestre, P. Andres, J. Miret, and M. Andres, *"Designing the properties of dispersion-flattened photonic crystal fibers"*, Opt. Express **9**, pp.687 (2001).

[52] A. Kudlinski, A. K. George, J. C. Knight, J. C. Travers, A. B. Rulkov, S. V. Popov, and J. R. Taylor, *"Zero-dispersion wavelength decreasing photonic crystal fibers for ultraviolet-extended supercontinuum generation"*, Opt. Express **14**, pp.5715 (2006).

[53] J. C. Travers, A. B. Rulkov, B. A. Cumberland, S. V. Popov, and J. R. Taylor, *"Visible supercontinuum generation in photonic crystal fibers with a 400W continuous wave fiber laser"*, Opt. Express **16**, pp.14435 (2008).

[54] R. E. Kennedy, S. V. Popov, and J. R. Taylor, *"Ytterbium gain band self-induced modulation instability laser"*, Opt. Lett. **31**, pp.167 (2006).

[55] R. T. Murray, E. J. R. Kelleher, S. V. Popov, A. Mussot, A. Kudlinski, and J. R. Taylor, *"Synchronously pumped photonic crystal fiber-based optical parametric oscillator"*, Opt. Lett. **37**, pp.3156 (2012).

[56] J. Zhou, K. Tajima, K. Nakajima, K. Kurokawa, C. Fukai, T. Matsui and I. Sankawa, *"Progress on low loss photonic crystal fibers"*, Opt. Fiber Technol. **11**, pp.101 (2005).

[57] T. P. White, R. C. McPhedran, C. M. de Sterke, *"Confinement losses in microstructured optical fibers"*, Opt. Lett. **26**, pp.1660 (2001).

[58] U. Keller, *"Recent developments in compact ultrafast lasers"*, Nature **424**, pp. 831 (2003).

[59] A. H. Zewail, *"Femtochemistry: atomic-scale dynamics of chemical bond"*, J. Phys. Chem. A **104**, pp.5660 (2000).

[60] L. F. Mollenauer, P. V. Mamyshev, J. Gripp, M. J. Neubelt, N. Mamysheva, L. Grüner-Nielsen, and T. Veng, *"Demonstration of massive wavelength-division multiplexing over transoceanic distances by use of dispersion-managed solitons"*, Opt. Lett. **25**, pp.704 (2000).

[61] T. H. Maiman, *"Stimulated optical radiation in ruby"*, Nature **187**, pp.493 (1960).

[62] W. E. Lamb Jr., *"Theory of an optical laser"*, Phys. Rev. **134**, pp.A1429 (1964).

[63] M. DiDomenico, *"Small-signal analysis of internal (coupling type) modulation of lasers"*, J. Appl. Phys. **35**, pp.2870 (1964).

[64] L. E. Hargrove, R. L. Fork, and M. A. Pollack, *"Locking of He-Ne laser modes induced by synchronous intracavity modulation"*, Appl. Phys. Lett. **5**, pp.4 (1964).

[65] H. W. Mocker and R. J. Collins. *"Mode competition and self-locking effects in a q-switched ruby laser"*, Appl. Phys. Lett. **7**, pp.270 (1965).

[66] A. J. D. Maria, D. A. Stetser and H. Heynau, *"Self mode-locking of lasers with saturable absorbers"*, Appl. Phys. Lett. **8**, pp.174 (1966).

[67] I. P. Alcock, A. I. Ferguson, D. C. Hanna and A. C. Tropper, *"Mode-locking of a Neodymium-doped monomode fibre laser"*, Electron. Lett. **22** pp.268 (1986).

[68] I. N. Duling, *"All-fiber modelocked figure eight laser"*, In Optical Society of America 1990 Annual Meeting **5**, pp.306 (1990).

[69] I. N. Duling, *"All-fiber ring soliton laser mode locked with a nonlinear mirror"*, Opt. Lett. **16**, pp.539 (1991).

[70] F. Stutzki, F. Jansen, T. Eidam, A. Steinmetz, C. Jauregui, J. Limpert, and A. Tnnermann, *"High average power large-pitch fiber amplifier with robust single-mode operation"*, Opt. Lett. **36**, pp.689 (2011).

[71] W. S. Wong, X. Peng, J. M. McLaughlin, and L. Dong, *"Breaking the limit of maximum effective area for robust single-mode propagation in optical fibers"*, Opt. Lett. **30**, pp.2855 (2005).

[72] D. J. Richardson, J. Nilsson, and W. A. Clarkson, *"High power fiber lasers: current status and future perspectives"*, J. Opt. Soc. Am. B **27**, pp.B63 (2010).

[73] Y. Jeong, J. Sahu, D. Payne, and J. Nilsson, *"Ytterbium-doped large-core fiber laser with 1.36 kW continuous-wave output power"*, Opt. Express **12**, pp.6088 (2004).

[74] J. Limpert, F. Roser, T. Schreiber, and A. Tünnermann, *"High-power ultrafast fiber laser systems"*, IEEE J. Sel. Top. Quantum Electron. **12**, pp.233 (2006).

[75] F. Röser, J. Rothhard, B. Ortac, A. Liem, O. Schmidt, T. Schreiber, J. Limpert, and A. Tünnermann, *"131 W 220 fs fiber laser system"*, Opt. Lett. **30**, pp.2754 (2005).

[76] H. A. Haus, *"Mode-locking of lasers"*, IEEE J. Sel. Top. Quantum Electron. **6**, pp.1173 (2000).

[77] T. Brabec, Ch. Spielmann, P. F. Curley, and F. Krausz, *"Kerr lens mode locking"*, Opt. Lett. **17**, pp.1292 (1992).

[78] M. E. Fermann, M. J. Andrejco, Y. Silberberg, and M. L. Stock, *"Passive mode locking by using nonlinear polarization evolution in a polarization-maintaining erbium-doped fiber"*, Opt. Lett. **18**, pp.894 (1993).

[79] K. A. Stankov, *"A mirror with an intensity-dependent reflection coefficient"*, Appl. Phys. B **45**, pp. 191 (1988).

[80] U. Morgner, F. X. Kärtner, S. H. Cho, Y. Chen, H. A. Haus, J. G. Fujimoto, E. P. Ippen, V. Scheuer, G. Angelow, and T. Tschudi, *"Sub-two-cycle pulses from a Kerr-lens mode-locked Ti:sapphire laser"*, Opt. Lett. **24**, pp.411 (1999).

[81] U. Keller, K. J. Weingarten,F. X. Kartner, D. Kopf,B. Braun, I. D. Jung, R. Fluck, C. Honninger, N. Matuschek, J. Aus der Au, *"Semiconductor saturable absorber mirrors (SESAMs) for femtosecond to nanosecond pulse generation in solid-state lasers"*, IEEE J. Sel. Top. Quantum Electron. **2**, pp.435 (1996).

[82] S. Kivistö, T. Hakulinen, A. Kaskela, B. Aitchison, D. P. Brown, A. G. Nasibulin, E. I. Kauppinen, A. Härkönen, and O. G. Okhotnikov, *"Carbon nanotube films for ultrafast broadband technology"*, Opt. Express **17**, pp.2358 (2009).

[83] A. K. Geim and K. S. Novoselov, *"The rise of graphene"*, Nature Materials **6**, pp.183 (2007).

[84] N. Akhmediev and A. Ankiewicz., *Dissipative Solitons*, Springer (2005).

[85] A. Chong, J. Buckley, W. Renninger, and F. Wise, *"All-normal-dispersion femtosecond fiber laser"*, Opt. Express **14**, pp.10095 (2006).

[86] A. Chong, W. H. Renninger, and F. W. Wise, *"Properties of normal-dispersion femtosecond fiber lasers"*, J. Opt. Soc. Am. B **25**, pp.140 (2008).

[87] B. G. Bale, S. Boscolo, and S. K. Turitsyn, *"Dissipative dispersion-managed solitons in mode-locked lasers"*, Opt. Lett. **34**, pp.3286 (2009).

[88] E. J. R. Kelleher, J. C. Travers, Z. Sun, A. G. Rozhin, A. C. Ferrari, S. V. Popov, and J. R. Taylor, *"Nanosecond-pulse fiber lasers mode-locked with nanotubes"*, Appl. Phys. Lett. **95**, pp.111108 (2009).

[89] D. Mao, X. Liu, L. Wang, H. Lu, and H. Feng, *"Generation and amplification of high-energy nanosecond pulses in a compact all-fiber laser"*, Opt. Express **18**, pp.23024 (2010).

[90] W. H. Renninger, A. Chong, and F. W. Wise, *"Area theorem and energy quantization for dissipative optical solitons"*, J. Opt. Soc. Am. B **27**, pp.1978 (2010).

[91] B. N. Nyushkov, V. I. Denisov, S. M. Kobtsev, V. S. Pivtsov, N. A. Kolyada, A. V. Ivanenko and S. K. Turitsyn, *"Generation of 1.7-μJ pulses at 1.55 μm by a self-mode-locked all-fiber laser with a kilometers-long linear-ring cavity"*, Laser Phys. Lett. **7**, pp.661 (2010).

[92] S. Lefrançois, K. Kieu, Y. Deng, J. D. Kafka, and F. W. Wise, *"Scaling of dissipative soliton fiber lasers to megawatt peak powers by use of large-area photonic crystal fiber"* Opt. Lett. **35**, pp.1569 (2010).

[93] M. Baumgartl, B. Ortaç, C. Lecaplain, A. Hideur, J. Limpert, and A. Tünnermann, *"Sub-80 fs dissipative soliton large-mode-area fiber laser"*, Opt. Lett. **35**, pp.2311 (2010).

[94] C. E. S. Castellani, E. J. R. Kelleher, J. C. Travers, D. Popa, T. Hasan, Z. Sun, E. Flahaut, A. C. Ferrari, S. V. Popov, and J. R. Taylor, *"Ultrafast Raman laser mode-locked by nanotubes"*, Opt. Lett. **36**, pp.3996 (2011).

[95] R. Paschotta, R. Häring, E. Gini, H. Melchior, U. Keller, H. L. Offerhaus, and D. J. Richardson, *"Passively Q-switched 0.1-mJ fiber laser system at 1.53 m"*, Opt. Lett. **24**, pp.388 (1999).

[96] S. Yang, Y. Zhou, J. Li, and K. K. Y. Wong, *"Actively Mode-Locked Fiber Optical Parametric Oscillator"*, IEEE J. Sel. Top. Quantum Electron. **15**, pp.393 (2009).

[97] G. K. L. Wong, S. G. Murdoch, R. Leonhardt, J. D. Harvey, and V. Marie, *"High-conversion-efficiency widely-tunable all-fiber optical parametric oscillator"* Opt. Express **15**, pp.2947 (2007).

[98] J. S. Y. Chen, S. G. Murdoch, R. Leonhardt, and J. D. Harvey, *"Effect of dispersion fluctuations on widely tunable optical parametric amplification in photonic crystal fibers"* Opt. Express **14**, pp.9491 (2006).

[99] C. Headly, G. P. Agrawal, *Raman Amplification in Fiber Optical Communication Systems*, 1st Edition Academic Press (2004).

[100] M. J. Damzen, V. I. Vlad, A. Mocofanescu, V. Babin, *Stimulated Brillouin Scattering: Fundamentals and Applications: Theory and Applications*, 1st Edition Taylor & Francis (2003).

[101] C. V. Raman, *"A new radiation"*, Indian J. Phys. **2**, pp.387 (1928).

[102] V. V. Raman and K. S. Krishnan, *"A new type of secondary radiation"*, Nature **121**, pp.501 (1928).

[103] E. P. Ippen, *"Low-power quasi-CW Raman oscillator"*, Appl. Phys. Lett. **16**, pp.303 (1970).

[104] R. H. Stolen, E. P. Ippen, and A. R. Tynes, *"Raman oscillation in glass optical waveguide"*, Appl. Phys. Lett. **20**, pp.62 (1972).

[105] B. A. Cumberland, S. V. Popov, J. R. Taylor, O. I. Medvedkov, S. A. Vasiliev, and E. M. Dianov, *"2.1 μm continuous-wave Raman laser in GeO_2 fiber"* Opt. Lett. **32**, pp.1848 (2007).

[106] J. C. Travers, S. V. Popov, and J. R. Taylor, *"Efficient continuous-wave holey fiber Raman laser"*, Appl. Phys. Lett. **87**, pp.031106 (2005).

[107] V. M. Mashinsky, V. B. Neustruev, V. V. Dvoyrin, S. A. Vasiliev, O. I. Medvedkov, I. A. Bufetov, A. V. Shubin, E. M. Dianov, A. N. Guryanov, V. F. Khopin, and M. Yu. Salgansky, *"Germania-glass-core silica-glass-cladding modified chemical-vapor deposition optical fibers: optical losses, photorefractivity, and Raman amplification"*, Opt. Lett. **29**, pp.2596 (2004).

[108] P.A. Champert, S.V. Popov and J. R. Taylor, *"Tunable, broad visible range, fibre-based Raman source"*, Elect. Lett. **36**, pp.2003 (2000).

[109] D. Georgiev, V. P. Gapontsev, A. G. Dronov, M. Y. Vyatkin, A. B. Rulkov, S. V. Popov, and J. R. Taylor, *"Watts-level frequency doubling of a narrow line linearly polarized Raman fiber laser to 589 nm"*, Opt. Express **13**, pp.6772 (2005).

[110] S. V. Chernikov, S. A. E. Lewis, and J. R. Taylor, *"Broadband Raman amplifiers in the spectral range of 1480-1620 nm"*, in Optical Fiber Communication Conference and the International Conference on Integrated Optics and Optical Fiber Communication, OSA Technical Digest Series, paper WG6 (1999).

[111] P.C. Reeves-Hall and J.R. Taylor, *"Wavelength tunable CW Raman fibre ring laser operating at 1486-1551 nm"*, Elect. Lett. **37**, pp.491 (2001).

[112] C. Lin, L. G. Cohen, R. H. Stolen, G. W. Tasker, W. G. French, *"Near-infrared sources in the 1-1.3 μm region by efficient stimulated Raman emission in glass fibers"*, Opt. Commun. **20**, pp.426 (1977).

[113] M. J. F. Digonnet, *Rare-Earth-Doped Fiber Lasers and Amplifiers, Revised and Expanded*, 2nd Edition CRC press (2001).

[114] T. S. McComb, R. A. Sims, C. C. C. Willis, P. Kadwani, V. Sudesh, L. Shah, and M. Richardson, *"High-power widely tunable thulium fiber lasers"*, Appl. Opt. **49**, pp.6236 (2010).

[115] C. E. S. Castellani, S. P. N. Cani, M. E. Segatto, M. J. Pontes, and M. A. Romero, *"Design methodology for multi-pumped discrete Raman amplifiers: case-study employing photonic crystal fibers"*, Opt. Express **17**, pp.14121 (2009).

[116] K. Smith and L. F. Mollenauer, *"Experimental observation of adiabatic compression and expansion of soliton pulses over long fiber paths"*, Opt. Lett. **14**, pp.751 (1989).

[117] J. Schröder, S. Coen, F. Vanholsbeek, T. Sylvestre, *"Passively mode-locked Raman fiber laser with 100 GHz repetition rate"*, Opt. Lett. **31**, pp.3489 (2006).

[118] D. A. Chestnut, J. R. Taylor, *"Wavelength-versatile subpicosecond pulsed lasers using Raman gain in figure-of-eight fiber geometries"* Opt. Lett. **30**, pp.2982 (2005).

[119] C. Aguergaray, D. Mechin, V. Kruglov, J. D. Harvey, *"Experimental realization of a Mode-locked parabolic Raman fiber oscillator"*, Opt. Express **18**, pp.8680 (2010).

[120] A. Chamorovskiy, J. Rautiainen, J. Lyytikäinen, S. Ranta, M. Tavast, A. Sirbu, E. Kapon, and O. G. Okhotnikov, *"Raman fiber laser pumped by semiconductor disk laser and mode-locked by a semiconductor saturable absorber mirror"*, Opt. Lett. **35**, pp.3529 (2010).

[121] A. Chamorovskiy, A. Rantamäki, A. Sirbu, A. Mereuta, E. Kapon, and O. G. Okhotnikov, "1.38-μm mode-locked Raman fiber laser pumped by semiconductor disk laser", Opt. Express **18**, pp.23872 (2010).

[122] T. Hasan, Z. Sun, F. Wang, F. Bonaccorso, P. H. Tan, A. G. Rozhin, A. C. Ferrari, *"NanotubePolymer Composites for Ultrafast Photonics"*, Adv. Mater. **21**, pp.3874 (2009).

[123] Z. Sun, T. Hasan, F. Torrisi, D. Popa, G. Privitera, F. Wang, F. Bonaccorso, D. M. Basko, A. C. Ferrari, *"Graphene Mode-Locked Ultrafast Laser"*, ACS Nano **4**, pp.803 (2010).

[124] F. Bonaccorso, Z. Sun, T. Hasan, A. C. Ferrari, *"Graphene photonics and optoelectronics"*, Nat. Phot. **4**, pp.611 (2010).

[125] S. Ijima, *"Helical microtubules of graphitic carbon"*, Nature **354**, pp.56 (1991).

[126] K. S. Novoselov, A. K. Geim, S. V. Morozov, D. Jiang, Y. Zhang, S. V. Dubonos, I. V. Grigorieva, A. A. Firsov, *"Electric field effect in atomically thin carbon films"*, Science **306**, pp.666 (2004).

[127] Unknown author, *"Nanotubes de carbone"*, Retrieved from: http://www-ibmc.u-strasbg.fr/ict/article83.html?lang=fr, Last Accessed: 15/12/2013.

[128] R. H. Baughman, A. A. Zakhidov, W. A. Heer, *"Carbon Nanotubes–the Route Toward Applications"*, Science **297**, pp.787 (2002).

[129] H. W. C. Postma, T. Teepen, Z. Yao, M. Grifoni, C. Dekker, *"Carbon Nanotube Single-Electron Transistors at Room Temperature"*, Science **293**, pp.76 (2001).

[130] E. Gaufres, N. Izard, X. Roux, D. M. Morini, S. Kazaoui, E. Cassan, and L. Vivien, *"Optical gain in carbon nanotubes"*, Appl. Phys. Lett. **96**, pp.231105 (2010).

[131] A. Modi, N. Koratkar, E. Lass, B. Wei, and P. M. Ajayan, *"Miniaturized gas ionization sensors using carbon nanotubes"*, Nature **424**, pp.171 (2003).

[132] T. Belin, F. Epron, *"Characterization methods of carbon nanotubes: a review"*, Mater. Sci. Eng. B **119**, pp.105 (2005).

[133] B. P. Grady, *"Carbon Nanotube Composites"*, Retrieved from: http://coecs.ou.edu/Brian.P.Grady/nanotube.html, Last Accessed: 15/12/2013.

[134] J. C. Travers, J. Morgenweg, E. D. Obraztsova, A. I. Chernov, E. J. R. Kelleher, S. V. Popov, *"Using the E22 transition of carbon nanotubes for fiber laser mode-locking"*, Laser Phys. Lett. **8**, pp.144 (2010).

[135] M. S. Dresselhaus, G. Dresselhaus, R. Saito, and A. Jorio, *"Raman spectroscopy of carbon nanotubes"*, Phys. Rep. **409**, pp.47 (2005).

[136] S. Set, H. Yaguchi, Y. Tanaka, M. Jablonski, Y. Sakakibara, A. Rozhin, M. Tokumoto, H. Kataura, Y. Achiba and K. Kikuchi, *"Mode-locked fiber lasers based on a saturable absorber incorporating carbon nanotubes*, In Optical Fiber Communications Conference, pp. PD44P13 (2003).

[137] S. Set, H. Yaguchi, Y. Tanaka and M. Jablonski, *"Laser mode locking using a saturable absorber incorporating carbon nanotubes"*, J. Lightwave Technol. **22**, pp.51 (2004).

[138] Y. Song, S. Set, S. Yamashita, C. Goh and T. Kotake, *"1300 nm pulsed fiber lasers mode-locked by purified carbon nanotubes"*, IEEE Phot. Tech. Lett. **17** pp. 1623 (2005).

[139] A. G. Rozhin, Y. Sakakibara, S. Namiki, M. Tokumoto, H. Kataura and Y. Achiba, *"Sub-200-fs pulsed erbium-doped fiber laser using a carbon nanotube-polyvinylalcohol mode locker"*, Appl. Phys. Lett. **88**, pp.051118 (2006).

[140] M. Solodyankin, E. Obraztsova, A. Lobach, A. Chernov, A. Tausenev, V. Konov and E. Dianov, *"Mode-locked 1.93 μm thulium fiber laser with a carbon nanotube absorber"*, Opt. Lett. **33**, pp.1336 (2008).

[141] K. Kieu and F. W. Wise, *"All-fiber normal-dispersion femtosecond laser"*, Opt. Express **16**, pp.11453 (2008).

[142] D. Steinberg, L. A. M. Saito, H. G. Rosa, E. A. De Souza, *"O-band passive mode-locked Raman fiber laser based on Single Wall Carbon Nanotubes as saturable absorbers"*, Microwave & Optoelectronics Conference (IMOC), pp.829 (2011).

[143] C. E. S. Castellani, E. J. R. Kelleher, D. Popa, T. Hasan, Z. Sun, A. C. Ferrari, S. V. Popov, J. R. Taylor, *"CW-pumped short pulsed 1.12 μm Raman laser using carbon nanotubes"*, Laser Phys. Lett. **10**, pp. 015101 (2013).

[144] C. E. S. Castellani, E. J. R. Kelleher, D. Popa, Z. Sun, T. Hasan, A. C. Ferrari, O. I. Medvedkov, S. A. Vasiliev, E. M. Dianov, S. V. Popov, J. R. Taylor, *"Mode-locking by nanotubes of a Raman laser based on a highly doped GeO_2 fiber"*, Conference on Lasers and Electro-Optics (CLEO), (2012).

[145] S. T. Davey, D. L. Williams, B. J. Ainslie, W. J. M. Rothwell, B. Wakefield, *"Optical gain spectrum of GeO_2-SiO_2 Raman fibre amplifiers"*, IEE PROC-J **136**, pp.301 (1989).

[146] E. Flahaut, R. Bacsa, A. Peigney, C. Laurent, *"Gram-scale CCVD Synthesis of Double-Walled Carbon nanotube"*, Chem. Commun. **12**, pp.1442 (2003).

[147] S. Osswald, E. Flahaut, H. Ye, Y. Gogotsi, *"Elimination of D-Band in Raman Spectra of Double-Wall Carbon Nanotubes by Oxidation"*, Chem. Phys. Lett. **402**, pp.422 (2005).

[148] W. H. Renninger, A. Chong, F. W. Wise, *"Giant-chirp oscillators for short-pulse fiber amplifiers"*, Opt. Lett. **33**, pp.3025 (2008).

[149] B. Kitiyanan, W. E. Alvarez, J. H. Harwell, and D. E. Resasco, *"Controlled production of single-wall carbon nanotubes by catalytic decomposition of CO on bimetallic CoMo catalysts"*, Chem. Phys. Lett. **317**, pp.497 (2000).

[150] A. Jorio, A. P. Santos, H. B. Ribeiro, C. Fantini, M. Souza, J. P. M. Vieira, C. A. Furtado, J. Jiang, R. Saito, L. Balzano, D. E. Resasco, and M. A. Pimenta, *"Quantifying carbon-nanotube species with resonance Raman scattering"*, Phys. Rev. B **72**, pp.075207 (2005).

[151] R. B. Weisman, S. M. Bachilo, *"Dependence of Optical Transition Energies on Structure for Single-Walled Carbon Nanotubes in Aqueous Suspension: An Empirical Kataura Plot"*, Nano Lett. **3**, pp.1235 (2003).

[152] S. M. Bachilo, L. Balzano, J. E. Herrera, F. Pompeo, D. E. Resasco, and R. B. Weisman, *"Narrow (n,m)-distribution of single-walled carbon nanotubes grown using a solid supported catalyst"*, J. Am. Chem. Soc. **125**, pp.11186 (2003).

[153] R. E. Peierls, *"Quelques proprietes typiques des corpses solides"*, Ann. I. H. Poincare **5**, pp.177 (1935).

[154] L. D. Landau, *"Zur Theorie der phasenumwandlungen II"*, Phys. Z. Sowjetunion **11**, pp.26 (1937).

[155] P. R. Wallace, *"The band theory of graphite"*, Phys. Rev. **71**, pp.622 (1947).

[156] J. W. McClure, *"Diamagnetism of graphite"*, Phys. Rev. **104**, pp.666 (1956).

[157] K. S. Novoselov, D. Jiang, F. Schedin, T. J. Booth, V. V. Khotkevich, S. V. Morozov, and A. K. Geim, *"Two-dimensional atomic crystals"*, Proc. Natl Acad. Sci. USA **102**, pp.10451 (2005).

[158] A. N. Obraztsov, E. A. Obraztsova, A. V. Tyurnina, and A. A. Zolotukhin, *"Chemical vapor deposition of thin graphite films of nanometer thickness"*, Carbon **45**, pp.2017 (2007).

[159] A. Reina, X. Jia, J. Ho, D. Nezich, H. Son, V. Bulovic, M. S. Dresselhaus, and J. Kong, *"Large Area, Few-Layer Graphene Films on Arbitrary Substrates by Chemical Vapor Deposition"*, Nano Lett. **9**, pp.30 (2009).

[160] Y. Hernandez, V. Nicolosi, M. Lotya, F. M. Blighe, Z. Sun, S. De, I. T. McGovern, B. Holland, M. Byrne, Y. K. Gun'Ko, J. J. Boland, P. Niraj, G. Duesberg, S. Krishnamurthy, R. Goodhue, J. Hutchison, V. Scardaci, A. C. Ferrari, and J. N. Coleman, *"High-yield production of graphene by liquid-phase exfoliation of graphite"*, Nature Nanotech. **3**, pp.563 (2008).

[161] A. C. Ferrari, J. C. Meyer, V. Scardaci, C. Casiraghi, M. Lazzeri, F. Mauri, S. Piscanec, D. Jiang, K. S. Novoselov, S. Roth, and A. K. Geim, *"Raman Spectrum of Graphene and Graphene Layers"*, Phys. Rev. Lett. **97**, pp.187401 (2006).

[162] A. C. Ferrari, and D. M. Basko, *"Raman spectroscopy as a versatile tool for studying the properties of graphene"*, Nature Nanotech. **8**, pp.235 (2013).

[163] P. Blake, E. W. Hill, A. H. C. Neto, K. S. Novoselov, D. Jiang, R. Yang, T. J. Booth, and A. K. Geim, *"Making graphene visible"*, Appl. Phys. Lett. **91**, pp.063124 (2007).

[164] B. Partoens, and F. M. Peeters, *"From graphene to graphite: Electronic structure around the K point"*, Phys. Rev. B **74**, pp.075404 (2006).

[165] H. S. P. Wong, D. Akinwande, *Carbon Nanotube and Graphene Device Physics*, Cambridge University Press (2011).

[166] C. Lee, X. Wei, J. W. Kysar, J. Hone, *"Measurement of the Elastic Properties and Intrinsic Strength of Monolayer Graphene"*, Science **321**, pp.385 (2008).

[167] A. H. C. Neto, F. Guinea, N. M. R. Peres, K. S. Novoselov, and A. K. Geim, *"The electronic properties of graphene"*, Rev. Mod. Phys. **81**, pp.109 (2009).

[168] K. S. Novoselov, A. K. Geim, S. V. Morozov, D. Jiang, M. I. Katsnelson, I. V. Grigorieva, S. V. Dubonos, and A. A. Firsov, *"Two-dimensional gas of massless Dirac fermions in graphene"*, Nature **438**, pp.197 (2005).

[169] M. I. Katsnelsona, K. S. Novoselov, *"Graphene: New bridge between condensed matter physics and quantum electrodynamics"*, Solid State Commun. **143**, pp.3 (2007).

[170] E. H. Hwang, S. Adam, and S. D. Sarma, "*Carrier Transport in Two-Dimensional Graphene Layers*", Phys. Rev. Lett. **98**, pp.186806 (2007).

[171] I. Gierz, C. Riedl, U. Starke, C. R. Ast, and K. Kern, *"Atomic Hole Doping of Graphene"*, Nano Lett. **8**, pp.4603 (2008).

[172] S. Y. Zhou, D. A. Siegel, A. V. Fedorov, and A. Lanzara, *"Metal to Insulator Transition in Epitaxial Graphene Induced by Molecular Doping"*, Phys. Rev. Lett. **101**, pp.086402 (2008).

[173] H. Liu, Y. Liu, D. Zhua, *"Chemical doping of graphene"*, J. Mater. Chem. **21**, pp.3335 (2011).

[174] M. Y. Han, B. Özyilmaz, Y. Zhang, and P. Kim, *"Energy Band-Gap Engineering of Graphene Nanoribbons"*, Phys. Rev. Lett. **98**, pp.206805 (2007).

[175] R. R. Nair, P. Blake, A. N. Grigorenko, K. S. Novoselov, T. J. Booth, T. Stauber, N. M. R. Peres, A. K. Geim, *"Fine structure constant defines visual transparency of graphene"*, Science **320**, pp.1308 (2008).

[176] C. Casiraghi, A. Hartschuh, E. Lidorikis, H. Qian, H. Harutyunyan , T. Gokus , K. S. Novoselov, and A. C. Ferrari, "Rayleigh imaging of graphene and graphene layers", Nano Lett. **7**, pp.2711 (2007).

[177] D. Popa, Z. Sun, F. Torrisi, T. Hasan, F. Wang, and A. C. Ferrari, *"Sub 200 fs pulse generation from a graphene mode-locked ber laser"*, Appl. Phys. Lett. **97**, pp.203106 (2010);

[178] L. M. Zhao, D. Y. Tang, H. Zhang, X. Wu, Q. Bao, and K. P. Loh, *"Dissipative soliton operation of an ytterbium-doped fiber laser mode locked with atomic multilayer graphene"*, Opt. Lett. **35**, pp.3622 (2010).

[179] M. Zhang, E. J. R. Kelleher, F. Torrisi, Z. Sun, T. Hasan, D. Popa, F. Wang, A. C. Ferrari, S. V. Popov, and J. R. Taylor, "Tm-doped fiber laser mode-locked by graphene-polymer composite", Opt. Express **20**, pp.25077 (2012).

[180] L. Zhang, G. Wang, J. Hu, J. Wang, J. Fan, J. Wang, Y. Feng, *"Linearly Polarized 1180-nm Raman Fiber Laser Mode Locked by Graphene"*, IEEE Photon. J. **4**, pp.1809 (2012).

[181] H. Zhang, D. Tang, R. J. Knize, L. Zhao, Q. Bao, and K. P. Loh, *"Graphene mode locked, wavelength-tunable, dissipative soliton fiber laser"*, Appl. Phys. Lett. **96**, pp.111112 (2010).

[182] Z. Sun, D. Popa, T. Hasan, F. Torrisi, F. Wang, E. J. R. Kelleher, J. C. Travers, V. Nicolosi, A. C. Ferrari, *"A stable, wideband tunable, near transform-limited, graphene-mode-locked, ultrafast laser"*, Nano Res. **3**, pp.653 (2010).

[183] J. Sotor, G. Sobon, I. Pasternak, A. Krajewska, W. Strupinski, and K. M. Abramski, *"Simultaneous mode-locking at 1565 nm and 1944 nm in fiber laser based on common graphene saturable absorber"*, Opt. Express **21**, pp.18994 (2013).

[184] C. E. S. Castellani, E. J. R. Kelleher, Z. Luo, K. Wu, C. Ouyang, P. P. Shum, Z. Shen, S. V. Popov, J. R. Taylor, *"Harmonic and single pulse operation of a Raman laser using graphene"*, Laser Phys. Lett. **9**, pp. 223 (2012).

[185] Z. Luo, T. Yu, J. Z. Shang, Y. Y. Wang, S. H. Lim, L. Liu,G. G. Gurzadyan, Z. X. Shen and J. Y. Lin, *"Large-Scale Synthesis of Bi-layer Graphene in Strongly Coupled Stacking Order"*, Adv. Funct. Mater., **21**, pp.911 (2011).

[186] N. Papasimakis, Z. Luo, Z. X. Shen, F. D. Angelis, E. D. Fabrizio, A. E. Nikolaenko and N. I. Zheludev, *"Graphene in a photonic metamaterial"*, Opt. Express **18**, 8353 (2010).

[187] S. V. Chernikov, D. V. Gapontsev, S. A. E. Lewis, J. R. Taylor, *"Broadband silica fibre Raman amplifiers at 1.3 μm and 1.5 μm"*, Proceedings of the 24th European Conference on Optical Communication (1998).

[188] E. Desurvire, M. Papuchon, J. P. Pocholle, J. Raffy, *"High-gain optical amplification of laser diode signal by Raman scattering in single-mode fibres"*, Electron. Lett. **19**, pp.751 (1983).

[189] J. Hegarty, N. A. Olsson, L. Goldner, *"CW pumped Ramam preamplifier in a 45 km-long fibre transmission system operating at 1.5 μm and 1 Gbitls"*, Electron. Lett. **21**, p.290 (1985).

[190] E. M. Dianov, *"Raman fiber amplifiers"*, Proc. SPIE 4083, Advances in Fiber Optics **90**, (2000).

[191] F. L. Galeener, J. C. Mikkelsen, R. H. Geils, and W. J. Mosby, *"The relative Raman cross sections of vitreous SiO_2, GeO_2, B_2O_3, and P_2O_5"*, Appl. Phys. Lett. **32**, pp.34 (1978).

[192] N. Shibata, M. Horigudhi, and T. Edahiro, *"Raman spectra of binary high-silica glasses and fibers containing SiO_2, GeO_2, B_2O_3, and P_2O_5"*, J. Non-Cryst. Solids **45**, pp.115 (1981).

[193] E. M. Dianov, A. A. Abramov, M. M. Bubnov, A. V. Shipulin, A. M. Prokhorov, S. L. Semjonov, A. G. Schebunjaev, G. G. Devjatykh, A. N. Guryanov, V. F. Khopin, *"Demonstration of 1.3-μm Raman Fiber Amplifier Gain of 25 dB at a Pumping Power of 300 mW"*, Opt. Fiber Technol. **1**, pp.236 (1995).

[194] E. M. Dianov, *"Advances in Raman Fibers"*, J. Lightwave Technol. **20**, pp.1457 (2002).

[195] A. S. L. Gomes, V. L. daSilva, B. J. Ainslie, S. P. Craig and J. R. Taylor, *"Picosecond stimulated Raman scattering in P_2O_5-SiO_2 based single mode optical fibre"*, Opt Commun **64**, pp.373 (1987).

[196] E. M.Dianov, M .V. Grekov, I. A. Bufetov, S. A. Vasiliev, O. I. Medvedkov, V. G. Plotnichenko, V. V. Koltashev, A. V. Belov, M. M. Bubnov, S. L. Semjonov and A. M. Prokhorov, *"CW high power 1.24 μm and 1.48 μm Raman lasers based on low loss phosphosilicate fibre"*, Electron. Lett., **33**, pp.1542 (1997).

[197] Z. Q. Luo, C. C. Ye, H. Y. Fu, H. H. Cheng, J. Z. Wang, and Z. P. Cai, *"Raman fiber laser harmonically mode-locked by exploiting the intermodal beating of CW multimode pump source"*, Opt. Express **20**, pp.19905 (2012).

[198] T. Sun, G. Kai, Z. Wang, S. Yuan, and X. Dong, *"Enhanced nonlinearity in photonic crystal fiber by germanium doping in the core region"*, Chin. Opt. Lett. **6**, pp.93 (2008).

[199] F. Couny, F. Benabid, and P. S. Light, *"Subwatt Threshold cw Raman Fiber-Gas Laser Based on H_2-Filled Hollow-Core Photonic Crystal Fiber"*, Phys. Rev. Lett. **99**, pp.143903 (2007).

[200] F. Benabid, J. C. Knight, G. Antonopoulos, and P. St. J. Russell, *"Stimulated Raman Scattering in Hydrogen-Filled Hollow-Core Photonic Crystal Fiber"*, Science **298** pp.399 (2002).

[201] F. Benabid, G. Bouwmans, J. C. Knight, P. St. J. Russell, and F. Couny, *"Ultrahigh Efficiency Laser Wavelength Conversion in a Gas-Filled Hollow Core Photonic Crystal Fiber by Pure Stimulated Rotational Raman Scattering in Molecular Hydrogen"*, Phys. Rev. Lett. **93**, pp.123903 (2004).

[202] R. Kashyap, *"The Fiber Fuse - from a curious effect to a critical issue: A 25^{th} year retrospective"*, Opt. Express **21**, pp.6422 (2013).

[203] S. D. Jackson, *"Towards high-power mid-infrared emission from a fibre laser"*, Nat. Photonics **6**, pp.423 (2012).

[204] G. M. Hale, and M. R. Querry, *"Optical Constants of Water in the 200-nm to 200-μm Wavelength Region"*, Appl. Opt. **12**, pp.555 (1973).

[205] E. M. Dianov, I. A. Bufetov, V. M. Mashinsky, V. B. Neustruev, O. I. Medvedkov, A. V. Shubin, M. A. Melkumov, A. N. Guryanov, V. F. Khopin, and M. V. Yashkov, *"Raman fibre lasers emitting at a wavelength above 2 μm"*, Quantum Electron. **34**, pp.695 (2004).

[206] S. D. Jackson, and G. A. Sanchéz, *"Chalcogenide glass Raman fiber laser"*, Appl. Phys. Lett. **88**, pp.221106 (2006).

[207] M. Bernier, V. Fortin, N. Caron, M. El-Amraoui, Y. Messaddeq, and R. Vallée, *"Mid-infrared chalcogenide glass Raman fiber laser"*, Opt. Lett. **38**, 127-129 (2013).

[208] V. Fortin, M. Bernier, D. Faucher, J. Carrier, and R. Vallée, *"3.7 W fluoride glass Raman fiber laser operating at 2231 nm"*, Opt. Express **20**, pp.19412 (2012).

[209] M. D. O'Donnell, K. Richardson, R. Stolen, C. Rivero, T. Cardinal, M. Couzi, D. Furniss, A. B. Seddon, *"Raman gain of selected tellurite glasses for IR fibre lasers calculated from spontaneous scattering spectra"*, Opt. Mater. **30**, pp.946 (2008).

[210] G. Qin, M. Liao, T. Suzuki, A. Mori, and Y. Ohishi, *"Widely tunable ring-cavity tellurite fiber Raman laser"*, Opt. Lett. **33**, pp.2014 (2008).

[211] M. N. Islam, *Raman Amplifiers for Telecommunications 1: Physical Principles*, Springer (2004).

[212] E. M. Dianov and V. M. Mashinsky, *"Germania-Based Core Optical Fibers"*, J. Lightwave Technol. **23**, pp.3500 (2005).

[213] J. Nishii, S. Morimoto, I. Inagawa, R. Iizuka, T. Yamashita, T. Yamagishi, *"Recent advances and trends in chalcogenide glass fiber technology: a review"*, J. Non-Cryst. Solids **140**, pp.199 (1992).

[214] X. Zhu and N. Peyghambarian, *High-Power ZBLAN Glass Fiber Lasers: Review and Prospect"*, Adv. Optoelectron. **2010**, pp.23 (2010).

[215] V. Fortin, M. Bernier, J. Carrier, and R. Valle, *"Fluoride glass Raman fiber laser at 2185 nm"*, Opt. Lett. **36**, pp.4152 (2011).

[216] K. Richardson, D. Krol, and K. Hirao, *"Glasses for photonic applications"*, Int. J. Appl. Glass Sci. **1**, pp.74 (2010).

[217] J. Wang, S. Prasad, K. Kiang, R.K. Pattnaik, J. Toulouse, and H. Jain, *"Source of optical loss in tellurite glass fibers"*, J. Non-Cryst. Solids **352**, pp.510 (2006).

[218] M. Zhang, E. J. R. Kelleher, T. H. Runcorn, V. M. Mashinsky, O. I. Medvedkov, E. M. Dianov, D. Popa, S. Milana, T. Hasan, Z. Sun, F. Bonaccorso, Z. Jiang, E. Flahaut, B. H. Chapman, A. C. Ferrari, S. V. Popov, and J. R. Taylor, *"Mid-infrared Raman-soliton continuum pumped by a nanotube-mode-locked sub-picosecond Tm-doped MOPFA"*, Opt. Express **21**, pp.23261 (2013).

[219] D. Von der Linde, *"Characterization of the Noise in Continuously Operating Mode-Locked Lasers"*, Appl. Phys. B **39**, pp.201 (1986).